Πανεπιστήμιο Κρήτης
Σχολή Θετικών Επιστημών
Τμήμα Φυσικής

Μεταπτυχιακό πρόγραμμα Μικροηλεκτρονικής – Οπτοηλεκτρονικής

Μεταπτυχιακή Εργασία

Φωτοδυναμική θεραπεία (PDT) παρουσία εκχυλίσματος του *Hypericum Perforatum L* ως φωτοευαισθητοποιητή για την επίτευξη θανάτωσης των κυττάρων της HL-60 λευχαιμικής σειράς

Επιβλέπων: Καθ. Κ. Φωτάκης
Υπεύθυνοι Εργασίας: Επικ. Καθ. Ε. Δημητρίου
Δρ. Γ. Φιλιππίδης
Δρ. Θ. Παπάζογλου

Δημήτρης Καψοκαλύβας

Ηράκλειο 2004

University of Crete
School of Sciences
Department of Physics

Postgraduate Course in Microelectronics and Optoelectronics

Master Thesis

Photodynamic Therapy on HL-60 leukemic cell line with *Hypericum Perforatum L* extracts as photosensitizers

Supervisor: Prof. C. Fotakis
Advisors: Assist. Prof. H. Dimitriou
Dr. G. Filippidis
Dr. T. Papazoglou

Dimitris Kapsokalyvas

Heraklion 2004

Ευχαριστίες

Η παρούσα εργασία είναι αποτέλεσμα συνεργασίας πολλών ανθρώπων τους οποίου θα ήθελα να ευχαριστήσω για την ευγενική προσφορά τους. Καταρχήν θα ήθελα να ευχαριστήσω τον κ. Κ. Φωτάκη πρόεδρο του Ι.Η.Δ.Λ. του Ι.Τ.Ε γιατί ενέκρινε την διεξαγωγή της εργασίας στο Ι.Η.Δ.Λ. Θα ήθελα να ευχαριστήσω ακόμα τον κ. Θ. Παπαζογλου επικεφαλής του τμήματος Βιοϊατρικών εφαρμογών του Ι.Η.Δ.Λ και την κα. Ε. Δημητρίου επικεφαλής του τμήματος Παιδιατρικής Αιματολογίας –Ογκολογίας του Τμήματος Ιατρικής γιατί υποστήριξαν υλικά και επιστημονικά την εργασία αυτή. Επίσης να ευχαριστήσω και τον κ. Δ. Σκάλκο του τμήματος Επιστήμης Υλικών και Μηχανικής του Πανεπιστημίου Ιωαννίνων γιατί μας πρόσφερε τα εκχυλίσματα του φυτού *Hypericum Perforatum L.*

Να ευχαριστήσω ακόμα τον Γ. Φιλιππίδη και τον Γ. Κωνσταντουδάκη για την άμεση συνεργασία που είχαμε. Επίσης ένα μεγάλο ευχαριστώ στους Γιάννη Βόγγλη και στη Χρυσούλα Πιτσούλη για την ανιδιοτελή βοήθεια τους σε θέματα που αφορούσαν το Confocal Μικροσκόπιο. Θα ήθελα να ευχαριστήσω επίσης του καθηγητές μου για όσα μου πρόσφεραν και ιδιαίτερα τους κ. Δ. Χαραλαμπίδη και κ. Ν. Φλυτζάνη.

Ένα μεγάλο ευχαριστώ στη Θεοδώρα Σαριδάκη για όσα μου πρόσφερε τόσο σε επιστημονικά θέματα όσο και για την ηθική υποστήριξη σε όλη τη διάρκεια της εργασίας. Τέλος το μεγαλύτερο ευχαριστώ στην οικογένειά μου που με στήριξε και με στηρίζει με υπομονή και κατανόηση όλα αυτά τα χρόνια που βρίσκομαι στην Κρήτη.

Στον πατέρα μου

Abstract

Autologous bone marrow transplantation is a therapeutic modality that increases the survival rates for children with poor prognosis malignancies but relapse rates are high and attributed partially to the existence of residual malignant cells. The photodynamic treatment (PDT) has been developed among purging strategies. In this study we investigated the effect of the methanolic extract (ME) and its fraction (PMF) of Hypericum perforatum L. (St. John's wort), as a new photosensitizer on the leukemic cell line HL-60 and cord blood hemopoietic progenitors. The subcellular localization of the photosensitizer was also investigated with non linear and confocal microscopy. Cells were incubated with the PMF or ME for one hour before irradiation with Laser at 532nm. The concentrations of PMF or ME used were 30, 40, 50 and 60 μg/ml. Each of them was tested at 3, 5, 7 minutes of irradiation (74.87, 124.79, 174.7 J/cm^2 respectively). Laser photoirradiation in the presence of both PMF and ME induces the killing of HL-60 cells. This effect is dose dependent. At all the tested irradiation doses and photosensitizer concentrations a 99.9999% cell death was observed 24 hrs after irradiation but only concentrations of 50 and 60 μg/ml of PMF or ME resulted in cell killing at the end of the culture. No colony growth from cord blood mononuclear cells was observed under the tested experimental conditions. There was not cell death when cells were incubated only with PMF or ME without irradiation. The extracts were found to localize in the cytoplasm. PDT with both PMF and ME induces the killing of HL-60 leukemic cells and the optimal conditions of treatment were determined. This effect of PDT/ PMF was also exerted on cord blood progenitor cells indicative of the non selective uptake of the photosensitizer by malignant cells. Though this suggests that PDT/ PMF cannot be helpful in autologous bone marrow purging, PMF can however be beneficial in the PDT treatment of tumors.

Περίληψη

Η αυτόλογη μεταμόσχευση αιμοποιητικών κυττάρων έχει υψηλό ποσοστό υποτροπών λόγω εμπεριεχόμενων υπολειπόμενων κακοηθών κυττάρων. Μεταξύ των τεχνικών κάθαρσης που έχουν αναπτυχθεί είναι και η φωτοδυναμική θεραπεία (PDT). Σε αυτήν την μελέτη ερευνήσαμε την επίδραση του μεθανολικού εκχυλίσματος (ΜΕ) και του πολικού εκχυλίσματος (PMF) του *Hypericum perforatum L*, ως νέου φωτοευαισθητοποιητή στη λευχαιμική σειρά HL- 60 κυττάρων και σε προγονικά αιμοποιητικά κύτταρα αίματος ομφάλιου λώρου. Ο ενδοκυττάριος εντοπισμός του φωτοευαισθητοποιητή διερευνήθηκε με χρήση μη γραμμικής και confocal μικροσκοπίας. Τα κύτταρα επωάστηκαν με PMF ή ΜΕ για μια ώρα πριν από την ακτινοβόληση με λέιζερ στα 532nm. Οι συγκεντρώσεις PMF ή ΜΕ που χρησιμοποιήθηκαν ήταν 30, 40, 50 και 60 μg/ml. Κάθε δείγμα ακτινοβολήθηκε για 3, 5 και 7 λεπτά (74,87, 124.79, 174.7 J/cm ^{2} δόση ενέργειας αντίστοιχα). Η ακτινοβολία λέιζερ παρουσία PMF και ΜΕ προκαλεί το θάνατο των HL- 60 κυττάρων. Αυτή η επίδραση είναι δόσο-εξαρτώμενη. Σε όλες τις δόσεις ακτινοβολίας και συγκέντρωση φωτοευαισθητοποιητή που δοκιμάσθηκαν παρατηρήθηκε 99,9999% θάνατος των κυττάρων 24 ώρες μετά από την ακτινοβόληση αλλά μόνο σε συγκεντρώσεις 50 και 60 μg/ml PMF ή ΜΕ παρατηρήθηκε κυτταρικός θάνατος μετά την ολοκλήρωση της καλλιέργειας. Επίσης δεν παρατηρήθηκε ανάπτυξη αποικιών από μονοπύρηνα κύτταρα αίματος ομφάλιου λώρου υπό τις ίδιες πειραματικές συνθήκες.. Δεν υπήρξε θάνατος κυττάρων όταν επωάστηκαν μόνο με PMF ή ΜΕ χωρίς ακτινοβολία. Ο φωτοευαισθητοποιητής βρέθηκε να εντοπίζεται στο κυτταρόπλασμα. Φωτοδυναμική θεραπεία με PMF και ΜΕ προκαλεί το θάνατο των HL-60 λευχαιμικών κυττάρων υπό τις παραμέτρους της PDT που καθορίστηκαν. Η ίδια επίδραση PMF παρατηρήθηκε και στα προγονικά αιμοποιητικά κύτταρα αίματος ομφάλιου λώρου, ενδεικτικό της μη επιλεκτικής σύνδεσης του φωτοευαισθητοποιητή σε κακοήθη κύτταρα. Αν και αυτό δείχνει ότι ο συνδυασμός PDT και PMF δεν μπορεί να είναι χρήσιμος στην κάθαρση αυτόλογων μοσχευμάτων μυελού των οστών, το εκχύλισμα PMF μπορεί εντούτοις να είναι έχει καθοριστικό ρόλο στη φωτοδυναμική θεραπεία των όγκων.

Contents

Part A

Part B

1. Photodynamic Therapy (PDT)

1.1 Laser tissue Interaction Mechanisms

The variety of interaction mechanisms that may occur when applying laser light to biological tissue is manifold [1]. Specific tissue characteristics as well as laser parameters contribute to this diversity. Most important among optical tissue properties are the coefficients of reflection, absorption, and scattering. Together, they determine the total transmission of the tissue at a certain wavelength. Thermal tissue properties - such as heat conduction and heat capacity are also important. Additionally, the following parameters are given by the laser radiation itself: wavelength, exposure time, applied energy, focal spot size, energy density, and power density. Among these, the exposure time is a critical parameter when selecting a certain type of interaction, as it will be shown.

During the first decades after invention of the laser by Maiman (1960), many studies have been conducted investigating potential interaction effects by using all types of laser systems and tissue targets. Although the number of possible combinations for the experimental parameters is unlimited, mainly five categories of interaction types have been classified today. These are *photochemical interactions, thermal interactions, photoablation, plasma-induced ablation,* and *photodisruption.* Photochemical interactions take place at very low power densities and refer to the chemical interactions that take place during irradiation. These types of interactions play a significant role during PDT. Thermal interactions can be subdivided to coagulation, vaporization, carbonization and melting. These interactions take place when a certain temperature is reached which leads to the desired thermal effect.

Photoablation is the decomposition of a material when exposed to high intense laser irradiation. This means the removal of tissue in a very clean and exact fashion without any appearance of thermal damage such as coagulation or vaporization. Plasma-induced ablation takes place at intensities exceeding 10^{11} W/cm^2 and involves the ablation by ionizing plasma formation. This leads to a well defined removal of tissue without evidence of thermal or mechanical damage. Finally photodisruption takes place at very high intensities and longer exposure times and involves plasma formation but also shock wave generation, cavitation and jet formation. Again tissue removal is achieved but the mechanical side effects become more significant and

might determine the total effect upon the tissue. It should be stated that all these seemingly different interaction types share a single common property: the characteristic energy density ranges from approximately 1 J/cm^2 to 1000 J/cm^2. This is surprising, since the power density itself varies over 15 orders of magnitude! Thus, a single parameter distinguishes and primarily controls these processes: the duration of laser exposure which is mainly identical with the interaction time itself.

A double-logarithmic map with the five basic interaction types is shown in Fig. 1.1 as found in several experiments. The ordinate expresses the applied power density or irradiance in W/cm^2. The abscissa represents the exposure time in seconds. Two diagonals show constant energy fluences at 1 J/cm^2 and 1000 J/cm^2, respectively. According to this chart, the time scale can be roughly divided into five sections: continuous wave or exposure times > 1 s for *photochemical interactions,* 1 min down to 1 µs for *thermal interactions,* 1 µs down to 1 ns for *photoablation,* and < 1 ns for *plasma-induced ablation* and *photodisruption.* The difference between the last two is attributed to different energy densities.

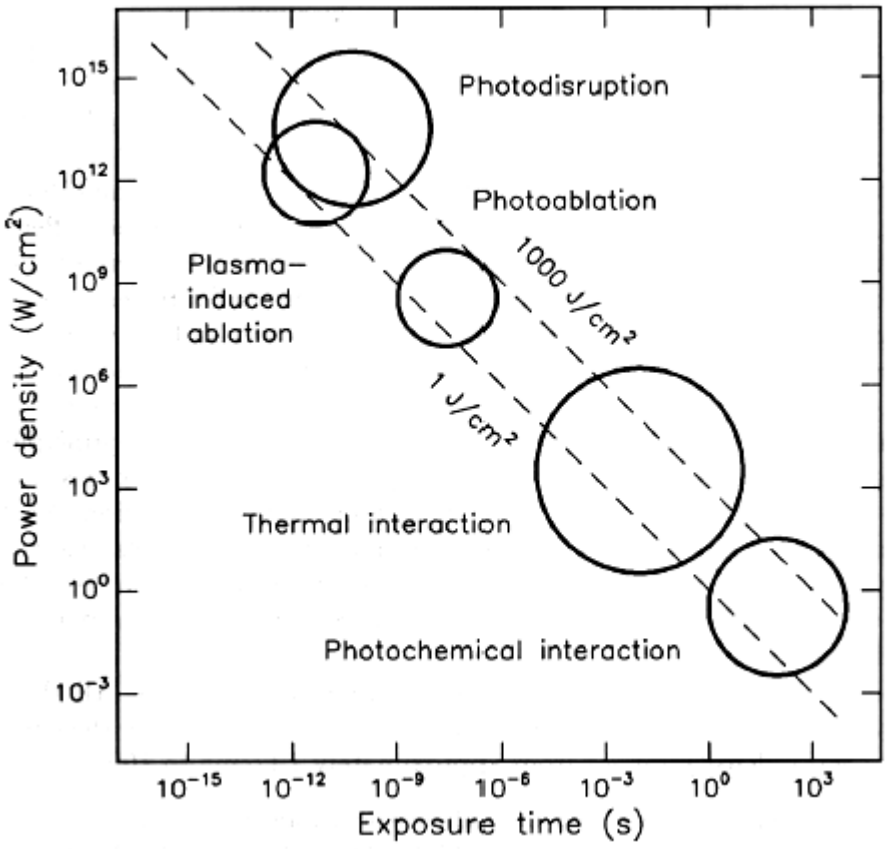

Figure 1.1: Map of laser-tissue interactions. The circles give only a rough estimate of the associated laser parameters [2].

Obviously, Fig. 1.1 depicts the statement from above that the total energy density relevant for medical laser applications ranges from about 1J/cm^2 to 1000 J/cm^2 and this energy density can be even lower around some mJ/cm^2 referring to fluorescence detection applications. The reciprocal correlation between power density and exposure time clearly demonstrates that roughly the same energy density is required for any intended type of interaction. Thus, the exposure time appears to be the main parameter responsible for the variety of interaction mechanisms.

Adjacent interaction types cannot always be strictly distinguished. Thermal effects may also play an important role during photochemical interaction. And even ultrashort laser pulses with pulse durations shorter than 100 ps - each of them having no thermal effect - may add up to a measurable increase in temperature if applied at repetition rates higher than 10-20 Hz, depending on the laser. These two examples reveal the need for a better understanding of each laser-tissue interaction. This task, of course, is aggravated due to the lack of homogeneity of most tissues which cannot change. However, the basic physics involved in each interaction becomes accessible if enough data are collected to fit unknown parameters.

1.2 Photodynamic Therapy in cancer

1.2.1 Introduction

Light has been used as a therapy for more than three thousand years [3]. Ancient Egyptian, Greek, Indian and Chinese civilizations used light to treat various diseases, including psoriasis, rickets, vitiligo and skin cancer. At the end of the nineteenth century in Denmark, Niels Finsen further developed ‘phototherapy’, or the use of light, to treat diseases. He found that red-light exposure prevents the formation and discharge of smallpox pustules and can be used to treat this disease. He also used ultraviolet light from the sun to treat cutaneous tuberculosis. This was the beginning of the modern light therapy, and Finsen was awarded a Nobel Prize for his discoveries in 1903. More than 100 years ago, researchers also observed that a combination of light and certain chemicals could induce cell death. In 1900, German medical student Oscar Raab reported that certain wavelengths were lethal to infusoria, including a species of *Paramecium,* in the presence of acridine. In the same year, a French neurologist, J.Prime, found that epilepsy patients who were treated with oral eosin developed dermatitis in sun-exposed areas. Later, Herman Von Tappeiner and A.

Jesionek treated skin tumours with eosin applied locally and subsequent exposure to white light in 1903; they described this phenomenon as 'Photodynamic Action' [4]. Experiments to test combinations of reagents and light led to modern photodynamic therapy (PDT).

PDT [5, 6] involves two individually non-toxic parameters that are combined to induce cellular and tissue effects in an oxygen-dependent manner (Fig. 1.2). The first parameter of PDT is the *photosensitizer*, a photosensitive molecule that localizes to a target cell and/or tissue. The second parameter involves the administration of light of a specific wavelength that activates the sensitizer. The photosensitizer transfers energy from laser light to molecular oxygen of the tissue, to generate reactive oxygen species (ROS). These reactions occur in the immediate locale of the light-absorbing photosensitizer. Therefore, the biological responses to the photosensitizer are activated only in the particular areas of tissue that have been exposed to light. Other photochemical reactions that do not use oxygen as an intermediate [7] have also been developed, for example photoaddition to DNA. These reactions are called 'photochemotherapy'. Such a photochemotherapeutic, called 'psoralens', has been combined with ultraviolet A to treat psoriasis, vitiligo and to enhance immunotherapy [8].

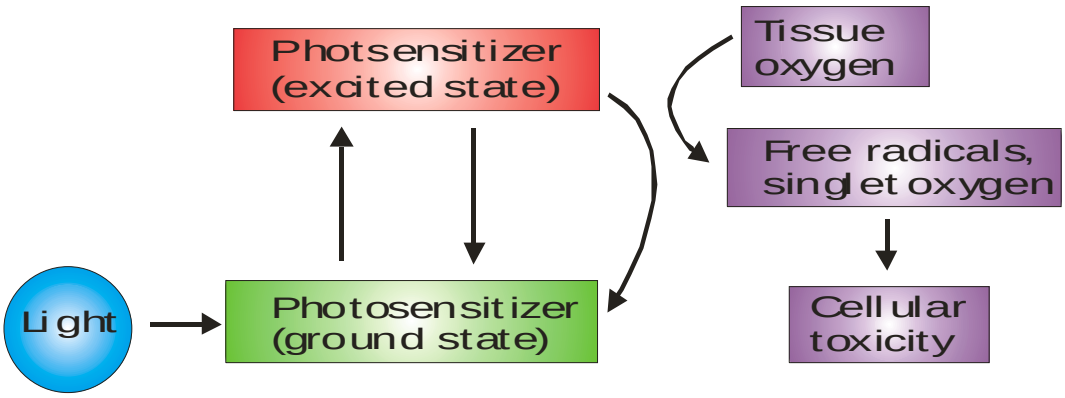

Figure 1.2: Mechanism of action of photodynamic therapy (PDT). PDT requires three elements: light, a photosensitizer and oxygen. When the photosensitizer is exposed to specific wavelengths of light, it becomes activated from a ground to an excited state. As it returns to the ground state, it releases energy, which is transferred to oxygen to generate reactive oxygen species (ROS), such as singlet oxygen and free radicals. These ROS mediate cellular toxicity.

The therapeutic application of PDT to patients with cancer took a long time to develop since the first experiments of Von Tappeiner and Jesionek that were carried out in 1903. In 1972, I. Diamond and colleagues postulated that the combination of the tumour-localizing and tumour-phototoxic properties of porphyrins might be

exploited to kill cancer cells [9]. A significant breakthrough occurred in 1975 when Thomas Dougherty and co-workers reported that administration of haematoporphyrin derivative (HPD) and red light completely eradicated mammary tumour growth in mice[10]. In the same year, J.F.Kelly and co-workers reported that light activation of HPD also eliminated bladder carcinoma in mice [11]. In 1976, they initiated the first trials in humans with HPD — in patients with **bladder cancer** [12]. Following the preliminary success in treating bladder and skin tumours, Y. Hayata and colleagues used PDT to treat obstructing **lung tumours**[13] and patients with **gastric carcinoma** [16]. In 1984, J.S.McCaughan and colleagues used PDT to treat patients with **oesophageal cancer**[14]. O.J. Balchum and colleagues used PDT to treat patients with lung cancer[15]. All these studies showed promising responses in early-stage patients, so PDT was recommended for patients with early stage cancers that were inoperable, due to other complications. Patients with **breast cancer** [17, 18], gynaecological tumours [19-21], **intraocular tumours**[22-25], **brain tumours [**26,27], **head** and **neck tumours [**28,29], **colorectal cancer** [30,31], cutaneous malignancies[32,33], intraperitoneal tumours [34] ,**mesothelioma** [35], cholangiocarcinoma [36] and **pancreatic cancer** [37] were subsequently treated with PDT. However, this approach has shown only limited success in further studies, due to issues related to specificity and potency of photosensitizers. Another confounding factor is that PDT has been tested largely in patients with advanced-stage diseases that were refractory to other treatments. In such cases, a local effect cannot usually significantly alter the outcome of a systemic disease. More selective and potent sensitizers have been developed, and are now under investigation in clinical trials (Table 1.1). With this new line of drugs, as well as with better localization methods and improved protocols and equipment, the efficacy of PDT might be improved [38].

The increasing interest in medicine for PDT is granted, representing an experimental tool for the detection and treatment of tumors located in the lung, esophagus, colon, peritoneum, pleura, genitourinary tract, brain, eye, and skin. Intensive clinical research ended in the approval of PDT for the management of selected malignancies in Canada, Japan, France, the Netherlands, Germany, and the United States [39].

Sensitizer	Trade name	Potential indications	Activation wavelength (nm)
HPD (partially purified), porfimer sodium	Photofrin	Cervical, endobronchial, oesophageal bladder and gastric cancers, and brain tumours	630
BPD-MA	Verteporfin	Basal-cell carcinoma	689
m-THPC	Foscan	Head and neck tumours, prostate and pancreatic tumours	652
5-ALA	Levulan	Basal-cell carcinoma, head and neck, and gynaecological tumours Diagnosis of brain, head and neck, and bladder tumours	635
5-ALA-methylesther	Metvix	Basal-cell carcinoma	375-400
5-ALA benzylesther	Benzvix	Gastrointestinal cancer	635
5-ALA hexylesther	Hexvix	Diagnosis of bladder tumours	635
SnET2	Purlytin	Cutaneous metastatic breast cancer, basal-cell carcinoma, Kaposi's sarcoma, prostate cancer	374-400
Boronated protoporphyrin	BOPP	Brain tumours	664
HPPH	Photochlor	Basal-cell carcinoma	630
Lutetium texaphyrin	Lutex	Cervical, prostate and brain tumours	665
Phthalocyanine-4	Pc4	Cutaneous/subcutaneous lesions from diverse solid tumour origins	732
Taporfin sodium	Talaporfin	Solid tumours from diverse origins	670

Table 1.1: Photosensitizers for malignant diseases under investigation in clinical trials

The main advantages of PDT over other therapies, for instance chemotherapy, include rather significant degree of selectivity of drug accumulation in the tumor tissue, the absence of systemic toxicity of the drug alone, the ability to irradiate only tumor, the possibility of treating multiple lesions simultaneously and the ability to retreat a tumor in order to improve the response.

Moreover, numerous investigations demonstrate possible practical applications of photosensitization in the different conditions, such as dermatological diseases [40], atherosclerosis [41], infectious diseases [42], rheumatoid arthritis [43], age-related macular degeneration [44], AIDS [45] and hematological diseases.

In order to examine and explain how PDT works the answer will be divided in three sections, photophysics, photochemistry and photobiology because it is a

complex matter and involves three different scientific fields that each one of them alone can not provide a full and explanatory view of the photodynamic effect.

1.2.2 Photophysics

1.2.2.1 Absorption and Fluorescence

Emission of light in the form of fluorescence often accompanies deactivation of an electronically excited species [46]. Fluorescence is defined as the radiative transition between two electronic states of the same spin multiplicity. Most organic molecules have "paired" electrons in their ground state molecular orbital configuration. The spins are balanced (e.g., $s_1 = +½$ and $s_2 = - ½$, $S = \Sigma s = 0$) and the spin multiplicity (M_s, $= 2S + 1 = 1$) is singlet. Alternatively, inversion of the spin of the excited electron results in the two unpaired electrons having the same spin orientation. The overall spin S is 1 (e.g. $s_1 = +½$ and $s_2 = + ½$), the spin multiplicity ($M_s = 2S + 1$) is 3, and a triplet state results.

Most commonly, fluorescence refers to singlet-singlet transitions, especially the transition between the lowest, or first, excited singlet state (S_1) and the ground state (S_o). Other types of less common fluorescence processes do occur, such as that from the second (S_2) excited singlet state, and the doublet-doublet fluorescence exhibited in the radiative relaxation between excited and ground state free radicals (one unpaired electron, $S = ½$ $M_s = 2S + 1 = 2$). However our study is focused on S_1-S_o fluorescence, which is by far the most common type.

The relationship between absorbance and fluorescence can be illustrated using simple potential energy diagrams (Fig.1.3) that show the relative electronic and vibrational energy levels as a function of internuclear separation in the affected bond.

The absorption process involves interaction of the molecule in the ground state with a photon to promote an electron from a lower energy to a higher energy molecular orbital. The absorbance (A) of a sample is proportional to the concentration c (in molarity M) of absorbing species in a sample of pathlength ℓ (cm) traversed by the light and is generally independent of the intensity of the excitation light, although the latter may not hold under high-intensity laser irradiation. In transparent media the pathlength is simply the thickness of the sample, but it is more complex to determine in opaque or highly scattering materials. This results in the common expression of the

Beer-Lambert law $A = \varepsilon c \ell$ Eq. (1). The molar absorption coefficient (ε in M^{-1} cm^{-1}) is the proportionality factor and its magnitude reflects the probability of the absorption of a photon of a given energy by the molecule. The absorption spectrum of a compound is constructed by plotting ε as a function of excitation wavelength.

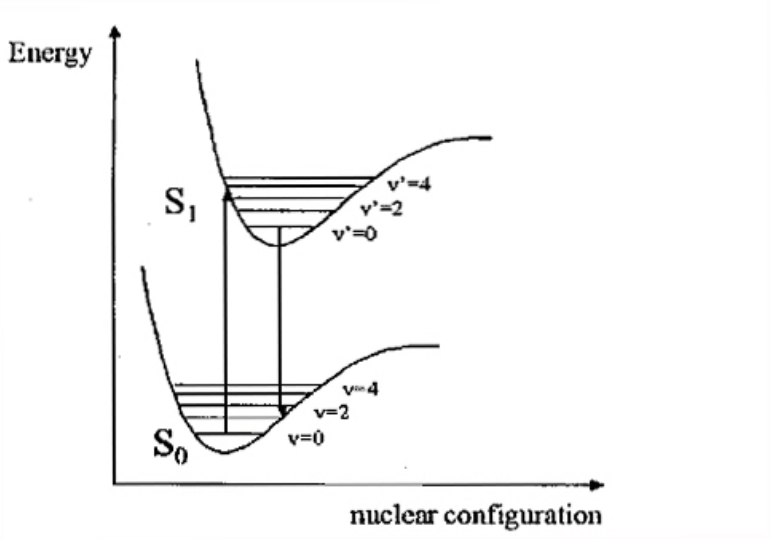

Figure 1.3: Potential energy diagram showing absorption and emission transitions between vibrational sublevels in ground and electronically excited states.

The absorption process takes place on a time scale (~10^{-15} sec) much faster than that of molecular vibration; thus, absorption occurs in a "vertical" manner, i.e., the internuclear geometry will be identical immediately before and after absorption to form the excited state. This is the *Franck-Condon* principle. In the excited state, the electron is promoted to an antibonding orbital such that the bond order is reduced, the atoms in the bond are less tightly held, and the equilibrium bond length is subsequently longer. This is shown as a displacement to the right of the excited state potential curve with respect to the ground state in Fig. 1.3. The vibrational level that is initially populated is that, where vertical overlap at the energy of the absorbed photon occurs and is generally $v' > 0$. In Fig. 1.3 the absorption is shown to the v' = 3 level of the S_1 state. The simplest fluorescence in terms of photophysics would be the exact reverse of the absorption process, emitting light of a wavelength identical to that absorbed. This is termed "resonance" fluorescence. In Fig. 1.3 this would correspond to a transition from the v' = 3 level of the S_1 state back to the $v' = 0$ level of the S_0 state. Such fluorescence can be observed from atoms or molecular gases at very low pressures but is not usually apparent for larger molecules in condensed phases such as liquids and solids. This is due to the fact that vibrational deactivation, through

intermolecular collisions, occurs more rapidly than the fluorescence emission process, with the result that fluorescence generally occurs from the lowest vibrational level (v′= 0) of the electronic excited state.

The transition that is associated with the emission of a photon is also so rapid that no change in nuclear configuration can occur during the process. The Franck-Cordon principle again dictates that the vibrational level that is initially populated in the electronic ground state will be that which shows "vertical" overlap with the v′= 0 level of the S_1 state. This would be the v = 1 level in the example shown in Fig. 1.3. Thus, the energy of the emitted photon will be significantly lower than the absorbed photon and the fluorescence is red shifted with respect to absorption.

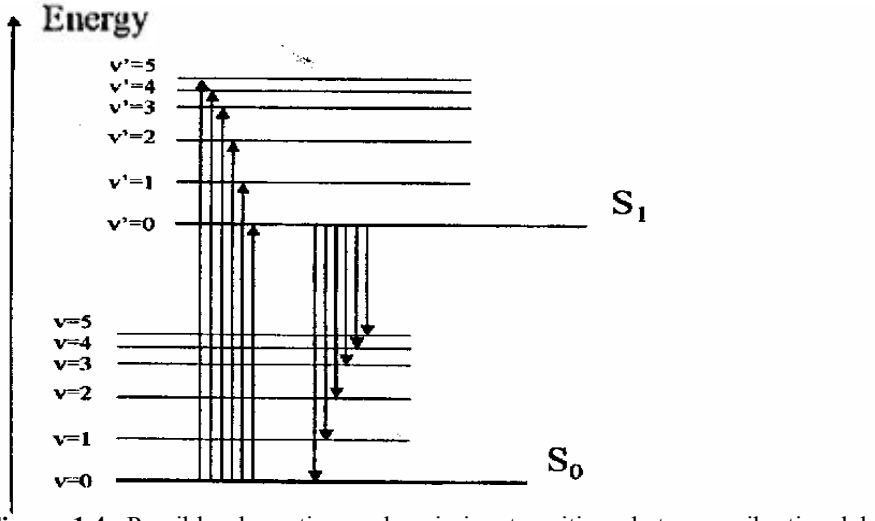

Figure 1.4: Possible absorption and emission transitions between vibrational levels in ground and excited states. Emission occurs at lower energy and is red shifted with respect to absorption bands.

Several other points should be pointed out in this diagram. The energy level spacings between adjacent vibrational levels decreases with increasing energy, and a similar spacing of vibrational levels is often seen in the ground (S_0) and excited (S_1) states. This results in the "mirror image" relationship commonly observed between absorption and emission spectra. This is shown in more detail in Fig.1.4. The electronic excited state energy of S_1 can be obtained from the transition between the v= 0 levels in both states -S_0 and S_1- and is termed the 0-0 transition. Due to slight changes in internuclear distances at equilibrium in both states, the 0-0 transition energy ($E_{0\text{-}0}$) is often not identical in absorbance and fluorescence but can be estimated from the wavelength at which these two spectra overlap. This difference is also termed the Stokes shift.

1.2.2.2 Deactivation of the S_1 state

Fluorescence is only one of the possible mechanisms by which an excited molecule can undergo relaxation to the ground state. The Jablonski diagram in Fig. 1.5 shows that there are a number of potential transitions open to the S_1 state after population by excitation and internal conversion from upper states. Here the formalism of a solid arrow depicting a radiative transition and a wavy arrow depicting a nonradiative transition has been followed. The molecule can undergo both nonradiative -internal conversion, (i.c.)- and radiative (fluorescence) relaxation to the ground state (S_o) or nonradiative transition -intersystem crossing (i.s.c.)- to the lowest excited triplet state (T_1).

1.2.2.3 Internal Conversion

The energy separation between consecutive singlet levels (S_o, S_1, S_2, ... S_n) tends to decrease with increasing electronic energy. Generally, the rate of radiationless transition from one state to another is inversely proportional to the energy separation (the "energy gap law") and nonradiative transitions between upper states (S_n to S_{n-1},) occur rapidly to populate the lowest excited state, S_1. These types of transitions are denoted *internal conversion* as they occur between states of the same

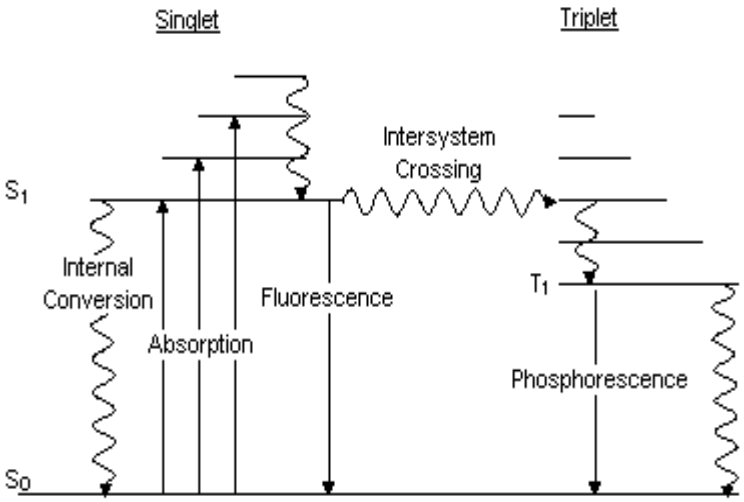

Figure 1.5: Modified Jablonski diagram showing radiative (soIid arrows) and nonradiative (wavy arrows) transitions between ground state (S_0) and excited singlet (S_2, S_1,) and triplet (T_1,) states. i.c., internal conversion; i.s.c., intersystem crossing.

spin multiplicity. For this reason, the fluorescence emission spectrum is typically independent of the excitation wavelength, e.g., a molecule that is directly excited into

the S_3 state by absorption of a higher energy photon will relax by internal conversion to the S_1 state before emission can occur. This is an example of Kasha's generalization that radiative processes or excited state reactions arise from the lowest electronically excited states (S_1 or T_1). The energy gap between S_1 and S_0 is considerably larger than between other adjacent states. Thus the S_1 state lifetime is much longer than the higher singlet states and radiative emission can effectively compete with nonradiative processes from this level.

1.2.2.4 Intersystem Crossing

Selection rules dictate that transitions between states of like spin multiplicity (e.g., singlet-singlet) are allowed and will be much more probable than transitions between states of different multiplicity (e.g., singlet-triplet). *Intersystem crossing* (i.s.c.) is defined as a nonradiative transition between states of different multiplicity and occurs via inversion of the spin of the excited electron resulting in the two unpaired electrons having the same spin orientation. The overall spin S is 1 and the spin multiplicity is 3 to give a triplet state. Although transitions between states of different multiplicity are formally forbidden, intersystem crossing occurs via other mechanisms. These include spin-orbit and vibronic coupling mechanisms that lessen the "pure" character of the initial and final states. One additional possibility is that photochemical reaction, rather than relaxation, may occur from the S_1 state. Thus, the efficiency of the fluorescence pathway depends on the value of the rate constant for fluorescence emission in relation to the rate constants for the other possible processes from S_1. Direct absorption into the triplet state from the ground state singlet (S_o) is spin forbidden but the triplet excited state can be accessed indirectly through intersystem crossing from S_1 to T_1. Intersystem crossing is also formally spin forbidden; the excited states in large organic molecules are not well described in terms of pure spin multiplicities but can be described in terms of mixed singlet and triplet state character. This lowers the importance of the spin selection rule. The reverse intersystem crossing (isc') from T_1 to S_1 is also formally spin forbidden. The opposite transition from the excited triplet to the ground singlet is called *phosphorescence* and is also spin forbidden, hence it occurs very slowly with a radiative lifetime in the order of seconds or longer.

1.2.2 Photochemistry

The group of photochemical interactions stems from empirical observations that light can induce chemical effects and reactions within macromolecules or tissues[1]. One of the most popular examples was created by the evolution itself: the energy release due to photosynthesis. In the field of medical laser physics, photochemical interaction mechanisms play a significant role during *photodynamic therapy (PDT).* Frequently, *biostimulation* is also attributed to photochemical interactions, although this is not scientifically ascertained.

Photochemical interactions take place at very low power densities (typically 1 W/cm^2) and long exposure times ranging from seconds to continuous wave. Careful selection of laser parameters yields a radiation distribution inside the tissue that is determined by scattering. In most cases, wavelengths in the visible range are used which correspond to the photosensitizers absorption maximum. The penetration depth of visible light into the tissue is small and this is a drawback if deeper tissue structures are to be reached. UV radiation is not recommended because of its mutagenic effect on DNA.

During PDT, spectrally adapted chromophores are injected into the body. Monochromatic irradiation may then trigger selective photochemical reactions, resulting in certain biological transformations. A chromophore compound which is capable of causing light-induced reactions in other non-absorbing molecules is called a *photosensitizer.* After resonant excitation by laser irradiation, the photosensitizer performs several simultaneous or sequential decays which result in intramolecular transfer reactions. At the end of these diverse reaction channels, highly cytotoxic reactants are released causing an irreversible oxidation of essential cell structures. Thus, the main idea of photochemical treatment is to use a chromophore receptor acting as a catalyst. Its excited states are able to store energy transferred from resonant absorption, and their deactivation leads to toxic compounds leaving the photosensitizer in its original state. Therefore, this type of interaction is also called *photosensitized oxidation.*

Most photosensitizers belong to the group of organic dyes. Their electronic states are characterized by singlet states (total electron spin momentum s = 0) and triplet states *(s* =1). Furthermore, each electronic state is subdivided into a band of vibrational states. Intersystem crossing is permitted but is associated with an increased

lifetime. Potential reaction kinetics of the photosensitizer are listed in Table 1.2. The reaction types can be characterized by either *excitation, decays, Type I* or *Type II reactions,* and *carotenoid protection.*

Excitation	
• Singlet state absorption	$^*S + h\nu \Rightarrow {}^1S^*$
Decays	
• Radiative Decays singlet decay	$^1S^* \Rightarrow {}^1S + h\nu$ (fluorescence)
• Non-radiative singlet decay	$^1S^* \Rightarrow {}^1S$
• Intersystem crossing	$^1S^* \Rightarrow {}^3S^*$ (or T_1)
• Radiative triplet decay	$^3S^* \Rightarrow {}^1S + h\nu$ (phosphorescence)
• Non-radiative triplet decay	$^3S^* \Rightarrow {}^1S$
Type I reactions	
• Hydrogen transfer	$^3S^* + RH \Rightarrow SH^\bullet + R^\bullet$
• Electron transfer	$^3S^* + RH \Rightarrow S^{\bullet -} + RH^{\bullet +}$
• Formation of hydrogen dioxide	$SH^\bullet + {}^3O_2 \Rightarrow {}^1S + HO_2^\bullet$
• Formation of superoxide anion	$S^{\bullet -} + {}^3O_2 \Rightarrow {}^1S + O_2^{\bullet -}$
Type II reactions	
• Intramolecular exchange	$^3S^* + {}^3O_2 \Rightarrow {}^1S + {}^1O_2^*$
• Cellular oxidation	$^1O_2^* + Cell \Rightarrow Cell_{ox}$
Carotenoid protection	
• Singlet oxygen extinction	$^1O_2^* + {}^1CAR \Rightarrow {}^3O_2 + {}^3CAR^*$
• Deactivation	$^3CAR^* \Rightarrow {}^1CAR + heat$

Table 1.2: Kinetics of photosensitization (S: photosensitizer, RH: substrate with H-bond, CAR: carotenoid, the triplet state is denoted as $^3S^*$) [1].

After the absorption of laser photons, the photosensitizer is first transferred from its ground state to the extremely unstable excited singlet state $^1S^*$ with a half life ranging from 10^{-6} to10^{-9} seconds. Then, three potential decay channels are available: non-radiative and radiative singlet decay to the singlet ground state, and intersystem crossing to an excited triplet state. Usually, the singlet excited photosensitizer either decays back to the ground state, resulting in the fluorescence (~10^{-9} s) or undergoes intersystem crossing to the longer lived (10^{-3} - 10 second) triplet excited state. Tumor destruction is most efficient using compounds with a long tripled half-life and a high quantum yield for the triplet excited state. The interaction of the triplet sensitizer with surrounding molecules results in two types of photo-oxidative reaction which are called *Type I* and *Type II* reactions (Table 1.2).

1.2.2.1 Type I and Type II reactions

During Type I reactions, the triplet state ($^3S^*$ or T_1) interacts with a target molecule, other than oxygen, through proton transfer or electron transfer, resulting in the release of free neutral or ionized radicals ($R^\bullet$, $RH^{\bullet+}$). Further reaction with triplet oxygen may lead to the formation of hydrogen dioxide ($HO_2^\bullet$) or superoxide anions ($O_2^{\bullet -}$) which initiate free radical chain reactions.

In Type II reactions, the triplet state of the photosensitizer directly interacts with molecular triplet oxygen $^3O_2$ which then is transferred to an excited singlet state $^1O_2$*. During this energy transfer process, the electronic spins are flipped in the following manner:

↑↑ ↑↑ ↑↓ ↑↓

$^3S^* + {}^3O_2 \Rightarrow {}^1S + {}^1O_2^*$

Singlet oxygen is short lived ($^1O_2$, lifetimes 4×10^{-6} s in water, $50 - 100 \times 10^{-6}$ s in lipid, $0{,}04 \times 10^{-6}$ s in cellular environment) and a highly reactive, oxidative species. The result is the oxidization of cells which leads to necrosis or apoptosis which are the natural pathways of cell death. The *in situ* generation of singlet oxygen via type II pathway appears to play the central role in photodynamic cytotoxicity because of the highly efficient interaction of the $^1O_2$ species with different biomolecules. For instance, singlet oxygen was identified as the toxic agent in photoactivation of tumor cells. To avoid additional oxidation of healthy cells, carotin is injected after laser exposure which then converts the toxic singlet oxygen to harmless triplet oxygen.

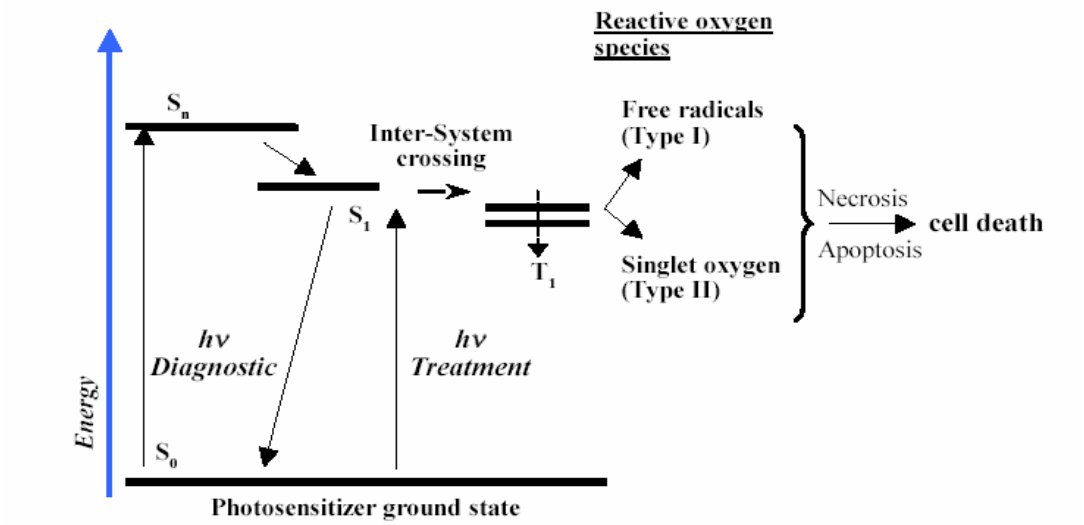

Figure 1.6: Jablonski's energy level diagram showing the sensitizer's pathway to forming reactive oxygen species which lead to cell death

Which mechanism is favored mainly depends on the concentration of available triplet oxygen and appropriate target molecules. Type I and Type II reactions may occur simultaneously and the ratio between the two processes is highly influenced by sensitizer, substrate and oxygen concentration, as well as the binding of sensitizer to substrate. In general high substrate and low oxygen concentrations lead to Type I reactions while low substrate and high oxygen concentrations lead to Type II reactions [5]. There is much indirect evidence to suggest that singlet oxygen is the major damaging species in PDT, but direct measurement of singlet oxygen production in complex biological systems appears to be extremely difficult. Most indirect methods such as the use of chemical quenchers of reactive intermediates or D_2O (which prolongs the singlet oxygen lifetime and so can increase photosensitization) are not entirely specific for singlet oxygen. In particular, indications are that superoxide ion (O_2^-) may be involved in some aspects of PDT damage.

From the above it is evident that PDT effects should be oxygen-dependent. In Fig. 1.6 a short summary of the sensitizer's pathway in PDT is illustrated. After excitation, follows intersystem crossing to a triplet excited state which in turn triggers a number of chemical reactions leading to cell death.

1.2.3 Photobiology

After examining the photophysics and the photochemistry of the irradiation of the photosensitizer, the result of the exited photosensitizer to the target cell will be examined. Keeping in mind that the endpoint is the death of tumor cells, the uptake and localization of the photosensitizer will be discussed, and how this is important for the photodynamic therapy and which are the pathways leading to cell death.

1.2.3.1 The cell

The elegant scientific exploration of sub-cellular molecular anatomy of the last decades have reinforced the cell concept as the smallest integrating unit in biology. The cell is a pseudo-intelligent computer that receives, screens, changes, reacts to and adapts to a host of environmental signals, all of this activity apparently designed, through evolution, for cell survival and host survival. As such, there are essential cellular components (the plasma membrane, mitochondria, lysosomes, endoplasmic reticulum, the nucleus, and other cellular organelles) each can be considered a

'vulnerable site' whose destruction or malfunction threatens the function of the cellular unit. Mitochondria, lysosomes, plasma membrane, endoplasmic reticulum have been evaluated as potential PDT targets.

1.2.3.2 Uptake and localization of photosensitizers in the tumor cells

An important factor in photodynamic therapy is the ability of the photosensitizer to identify the target that is the cancer cell and this parameter is called selectivity. An ideal photosensitizer should not attack healthy cells, though this is not always true. Since the target has been selected the photosensitizer tends to accumulate in various sites of the cell. The incubation parameters and mode of delivery as well as the chemical nature of the photosensitiser can all influence subcellular localisation, creating a number of potential targets for photodamage [5].

What are the factors that determine specific localization of photosensitizer in the cells? It's generally accepted, that lipophilicity of the sensitizer and aggregation degree mostly determine the accumulating efficiency and localization specificity in the tumor cells [5]. After intravenous (i. v.) administration of hydrophobic sensitizers, the compounds are, in general, strongly bound to lipoproteins (high density lipoproteins (HDLs) and low density lipoproteins (LDLs)), distributed within the blood system and transported to the malignant tissue with a distinct selectivity. It is widely accepted today that the tumor selectivity increases to some extend with the lipophilic character of the sensitizing agent. The preferred accumulation of lipophilic sensitizers, within tumor tissues is in accordance with the observation that neoplastic cells express a particularly large number of LDL membrane receptors. Following receptor-mediated endocytosis, the sensitizer molecules preferentially accumulate in the lipophylic compartments of tumor cells, including plasma, mitochondrial, endoplasmic reticulum, nuclear and lysosomal membranes [47].

However, it should be clearly emphasized that other factors, such as lower tumor pH, also correlate with an enhanced uptake of photosensitizers [47]. The point is that low pH value of most tumors is related to their poor oxygen supply and high glycolytic activity.

After i.v. injection of hydrophilic photosensitizers, the drugs are largely carried by albumin and other serum proteins. Microscopic measurements reveal a preferred accumulation of these sensitizers within the interstitial space and the vascular stroma of the tumor tissue. Due to their hydrophilic character, the tendency

to diffuse across the plasma membrane into the cytoplasm is small. As outlined above, the site of the primary localization of the sensitizer strongly depends on the lipophilic or hydrophilic character of the drug considered. In general, hydrophobic drugs attack the tumor cells mainly by direct interactions. In contrast, water-soluble sensitizers kill hyperproliferating cells indirectly by damaging blood vessels and interrupting the supply of oxygen and other essential nutrients.

1.2.3.3 PDT induced cell damage

The singlet oxygen, produced through the photochemical reactions, is very reactive. It is characterized by a short lifetime (~0,04μs) and free pathlength before reacting with another molecule. Because of limited migration of $^1O_2$ from the site of formation, photosensitization damage to the cell or tissue is closely related to the localization of the sensitizer.

Hydrophobic (lipophilic) compounds preferentially bind membranes and will target structures such as the plasma membrane, mitochondria, lysosomes, endoplasmic reticulum and the nucleus [5]. Oxidative degradation of membrane lipids can cause the loss of membrane integrity, resulting in impaired membrane transport mechanisms, increased permeability and rupturing of membranes. Cross-linking of membrane associated polypeptides may result in the inactivation of enzymes, receptors and ion channels.

In practice, sensitizers tend not to accumulate in cell nuclei. So, photosensitization has generally a low potential of causing DNA damage and consequently mutations and carcinogenesis. PDT damage of plasma membrane can be observed within few minutes after light exposure. This type of damage is manifested as swelling and blebbing, shedding of vesicles containing plasma membrane marker enzymes, cytosolic and lysosomal enzymes, reduction active transport, depolarization of plasma membrane, inhibition of activities of plasma membrane enzymes such as Na^+ K^+ – adenosine triphosphatase (ATPase), a rise in Ca^{2+}, up- and down-regulation of surface antigens, etc[47].

Cellular membranes, including plasma, mitochondrial and sometimes nuclear membranes are severely damaged by oxidation of unsaturated fatty acid residues and of cholesterol. The released lysosomal enzymes, especially those of neutral proteinases, damage tumor. The examination of the mechanism of cell lysis indicates that oxidative damage of membrane transport proteins induces a rapid derangement of

ionic homeostasis of Na^+, K^+ , Ca^{2+}, etc., while membrane integrity still retained at this time. The release of all these physiologically active ions has been associated with an immediate induction of acute inflammatory reactions.

1.2.3.4 Cell death pathways induced after photosensitization

With increasing recognition of photosensitization as an efficacious treatment, there is also increased interest in elucidating the mechanisms by which it causes the death in the cells and tissue – in order to enhance this destructive action on target tissue and optimize therapeutic strategies.

Two distinct modes of cell death after photosensitization – *apoptosis* and *necrosis* – can be recognized based on differences in the morphological, biochemical and molecular changes of dying cell.

Apoptosis can be initiated by a wide variety of intracellular and extracellular stimuli and constitutes a mechanism for the removal of unnecessary, aged or damaged cells [48]. The most common feature of apoptosis is active participation of the cell in its self-annihilation. Cells undergoing apoptosis exhibit a quite distinct and profound set of coordinated structural changes that are characteristic of this process and independent from the death signal that originally induced them. The dying cell typically shrinks, widespread membrane blebbing occurs, followed by chromatin condensation and genomic DNA fragmentation. The cell further disassembles into membrane-enclosed vesicles called “apoptotic bodies” that are rapidly and cleanly ingested by neighboring cells and phagocytes. On the other hand, even during advanced stages of apoptosis, the structural integrity and the transport function of the plasma membrane are preserved. Also preserved and functionally active are the mitochondria and lysosomes. So, apoptosis looks like “black hole” of cell death: it draws everything inward and nothing escapes its biochemical event horizon. Therefore, during apoptosis, the cellular content is never accessible to the immune system minimizing the occurrence of inflammatory reactions.

This is in contrast to death by necrosis that occurs in response to chemical and physical insults [48]. This process is characterized by swelling of the entire cytoplasm and organelles which causes the plasma membrane to burst. Since the cellular content is spilled extracellularly, necrotic cell death evokes invariably an inflammatory response.

Early mechanistic studies of apoptosis, performed on cultured mammalian cells, have proved that each cell has the inherent capacity to trigger its own death when it is challenged by an appropriate signal [49]. Malignant cells often have an impaired ability to undergo apoptosis, so a selective triggering of this type of cell death has become an attractive therapeutic objective.

1.2.3.5 Apoptosis versus necrosis

Evidence for both apoptotic and necrotic regions has been found in tumor biopsies after PDT [5]. However, it remains to be determined how and to what extent the induction of these two types of cell death contributes to the mechanism of PDT-induced tumor ablation. This issue is further complicated by the fact that *in vivo* responses to PDT appear to be substantially influenced by a number of factors which include: the photosensitizer used and the way it is delivered to the tumor cells (i.e. bound to plasma lipoproteins or endocytosed), the irradiation protocol, the type of tumor and its level of oxygenation. Moreover, PDT induces a strong inflammatory response in the treated tissue secondary to the release of cytokines and other inflammatory mediators, which may contribute to the induction of apoptosis in both malignant and other host cells.

Several studies using cell lines as model systems have pointed out that crucial factors in determining the type of cell death, e.g. apoptosis or necrosis, following PDT are the subcellular localization of the photosensitizer and the light dose applied to activate it locally. These factors are particularly important since they determine the primary intracellular site and the intensity of the photodamage. Indeed, the close proximity of the photosensitizer and its target seems particularly required in photosensitization processes involving the formation of $^1O_2$ (Type II reactions), since this highly reactive oxidant molecule can diffuse only 20 nm and has a very short lifetime (<0.04 μs) [50].

There is strong evidence indicating that photoactive compounds localizing to the mitochondria promptly promote the apoptotic program, while PDT with compounds that target either the plasma membrane or lysosomes, can either delay or block the apoptotic program, predisposing the cell to necrosis [51,52].

1.3 PDT in Autologous Bone Marrow Transplantation

Bone marrow transplantation (BMT) is a therapeutic modality that increases the survival rates for children and adults with poor prognosis malignancies [53,54]. According to the basic principle of this treatment, transplant is taken from the patient while in remission and in the case of disease recurrence the autologous graft is administered to the patient. Autologous BMT obviates the need for a matched sibling donor and displays a smaller percentage of complications, such as acute or chronic graft versus host disease (GvHD), organ damage and fatal viral infections [55,56]. On the other hand, relapse rates are higher than those following allogeneic BMT [54,57]. Presumably, this is partly due to the existence of occult tumor cells in the bone marrow of patients, otherwise considered to have achieved remission. Thus, purging strategies have been developed aiming at the ex vivo removal or impairment of cancer cells [57]. Various physical, immunological and pharmacological approaches are currently used [58-61].

During the last decade clinical research has focused towards purging of malignant cells from the BM with the use of PDT. Photosensitizing dyes such as hematoporphyrin and merocyanine 540 (MC 540) with ultraviolet or visible light irradiation have been found to exert a cytotoxic effect on malignant hemopoietic cells [62-64], suggesting that these agents could be used for BM purging.

Specifically MC 540 has been found that stains living excitable cells [65]. It selectively accumulates in leukemic cells in cell sites as the cell membrane, mitochondria membranes, endoplasmic reticulum and the nuclei membrane. It has been reported that MC 540 binds with non saturated phospholipids of the outer lipid bilayer [66]. Other studies have shown that MC 540 selectively binds to sections of lipids bilayer which are cholesterol free and exhibit arrangement disorders [68].

PDT purging of autologous grafts seems to be a very promising technique. The selectivity of the sensitizers for malignant cells offers an advantage over other techniques.

2. *Hypericum Perforatum L* and Hypericin

2.1 *Hypericum perforatum* L

Hypericum perforatum L (St. John's wort) is a yellow-flowering, rhizomatous, perennial herb indigenous to Europe, which has been introduced to the Americas and grows wild in many meadows. The name comes from the fact that it traditionally flowers by and is harvested on St John's day; all above-ground parts are cut and dried for later use in the form of herbal tea, which has long been enjoyed both for its pleasant (though somewhat bitter) taste and for its medicinal properties.

Hypericum perforatum is a herb which has been used for centuries in the treatment of burns, bruises, swelling, inflammation, and anxiety, as well as bacterial and viral infections. Hypericum was prescribed as medicine by Hippocrates himself. The use of its top flowering parts was originally documented by ancient Greek medical herbalists Hippocrates, Theophrastus, and Dioscorides. Its top flowering parts contain a significant amount of *hypericin*. The scientific discovery of hypericin and it's characterization go back to the search for the constituents responsible for hypericism, a skin photosensitivity sometimes seen in cattle ingesting large amounts of *Hypericum* plants growing on pastures [68]. Hypericin was found in 27 out of 36 evaluated *Hypericum* species [69] and therefore seems to be an important secondary metabolite of this plant genus.

Figure 2.1: Photos and sketches of the Hypericum Perforatum flower.

The function of hypericins in *Hypericum* species is not very well known. They could function as deterrent allochemicals to defend the host plant against insects and other pests, since only very few insects have evolved behavioral, physical, or biochemical adaptations which allow them to feed with impunity on plants containing hypericins [68].

Actually, not hypericin itself, but mainly the proto-forms of hypericin and its congener pseudohypericin (i.e. protohypericin, protopseudohypericin) are present as dark colored granules in minute dark glands located on the stem, leaves, sepals, petals, stamens and ovules of fresh *H. perforatum* plants. These structures represent partially cyclic precursors, which upon irradiation with visible light, convert very efficiently into their naphthodianthrone (also called phenanthroperylenequinone) analogues hypericin and its congener pseudohypericin. Investigations on the photoactivity of these proto-forms revealed that they intrinsically exhibit a drastically lower, if any, photoactivity as compared to their naphthodianthrone counterparts [70]. These data suggest that the plant protects itself from photodependent autodestruction by keeping high protonaphthodianthrone/naphthodianthrone ratios. However, another view often put forward to explain the lack of activity of hypericins present in the plant is that the compounds are stored in impermeable pigment granules/vesicles, and therefore are not accessible to plant tissues unless damaged.

Hypericum plants have been of scientific interest for many years due to their widespread use in folk medicine for a range of purposes. Today, *Hypericum* extract is still widely used for the treatment of mild and moderate depression. The daily dose is about 500 mg extract corresponding to a total dose of 1–2 mg of hypericins. These doses of hypericin given orally do not provoke skin phototoxicity [71]. Several clinical studies demonstrate that St. John's wort is as effective as conventional synthetic antidepressants [72]. Surprisingly, recent evidence indicates that it is not hypericin but hyperforin that is responsible for much of the antidepressant activity of the herb [73].

2.2 Hypericin

2.2.1 Physical chemical and biological properties

Hypericin, is a polycyclic dianthraquinone isolated from *Hypericum Perforatum*. Its chemical formula is $C_{30}H_{16}O_8$ and its chemical name 4,5,7,4',5',7'-Hexahydroxy-2,2'-dimethylnaphthodianthrone. Its molecular weight is 504.45. In Fig. 2.2 is illustrated its two dimensional structure and as it is in its side on position. Hypericin is soluble in DMSO, ethanol, methanol, water, pyridin, acetonitril.

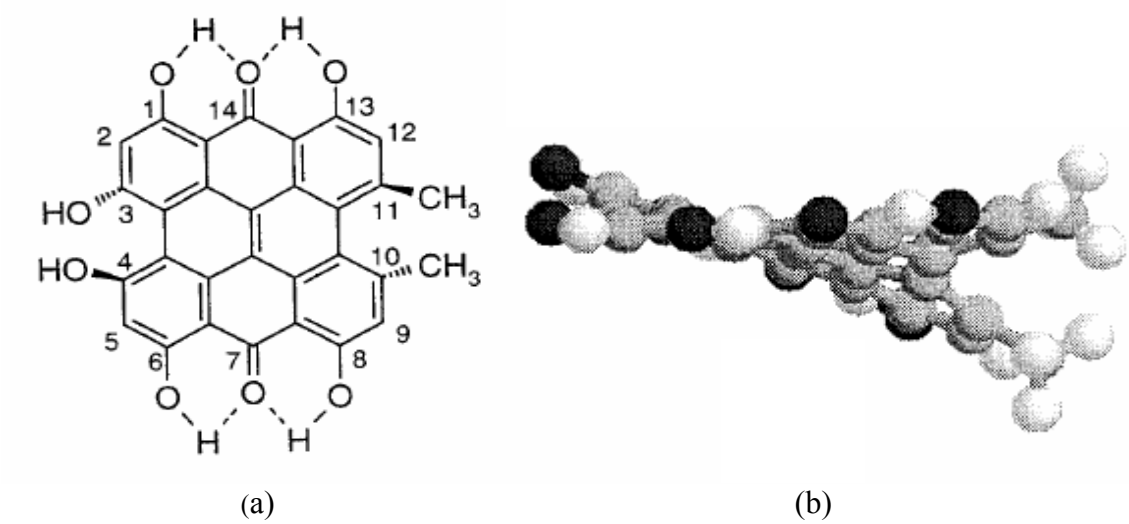

(a) (b)

Figure 2.2: a) Two-dimensional structure of hypericin and b) HY as seen in its side-on position.

Hypericin exhibits bright fluorescence, potent photosensitizing properties with a high singlet oxygen quantum yield [74,75] and minimal dark toxicity [76], characteristics that are all fundamental for the biological and clinical applications of this photosensitizer. The optical characteristics of hypericin depend on the solvent but it is documented that it absorbs in the visible. It has a maximum absorption around 590 nm (Fig. 2.3) when dissolved in DMSO (dimethyl sulfoxide), which is the most recommended solvent and maximum fluorescence around 600nm.

The discovery of the in vitro and in vivo antiviral activity of hypericin generated an enormous interest in this compound, mainly to evaluate its potential in the treatment of AIDS. Although the antiretroviral activity of hypericin has been demonstrated in vitro and in animal models [77-81], some recent clinical trials could not confirm these effects even when larger doses of hypericin were administered [82]. However, more in vivo

studies are warranted in order to fully understand the multiple antiviral activities of hypericin. Of interest, hypericin is nowadays under investigation as a photodependent blood sterilizer [83].

In the last decade, several in vitro studies have revealed the multifaceted photodynamic activity of hypericin. It has been shown that upon light activation hypericin inhibits protein kinase C (PKC) and other growth factor stimulated protein kinases [84–86], induces peroxidation of membrane lipids [87,88], increases superoxide dismutase activity and decreases cellular gluthatione levels [87,89], impairs mitochondrial functions [88,89], cross-links the molten globule form of acetylcholinesterase, but not the native protein [90], and causes photooxidation of lens α-crystallin [91].

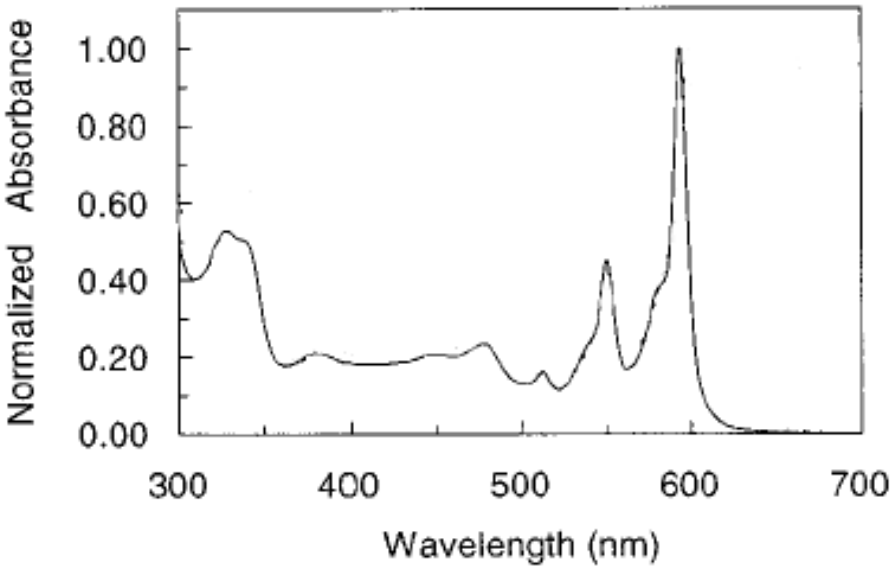

Figure 2.3: Absorption spectrum of hypericin

In view of the photobiological relevancy, excited state properties of hypericin have been widely studied, in order to understand the role of light on its biological activity.[92-95] Nevertheless its mechanism and site of action at the cellular level still remain unclear, and various photophysical processes have been proposed to account for its photosensitizing properties:

(i) An oxygen-dependent mechanism has first been reported [96] since irradiation of hypericin with visible light leads to the production of singlet oxygen ($^1O_2$). The postulation of the important role of singlet oxygen in Hypericin's activity was based on

its high quantum yield of formation, Φ_Δ [97-99]. The quantum yield, in ethanol for example, was reported to be 0.73, almost equal to its triplet yield. However, later this value was found to be considerably smaller (in ethanol, Φ_Δ =0.32) [100]. Reported values of Φ_Δ in other organic solvents are also lower than the original report and range from 0.17 in acetone to 0.37 in methanol [100], while that of liposome-bound hypericin has been reported as 0.35 [101] and 0.43 [102] The formation of singlet oxygen as a primary oxidizer occurs via energy transfer from the excited triplet state of hypericin towards the ground state of molecular oxygen.[103,104] However, although this type II oxygen-dependent photosensitization mechanism is the most widely reported, other observations lead to establish that oxygen is not always required for virucidal[105] and antitumoral[106] activities of hypericin.

(ii) Others studies suggest that the phototoxic activity may be due to complex mechanisms involving the superoxide anion and hypericinium ion, semiquinones and hydroxyl radicals implicating a type I radical mechanism.[107-112]

(iii) Finally, it is suggested that an alternative origin for the photoinduced virucidal activity of hypericin may involve its ability to produce a photogenerated pH drop[94,113, 114] through an intramolecular proton transfer in the excited state of the molecule, which is likely to precede solvent acidification.

Actually, a rapid (6-12 ps) proton transfer has been observed in the excited state of hypericin from one hydroxyl group to the adjacent carbonyl group,[94] and a light-induced pH drop has been observed inside phosphatidylcholine vesicles during steady state illumination of a hypericin containing solution.[115] These authors suggest that a deprotonation process might result from hypericin excited triplet state, without excluding the possibility that the singlet excited state could provide protons as well.

Also interesting is the fact that during the time course of intracellular acidification, (pH decrease) a decrease of the overall fluorescence emission of hypericin has been observed [114]. To interpret this, one has to recall previous studies showing that protonation of one or both of the carbonyl groups of hypericin, achieved through an intramolecular proton transfer in its excited state, is required to promote its fluorescence emission.[94] Consequently, a non-reversible proton release from the excited state of the chromophore to the bulk progressively precludes the fluorescence emission and can be

considered as the first step of formation of a non fluorescent photoproduct of the molecule.

Intracellular pH changes, as large as 0.4 pH unit as reported in [113], can be considered as a possible mechanism responsible for the photosensitizing properties of hypericin. Several investigations have demonstrated the critical role of pH in the replication cycle of certain enveloped viruses by regulating uncoating [116]. Intracelullar acidification down to 6.8 has also been reported to precede apoptosis in various cell lines[117-119] and can be involved in the hypericin induced apoptosis observed in glioma cell lines.[120] This intracellular acidification can also be directly involved in the photoinduced antitumoral activity of hypericin which has been previously observed on EMT6 mouse mammary carcinoma[104] or human glioma[120] cell lines. This assumption is supported by other studies on same EMT6 and glioma cell lines, which have shown that a decrease of intracellular pH constitutes a potent alternative for antitumor therapy [121].

Finally another important feature is that hypericin is a very photostable compound compared to other photosensitizers including Photofrin II and mTHPC [122]. For example the BD_{50} - the fluence required for the 50% bleaching of the dye - was found 100 J/cm^2 in a cellular environment for hypericin the same time that for PhotofrinII was 2 J/cm^2 and for mTHPC was 0.2 J/cm^2. This photostability could explain its high singlet oxygen quantum yield. Also this photostability could be very useful for prolonged irradiation on tumor and cancer cells.

Hypericin is not only a potent photosensitizer but also a fluorescent compound; for instance, in organic solvents the compound forms red solutions (λ_{abs}: 548, 591 nm in EtOH) that exhibit bright red fluorescence (λ_{em}: 594, 642 nm) [93]. For this reason Hypericin is used as a diagnostic tool for the fluorescence detection of flat neoplastic lesions in urine bladders [123].

2.2.2 Hypericin's subcellular localization and potential cellular targets

Hypericin features a pronounced acidity of the *bay* region hydroxyl groups with the result that hypericin is present as a monobasic salt in physiological conditions [77]. These hypericin salts are taken up by cellular lipid membrane structures and therefore

behave in all respects as lipophilic ion pairs. Not surprisingly, the pronounced hydrophobic character allows hypericin to localize in a time-dependent manner (2–4 h) in cytoplasmic membranes [104].

Cellular localization studies in cancer cell lines with different fluorescent organelle markers [124-126] revealed that this compound accumulates particularly in the membranes of the endoplasmic reticulum and Golgi complex. The cellular distribution of hypericin also appears to be influenced by the cell type, since in colon carcinoma Caco-2 cells hypericin preferentially accumulates not only in plasma but also in nuclear membranes [127]. In addition, the photodynamic killing efficacy of hypericin, which can be directly correlated to the intracellular accumulation of the drug, is dependent on the cell type [124].

It has been suggested that the cellular uptake of hypericin is determined by diffusion and solubility and does neither require an energy-dependent transport process nor the binding to specific receptors [104]. However, this view has been debated since ammonium chloride as well as brefeldin A, compounds known to perturb endocytotic events and membrane cycling from the endoplasmic reticulum to the Golgi, respectively, dramatically changed the intracellular distribution of hypericin [125]. Therefore, it appears that membrane-associated intracellular translocation processes may critically affect the final subcellular distribution of hypericin.

Due to its subcellular localization, it has been postulated that membranes are the principal cellular targets of hypericin [87,88,104,125,126], probably by means of ROS photogenerated locally or in the close vicinity of the cellular target. Investigations using isolated organelles or intact cells [126-128] have indicated that hypericin can affect critical mitochondrial functions in a photodependent manner. Hypericin photosensitization of isolated mitochondria led to inhibition of mitochondrial succinoxidase [104], a decrease in the respiratory control ratio and a drop in the mitochondrial membrane potential [127]. Hypericin also impaired mitochondrial functions in EMT6 mouse mammary carcinoma cells since total cellular ATP levels and cellular respiration were depressed after photosensitization [128]. In human glioma cells, hypericin induced a photogenerated intracellular pH drop leading to a release and inhibition of mitochondria outer membrane-bound hexokinase, with a concomitant

decrease in glucose phosphorylation and ATP content, and inhibition of cell proliferation [126]. Collectively, these data support the hypothesis that even though hypericin does not accumulate in mitochondria, these organelles are primary cellular sites of hypericin photodynamic action and indicate that the reported impairments in mitochondria bioenergetics are crucially involved in hypericin photocytotoxicity.

3. Material & Methods and Experimental setups

3.1 Materials and Methods

3.1.1 HL-60 cells

In order to determine any cytotoxic effect of *Hypericum perforatum* L (HP) extract during photodynamic treatment (PDT) HL-60 cell line was used. It is a promyelocytic cell line that derived from a patient with acute promyelocytic leukaemia. Cells were maintained in RPMI-1640 supplemented with 10% fetal calf serum (FCS), 1% penicillin-streptomycin, 1% L-glutamine and 1% sodium pyruvate at 37° C (all from Gibco, Life Technologies BRL) at 37^{o}C in 5% CO_2 fully humidified atmosphere. Under these conditions cells are reproduced logarithmically and their viability is over 95%.

Before the irradiation the cells were adjusted at 3×10^{6} cells/ml and were dispersed in 35mm Petri dishes at 1ml /dish. After irradiation every sample was washed twice by centrifugation at 1600 rounds per minute (rpm) with RPMI-1640. Washing is necessary in order to remove the photosensitizer from the sample as any remaining photosensitizer might exhibit dark toxicity.

Following washing cells were resuspended in RPMI and placed in six well plates. The viability was determined by the trypan blue dye exclusion method. The growth of cells was observed in liquid cultures for four weeks after irradiation. The cell viability was checked immediately after irradiation, 24 hours later, the first, second, third, and fourth week of culture. After every viability check, 1ml of RPMI was added to every sample.

3.1.2 Hemopoietic progenitors

3.1.2.1 Cord Blood cells

The phototoxicity of the HP extracts was examined on cord blood hematopoietic progenitor cells in order to evaluate the selectivity of the extract on normal hemopoietic cells.

Umbilical cord blood samples (n=3) were collected by gravity from the umbilical vein, after the completion of delivery. All deliveries were normal. The mononuclear cells were separated by Ficoll Hypaque (Lymphoprep-Nycomed d=1077g/ml) density

centrifugation. After washing twice an aliquot of cells the cells were adjusted at a concentration of 3×10^6 cells/ml and were treated with the photosensitizer. The cells were incubated for 1 hour and after they were irradiated. After irradiation the cells were washed twice with RPMI and were cultured in methylcellulose for the evaluation of PDT effect on committed hemopoietic progenitors.

3.1.2.2 Bone marrow cells

Bone marrow mononuclear cells from a child with ALL in remission were incubated with the desired amount of photosensitizer for one hour. After irradiation they were washed twice with α-MEM.

3.1.2.3 Semisolid Cultures

Growth of committed hemopoietic progenitors from both cord blood and bone marrow was assessed using methylcellulose semisolid cultures as follows:

Mononuclear cells after irradiation were resuspended in α-Minimum Essential Medium (a-MEM, Gibco, Life Technologies BRL), at a concentration of $1x10^5$/ml where possible. They were cultured in 1% methylocellulose (StemCell Technologies Inc, Vancouver, Canada), supplemented with 30% FCS (Gibco, Life Technologies BRL), 1% BSA (Sigma Chemicals, St Louis, USA), 10^{-4} M 2- mercaptoethanol (Sigma Chemicals, St Louis, USA) and 10% growth factors at a final volume of 1.1ml in 35mm petri dishes. Colony growth of myeloid progenitors (CFU-GM) was stimulated with Granulocyte - Colony Stimulating Factor (G-CSF Amgen, Roche), Interleukin-3 (IL-3, R&D Systems MN, USA) and Granulocyte Macrophage - Colony Stimulating Factor (GM-CSF, Leucomax, Sandoz) at a concentration of 40 ng/ml each. Colony growth of erythroid progenitors (BFU-E) was stimulated with Erythropoietin 4IU/ml (EPO, Eprex Cilag), IL-3 10 ng/ml and GM-CSF 5 ng/ml. Cultures were plated in duplicate, incubated at 37^o C in a 5% CO_2 fully humidified atmosphere for 14 days. They were identified and scored under an inverted microscope.

3.1.3 Photosensitization

The desired amount of the photosensitizer was prepared in solutions 1:1 ethanol-water and was added to the cell suspension. The sample was incubated for 1 hour at 37^o C in a

5% CO_2 fully humidified atmosphere. The 1 hour incubation should not be exceeded as the dark toxicity of the sensitizer might be substantial and in an unspecified manner. After the incubation the cells were irradiated for 3, 5 and 7 minutes which correspond to 74.9 J/cm^2, 124.8 J/cm^2 and 174,7 J/cm^2 light dose. After the irradiation the samples were washed twice by centrifugation.

3.1.4 *Hypericum Perforatum L* (HP) extracts

PMF (polar methanolic fraction) and ME (methanolic extract) were the extracts we used. The extracts were a generous gift of Dr D. Skalkos of the Department of Materials Science & Engineering of the University of Ioannina. ME was prepared after extraction of the dry herb with methanol. Further separation of the ME extract resulted in the polar fraction (90%) which is the PMF extract and the non polar fraction (10%) which doesn't contain any hypericins but mostly chlorophylls. So the PMF extract is slightly richer in hypericins than the ME extracts. These extracts contain naphthodianthrone derivatives mainly hypericin and pseudohypericin, flavonols (hyperoside, rutin quercitin, isoquercitin quercetin), flavonol glycosides, biflavones, phloroglucinols mainly hyperforin, tannins, coumarins, essential oils, chlorophylls, and others. The main biologically active constituents identified in the extracts of *Hypericum Perforatum* and their percentage concentration in the corresponding extract can be seen in Table 3.1. PMF contains 1.37% hypericins slightly higher to the 1.32% of the ME. Both PMF and ME were diluted in 1:1 water ethanol solution and were stored in small aliquots at -20 ^oC. Solutions at a concentration of 30, 40, 50 and 60 μg/ml were prepared.

Extracts	% of each Constituent (w/w)				
	Hypericins	*Hypericin*	*Pseudo-hypericin*	*Hyperforin*	*Chlorophylls*
ME	1.32	0.51	0.7	7.62	0.08
PMF	1.37	0.57	0.64	2.52	0.12

Table 3.1: Constituents and percentage concentration of PMF and ME extracts.

3.1.5 Hypericin

Pure hypericin (Purity > 98%) was obtained from AG Scientific. Hypericin was diluted in 1:1 water-ethanol solution and the stock solution was stored at -20^o C. The

desired concentration of hypericin was achieved by further dilution with ethanol and water.

3.1.6 Merocyanine 540 (MC 540)

MC 540 has been successfully used as photosensitizer for BM purging of malignant cells in PDT [64]. In the present study MC 540 was used to compare its subcellular localization with that of the PMF extract. Merocyanine-540 (MC 540) was obtained from Sigma Chemical Co (St. Louis, USA). A stock solution was prepared in 50% ethanol-water at 20 μg/ml and stored at -20°C in small aliquots.

3.1.7 Statistical analysis

The results are expressed as the mean value $\pm$ and the standard error (SE). Each sample was tested in triplicate. All experiments were carried out at least three times. Results are expressed as % of the corresponding cells before irradiation. As control was used the sample in which the photosensitizer was added but not irradiated. The results of the semi solid cultures are expressed as the number of CFU-GM and BFU-E colonies per 10^5 mononuclear cells.

3.2 Experimental setups

3.2.1 Photodynamic treatment Experimental Setup

The irradiation source is a diode pumped CW laser Millennia V (Spectra Physics) at 532 nm with 5.5W maximum output power. As seen in figure 1 the laser beam is directed by three mirrors to the expanding lens. The lens expands the beams diameter to 35 mm so as to fit perfectly the specimen's surface. The Petri dish is then placed on a piezoelectric crystal. The crystal is connected to a pulse generator (Goldstar) which supplies the crystal with sinusoidal electric current of 50 Hz frequency. The crystal vibrates to the corresponding frequency and the sample placed on the crystal vibrates to the same frequency. The stirring of the sample during irradiation results in homogeneous irradiation of all cells which otherwise tend to accumulate at the bottom of the Petri dish. Also the sample is kept on an aluminum plate that acts as an effective heat sink causing the temperature of the cell suspension to remain at 24±1°C. The setup, except for the laser and the pulse generator, is placed in a metallic box (30 cm width, 30 cm length, 50 cm height) for the protection of the specimen from the surroundings and the blocking of the deflected light. The front facet of the metal box was replaced by a sliding piece of transparent orange plastic that allowed the observation of the irradiated sample and simultaneously filtered out all laser scattering.

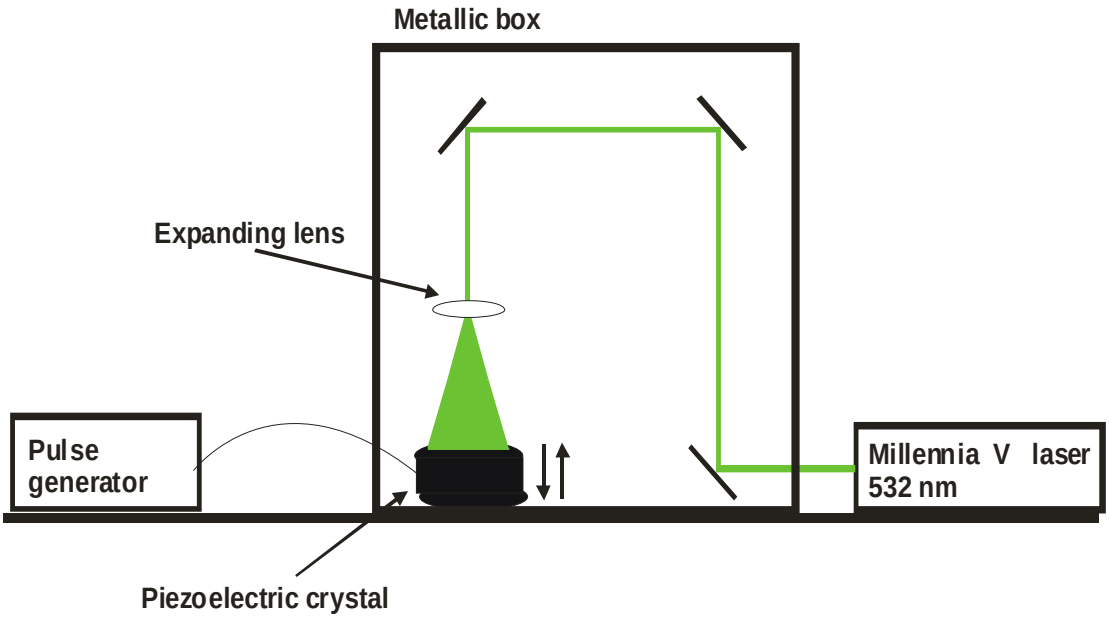

Figure 3.1: Photodynamic therapy Experimental Setup

3.2.2 Fluorescence measurement experimental setup

A CW Argon Ion laser (Spectra Physics) was used for the irradiation of the samples. We selected the 514 nm operation line of the laser for the excitation and the power was set at 100mW. A CVI spectrograph (CM 112), with a 600 gr/mm grating for visible light and a 1024 pixels diode array from CVI (AD 150), was used for the measurement of the fluorescence. The diode array was connected with a computer and the spectrum of fluorescence was displayed online. The wavelength calibration for the spectrograph was performed with a Hg-Ar lamp.

In Fig. 3.2 the setup is illustrated. The laser beam is directed to the cuvette(1×1 cm^2) which contains the sample. A special holder for the cuvette on the x-y-z-stage, was mounted to guarantee the same position for all samples corresponding to the position of the beam and the optical fiber. A multimode fiber (500μm core cladding diameter) was used. The optical fiber is mounted near the cuvette, at the same height and perpendicularly to the laser beam. The optical fiber collects the fluorescence and guides it to the spectrograph. The other end of the fiber was fixed to the entrance slit of a CVI-spectrograph of 100μm. A 1024 pixels diode array from CVI (AD 150) with 1nm resolution was used as a detector. The signal from the spectrograph was fed to a PC for A/D conversion and further analysis.

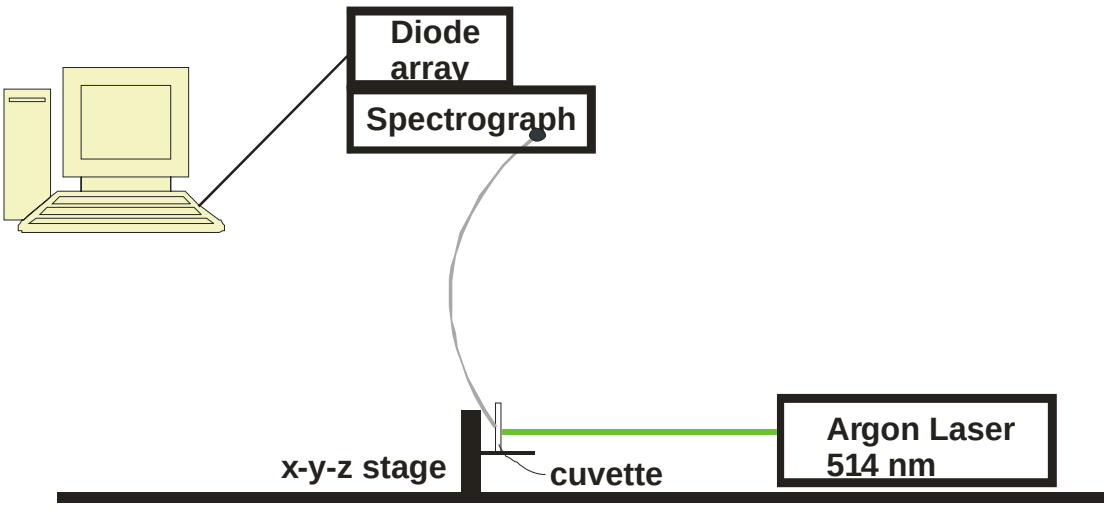

Figure 3.2: Experimental setup for the fluorescence measurements

4. Microscopy Techniques

4.1 Confocal Microscopy

Confocal microscopy became wide spread and popular the in last decade though it was discovered in 1957 by Minsky. The reason for that is the improvement on the laser technology, on the optics of the microscope, the electronics and finally on the software that accompanies it. The popularity of confocal microscopy arises from its ability to produce blur-free, crisp images of thick specimens at various depths. Confocal imaging rejects the out-of-focus information by placing a pinhole in front of the detector, so that only the region of the specimen that is in focus is detected. The practical effect of this is that the image comes from a thin section of the sample. By scanning many thin sections through the sample, a very clean three-dimensional image of the sample can be build up.

4.1.1 Basic Principle

Light from a laser passes through a small pinhole (top of figure 4.1) and expands to fill the entrance pupil of a microscope objective lens [131,132]. The objective lens focuses the light to a small spot on the specimen, at the focal plane of the objective lens. Light reflected back from the illuminated spot on the specimen is collected by the objective and is partially reflected by a beamsplitter to be directed at a pinhole placed in front of the detector. This confocal pinhole is what gives the system its confocal property, by rejecting light that did not originate from the focal plane of the microscope objective. Light rays from below the focal plane come to a focus before reaching the detector pinhole, and then they expand out so that most of the rays are physically blocked from reaching the detector by the detector pinhole. In the same way, light reflected from above the focal plane focuses behind the detector pinhole, so that most of that light also hits the edges of the pinhole and is not detected. However, all the light from the focal plane is focused at the detector pinhole and so is collected by the detector. This ability to reject light from above or below the focal plane enables the confocal microscope to perform depth discrimination and optical tomography. Scanning of the specimen is achieved by moving the detection beam along the specimen's surface. A true 3D image can be

processed by taking a series of confocal images at successive planes into the specimen and assembling them in computer memory.

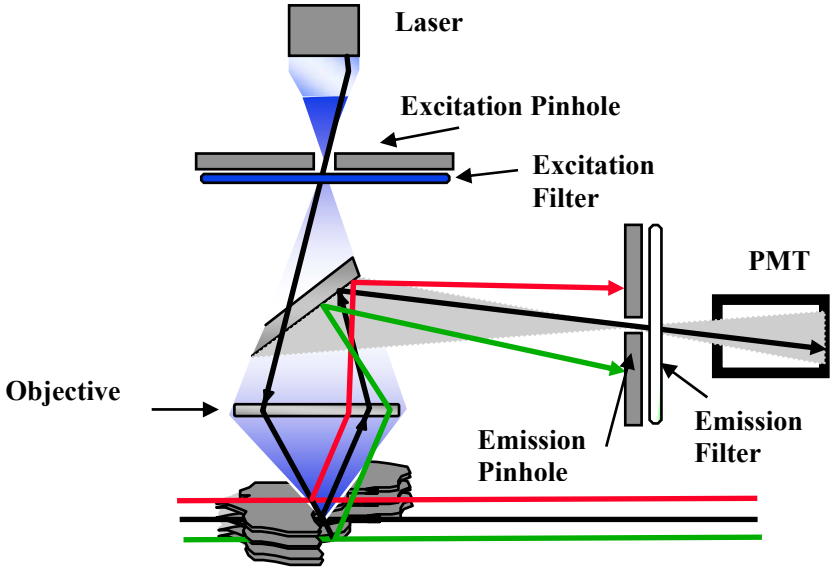

Figure 4.1: How a confocal image is formed

4.1.2 The Microscope

We used the state of the art **Bio-Rad Radiance 2100** CLSM (Confocal Laser Scanning Microscope). This microscope can be divided in four major components. The optical microscope on which the z drive is build up, the scan head which is placed on top of the microscope and drives the laser beam, the Instrument Control Unit (IOC) which contains the lasers the filters the detectors and all the electronic controls and the data acquisition unit –the computer- which processes and displays the scanned pictures.

4.1.3 Instrument Control Unit (ICU)

The control unit is a separate unit which contains the control circuits for the scan head and the lasers responsible for the excitation. Within the control unit are 3 lasers, an Argon laser with 4 lines (457, 477, 488, 514 nm), a He-Ne (543 nm) and a red diode laser (637 nm), power supplies and detectors. Excitation laser lines are routed via the ICU on the scan head. The modular construction of the ICU allows the easy exchange of detectors and lasers if required. The ICU links to the scan head by means of a conduit which contains a high efficiency, multi-mode emission fibre and a single-mode excitation fibre to preserve the polarisation state of the laser. Electrical control cables are also

routed through the conduit. Neutral density filters control the power of each laser line and interference filters control the emission wavelengths that reach the detectors. All functions are software controlled.

The ICU contains three prismatically enhanced photomultipliers (PMTs) specially designed which have twice the sensitivity of conventional PMTs covering the visible and near infra red spectrum.

4.1.4 Scan Head

The scan head (Fig. 4.2) is responsible for the scanning of the specimen in the x-y directions. It includes the incoming laser beams the galvanometers units responsible for the movement of the mirrors.

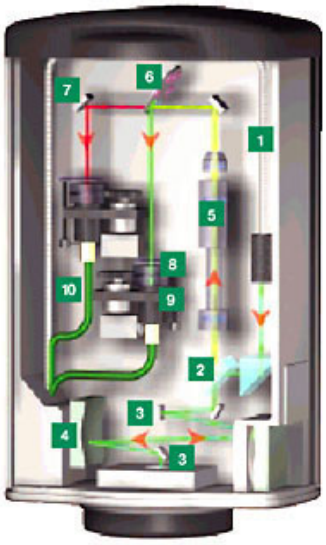

1. Polarisation preserving single-mode excitation fibre
2. Beamsplitter
3. Fast galvos
4. Concave mirror
5. Telescope with Sensitivity Enhancement Lens (SELS)
6. Dichroic chromatic reflectors
7. Steering mirror
8. Polarisers
9. Confocal aperture and collector lens
10. High sensitivity multi-mode emission fibre

Figure 4.2: The interior of the scan head. The various components are depicted.

In the Radiance 2100 scanhead both x and y-scan motions are produced by fast galvo-type mirrors (Fig. 4.3). Ideal scanning geometry is achieved by using two concave mirrors to perfectly image one galvanometer on the other. This produces rotation about a point on the second mirror and the back aperture of the objective is filled throughout the complete scan cycle. This is crucial with respect to maximising detection sensitivity and image uniformity. The scanning on the z-axis is achieved by a step motor employed on the specimens' base of the microscope.

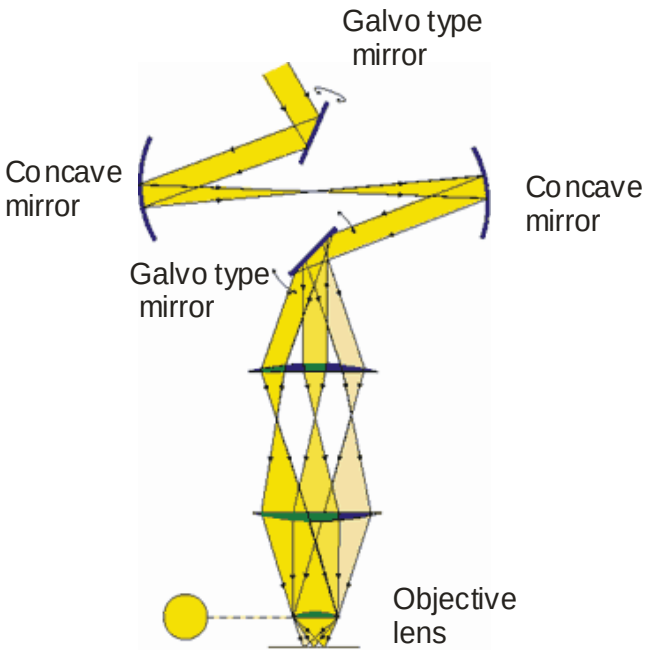

Figure 4.3: Sketch of the mirrors operation for the scanning in the x y directions. Two concave mirrors are employed to perfectly image the one galvanometer controlled mirror to the other

4.1.5 Lateral and Axial Resolution

The smallest separation between two point objects while still allowing them to be resolved is referred to as the limit of resolution. In confocal microscopy this is referred to as lateral resolution, distinguishing it from axial resolution which is measured along the optic axis. According to Rayleigh's criterion, two point objects are said to be just resolved when the center of one Airy disk falls on the first minimum of the other Airy disk.

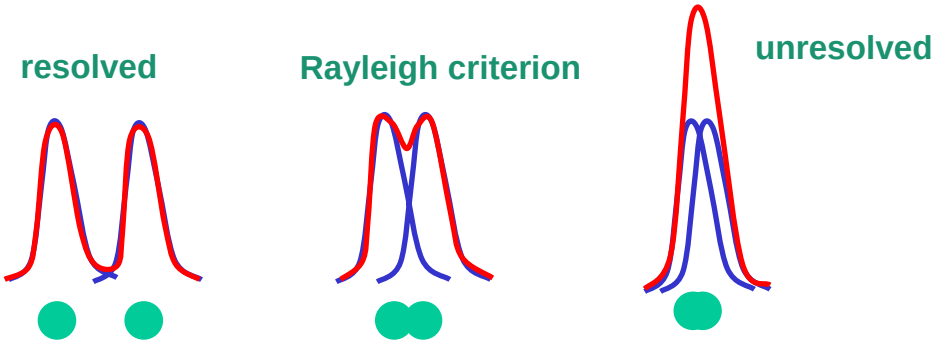

Figure 4.4: The Rayleigh's criterion for the resolution

The radius of an Airy disk is commonly defined to be the distance from its center to the first minimum and is equal to the lateral resolution of an objective lens (fig.4.4). The Airy disk radius is given by:

$$r_{Airy} = 1.22\ \lambda / 2\ N.A \qquad (1)$$

where λ = wavelength of light and, NA = numerical aperture of the objective lens. The numerical aperture of an objective lens is a measure of the angular size of the focusing cone of light as seen in Fig. 4.5 and is defined as follows:

$$N.A. = n \sin\theta \qquad (2)$$

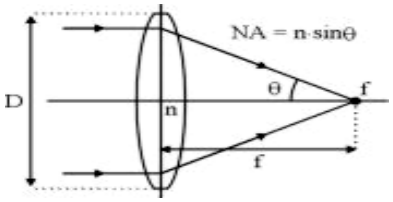

Figure 4.5: The numerical aperture (NA) of a microscope objective is a measure of its light gathering ability. Another measure is the f-number which is equal to f/D. The higher the NA and the lower the f-number, the more light is collected.

where θ is the half-angle of the cone and n is the index of refraction of the medium encompassing the cone. The magnification of the objective lens determines the maximum field of view. As is well known the performance of any imaging system is dependent on the numerical aperture (NA) of the objective lens. The larger the NA the better the spatial resolution of the system .The lateral resolution (R_{lat}) of a confocal microscope is considered the Airy disk produced by its optics

$$R_{lat} = r_{Airy} = 1.22\ \lambda / 2\ N.A. \qquad (3)$$

An accepted expression for the vertical or axial resolution is

$$R_{ax} = 2\lambda / n(\sin^2\theta) = [2\lambda] / [n(\sin^2 \sin^{-1}(N.A./n))] \qquad (4)$$

Where λ is the wavelength of the light n is the refractive index of the immersion medium and θ is the maximum light collecting angle of the objective lens. It is derived using paraxial (small angle) theory assuming the object being viewed is a perfect planar mirror. This expression should be considered only approximation which in some circumstances will fail to predict resolutions accurately.

The Radiance 2100 system employs a macroscopic (large), continuously variable circular aperture. The aperture should be set to Airy disk diameter to achieve theoretically optimal sectioning performance. This function is computer controlled and the formula used is

$$\text{Aperture Diameter} = 73.2\ \lambda\ mag_{obj} / N.A. \qquad (5)$$

where λ is the wavelength (in fluorescence the mid value of the band pass emission filter is used), mag_{obj} is the magnification of the objective and NA is the numerical aperture of the objective

4.1.6 Spherical and chromatic aberrations

Another important feature of this microscope is the Refractive index mismatch correction. If the lens' immersion medium and the sample's mounting material have different refractive indices, the light will be brought to a focus at a point displaced from the 'expected' position. The result of this 'unexpected refraction will be to distort the image's aspect ratio. This mismatch introduces a spherical aberration The LaserSharp2000 software of the system applies a correction factor to the calibration of the z-axis using an algorithm developed by White *et al.* [133] that works equally well for low and high Numerical Aperture (N.A.) lenses

To achieve results with the highest possible spatial integrity, planapochromatic lenses with high NA are used. These are highly corrected across the visible spectrum and have a very flat field of view.

4.1.7 Experimental details

For our observations we used the He-Ne laser line at 543nm. Also the 40X with 1.3 N.A. objective lens was used. The band pass filters were adjusted at 590-620 nm for the observation of PMF staining and at 570- 590nm for the observation of the MC 540. All the functions were electronically controlled from the computer software as it can be seen in Fig. 4.6. These functions were the selection of the laser, the laser intensity and the selection of appropriate filters for the PMTs. Also electronically controlled are the scanning parameters on the xyz axis. The z-axis step motor was set at 0.2μm

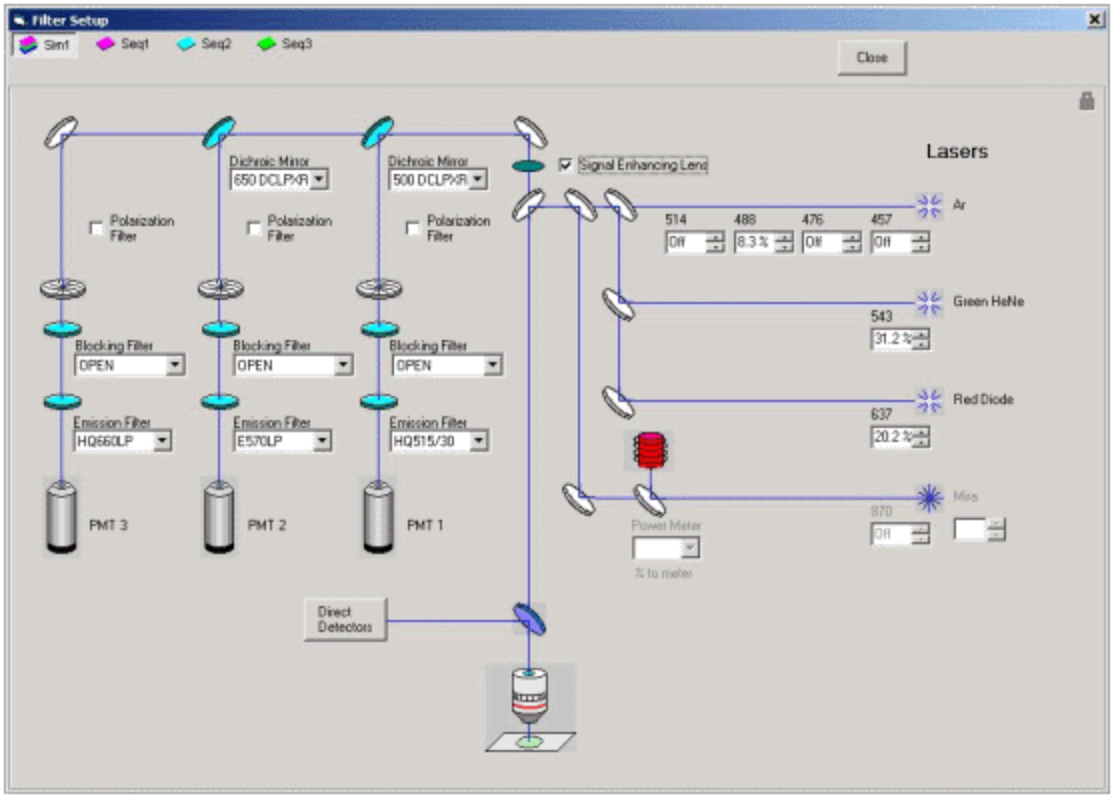

Figure 4.6: Computer control panel of the Radiance 2100 Microscope. All functions, filters, laser line and intensity are computer controlled.

For the 543 He-Ne laser line which we used and the band pass set to 590nm to 620nm with the 40X lens with NA = 1.3 the aperture diameter obtained from equation (5) is 1,22 mm. The lateral resolution for the 543nm laser line and the 40X lens is 255nm obtained by equation (3) and the axial resolution is 855nm obtained by equation (4). Also the software provides utilities offering the digital magnification of the scanned pictures. We made use of this utility which can offer up to 6x zoom to the digital picture.

4.2 Non linear Microscopy

A complementary technique of the confocal microscopy is non linear microscopy. Non linear microscopy can offer difraction limited resolution and optical sectioning of the specimen as confocal but it can also minimize side effects as photobleaching and sample destruction. Non-linear optical measurements used in conjuction with microscopy observation have created new opportunities. Second-order non-linear processes such as second-harmonic generation (SHG) or sum frequency generation (SFG), and third-order processes such as third-harmonic generation (THG), coherent anti-Stokes Raman scattering (CARS), and two-photon excited fluorescence (TPEF) have been used for the imaging and the understanding of biological systems and processes. We used a non linear microscope for the TPEF imaging of HL-60 cells and for the detection of the SHG signal.

By far the most well known form of non-linear microscopy is based on TPEF. It was firstly introduced by Denk, Webb and coworkers in 1990 [134]. The electronic transition of a fluorophore can be induced by the simultaneous absorption of two photons. These two photons, typically in the infrared spectral range, have energies approximately equal to half of the energetic difference between the ground and excited electronic states. Since the two-photon excitation probability is significantly less than the one-photon probability, two-photon excitation occurs with appreciable rates only in regions of high temporal and spatial photon concentration. The high spatial concentration of photons can be achieved by focusing the laser beam with a high numerical aperture (NA) objective lens to a diffraction-limited focus. The high temporal concentration of photons is made possible by the availability of high peak power pulsing lasers, with pulse width of the order of hundreds of femtoseconds (10^{-15}sec). The most important feature of two-photon microscopy is its intrinsic depth discrimination. This depth discrimination effect of the two-photon excitation arises from the quadratic dependence of two-photon fluorescence upon the excitation photon flux, which decreases rapidly away from the focal plane (fig. 4.7).

The ability to limit the region of excitation is very important, especially for biological specimen, since their photodamage is restricted only to the focal point. Since out-of-plane fluorophores are not excited, they are not subject to photobleaching. Moreover, TPEF microscopy exhibits an additional advantage. Two-photon excitation

wavelengths are red-shifted to approximately twice the one-photon excitation wavelengths. The significantly lower absorption and scattering coefficients ensure deeper tissue penetration. Finally, the wide separation between the excitation and emission spectra ensures that the excitation light can be rejected without filtering out any of the fluorescence photons, resulting in sensitivity enhancement and better signal-to-noise ratio (SNR).

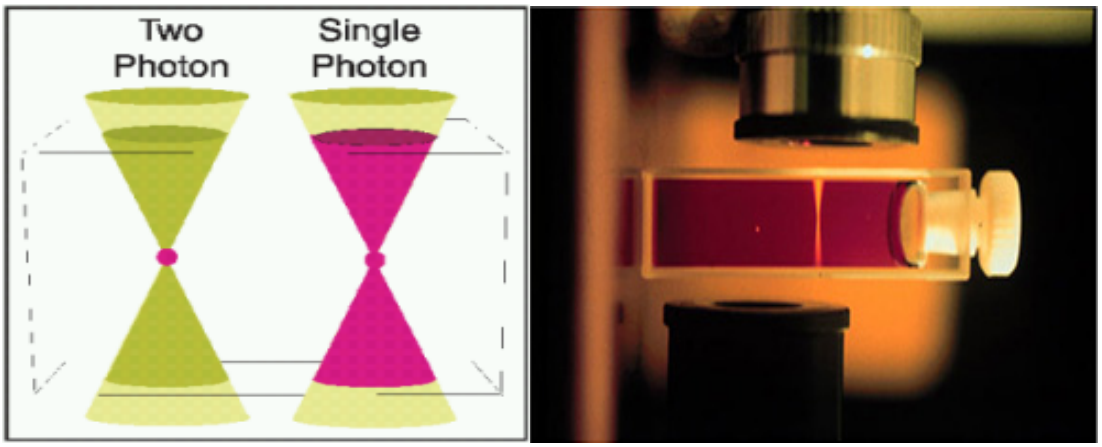

Figure 4.7: On the right a photograph shows a cuvette of fluorescent dye excited by single photon excitation (right line) and multiphoton excitation (localized spot of fluorescence at left) illustrating that two photon excitation is confined to the focus of the excitation beam [135]. On the left we see a picture of this phenomenon

SHG is a coherent phenomenon in contrast to TPEF which is non coherent. It is based on the Hyper Rayleigh Scattering (HRS). Light of the fundamental frequency ω is converted by the non linear material into light at the exactly the twice that frequency (2ω). SHG is a second-order non-linear phenomenon [136], and its strength is fully determined by the second-order susceptibility tensor $\chi^{(2)}$ of the non-linear medium. This tensor is non-vanishing only for non-centrosymmetric media. Under this symmetry constraint it is obvious that SHG can be mainly produced from structures with high degree of orientation and organization but without inversion symmetry, such as crystals or endogenous arrays of structural proteins in biological systems.

4.2.1 Experimental apparatus

In Figure 4.8 the layout of the developed setup for combined TPEF – SHG scanning microscopy is depicted, and its main parts are shown. We use as excitation source a diode pumped, femtosecond t-pulse laser (Amplitude Systemes product - high

power femtosecond oscillator) emmited at 1028nm. The laser material is an Ytterbium doped crystal. The average output power is 1 Watt, and it is characterized by long-term stability. The pulse duration is 200fs and the repetition rate is 50MHz. Using the above specifications, the energy of the single pulse is calculated to be 20nJ. This amount of energy limited in 200fs is extremely high and provides high efficiency of exciting non-linear phenomena. The beam is directed to a modified optical microscope (Nikon Eclipse ME600D) using suitable dichroic mirrors. The last dichroic mirror (99 % reflectivity at 1000nm) directs the fundamental beam to the objective lens. The objective lens offers the necessary tight focusing of the fundamental beam onto the sample. Simultaneously, it collects the TPEF originating from the sample in the backward direction, and collimates this signal, which is directed to the PMT at the top of the microscope. The average laser power on the specimen is 10mWatt. The biological sample is mounted between two cyclic glass slides. The thickness of each glass slide is 50-70 μm. The need for a thin slide originates from the short working distance of the objective lens. The slides are positioned at a special holder. This holder is connected mechanically with the x-y-z scanning stage. The x-y-z motorized scanning stage is a combination of three "one dimensional" Standa 8MT167-100 step motors. Their minimum step is 1 μm, and this sets a limit in the transversal and in the longitudinal resolution potential of this system. The combined movement of the three stages is computer controlled by a specially designed software (National Instruments, Labview program 6.1), so that a complicated scanning scheme is created. The average accumulation time in every step is 30msec.

Light is directed to the objective lens which focuses the beam and illuminates the sample. In the specimen TPEF and SHG are produced and they are measured from different detectors. TPEF is collected from the objective. Fluoresence is directed by a dichroic mirror to the detector. TPEF signal is collected using a photomultiplier tube (PMT Hamamatsu R4220) that is attached at the position of the eye-piece of the microscope. Because the optic path is the same for the excitation light and fluorescence the dichroic mirror enables their spatial separation. In front of the PMT a short pass filter (SPF 650 nm CVI) is placed at the top of the microscope, in order to cut off the reflected laser light. The PMT is connected with the Lock-in amplifier (SR810 Stanford Research Systems), where the created current is converted to a voltage indication. For the optical

observation of the biological samples through the objective lens, a CCD camera (Sony XC-57CE) is employed.

On the other hand the signal of SHG propagates with the laser, for thin samples like in our case, and is collected and colimmated by the condenser lens of the microscope (NA 0.9, working distance 1.9mm). A dichroic mirror is positioned under the condenser (99% at 45^0, 450 – 650nm). SHG signal is focused by means of a lens into the slit (100μm) of a monochromator. This is important for the proper operation of the monochromator, and prevents loss of the signal. The focal length of the lens is 3 cm. The monochromator (Digikrom CM110 CVI) consists of a grating (600 grooves/mm) adequate for visible light. For the detection of the signals a photomultiplier tube (PMT Hamamatsu R636-10) is employed. A short pass filter (SPF 700 nm CVI) is placed before the PMT in the forward direction, in order to cut-off the remainder of the laser light. The PMT is connected with the Lock-in amplifier. By using this configuration it is feasible to collect both SHG and TPEF signals in distinct sets of measurements (by tuning the monochromator to the proper wavelength)

By using the whole experimental apparatus it is possible to collect SHG and TPEF signals simultaneously (by detecting SHG images in the forward direction and TPEF images in the backward direction).

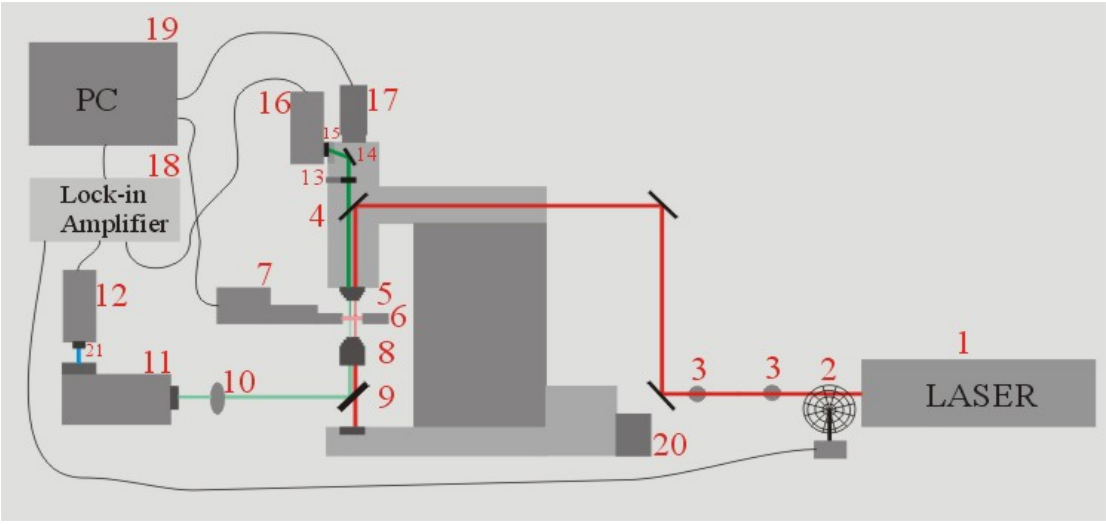

Figure 4.8: Experimental set-up for combined TPEF – SHG scanning microscopy. 1) Femtosecond laser (λ =1028 nm), 2) Chopper, 3) Iris, 4) Dichroic Mirror, 5) Objective lens, 6) Holder of the sample, 7) x-y-z motorized scanning stage, 8) Condenser lens, 9) Dichroic Mirror, 10) Focusing lens, 11) Monochromator, 12) Photo-multiplier tube (PMT), 13) Neutral density filter, 14) Flip-mount mirror, 15) Short Pass Filter, 16) PMT, 17) CCD camera, 18) Lock-in amplifier, 19) PC, 20) Light source, 21) Short Pass Filter. The

SHG signal is detected in the forward direction (PMT 12), while the TPEF is detected in the backward direction (PMT 16).

Two objective lenses were used an Edmund Scientific (100x, NA 1.25) and a Nikon (50x, NA 0.8). The lateral resolution provided by the Edmund Scientific (100x, NA 1.25) is about 430nm and the axial resolution is about 1093nm [137]. The lateral resolution provided by the Nikon (50x, NA 0.8) is about 670nm and the axial resolution is about 1960nm. The real lateral resolution though is restricted by the minimum step of the step motor which is 1μm. The axial resolution is determined by each lens used.

5. Fluorescence Measurements

The fluorescence of pure Hypericin and of PMF and ME extracts were measured and the results are presented in this section. The fluorescence of PMF in solutions with or without HL-60 cells was also evaluated and compared with that of MC 540 because MC 540 is a photosensitizer that has been successfully used for purging of autologous grafts.

5.1 Hypericin, PMF and ME

The fluorescence spectrum of the *Hypericum Perforatum L* extracts, PMF and ME, and the fluorescence of pure Hypericin were measured. It is known -by chemical analysis- that these extracts contain Hypericin and in order to verify this we applied spectroscopy. An Argon laser emitting at 514nm was used as an excitation source. The power of irradiation was 100 mW.

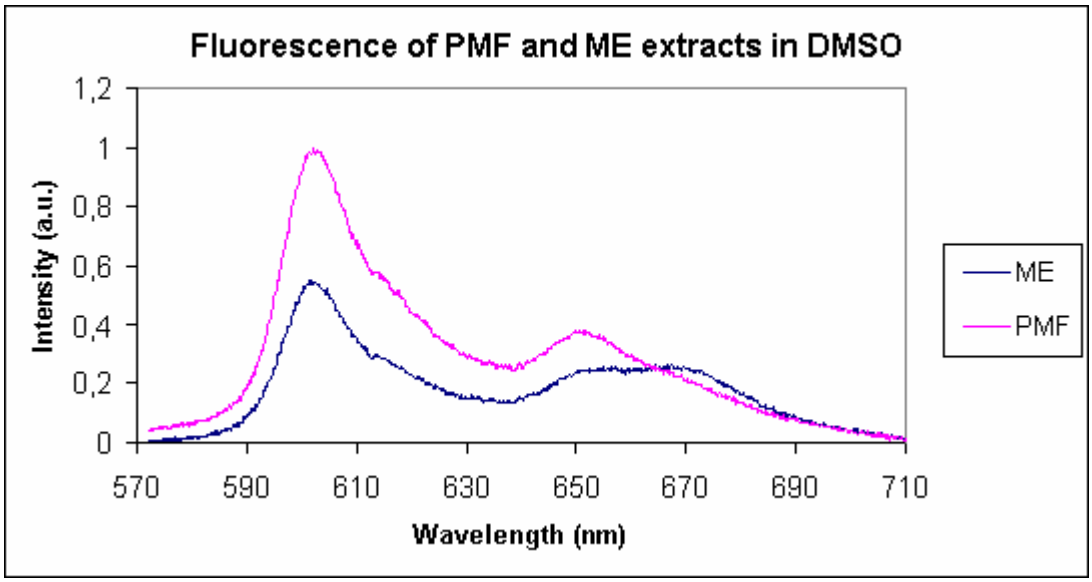

Figure 5.1: Normalized fluorescence of PMF and ME extracts in DMSO, accumulation time (a.t.) 45ms

One mg of PMF and ME were diluted in 3 ml of DMSO each and their fluorescence was measured (Fig. 5.1). Both spectra are similar. Fluorescence of PMF in DMSO exhibits major peak at 602nm and a minor peak at 652nm while ME exhibits a major peaks at 602nm and two minor peaks one at 652nm and one at 672nm. In both extracts the difference between the major and the minor peak is 40 nm. It can also be seen in the diagram that the fluorescence intensity signal of PMF at the peak is double that of ME. This high difference in the intensity was not expected

because although PMF has higher hypericin content this difference does not exceed 0.05%.

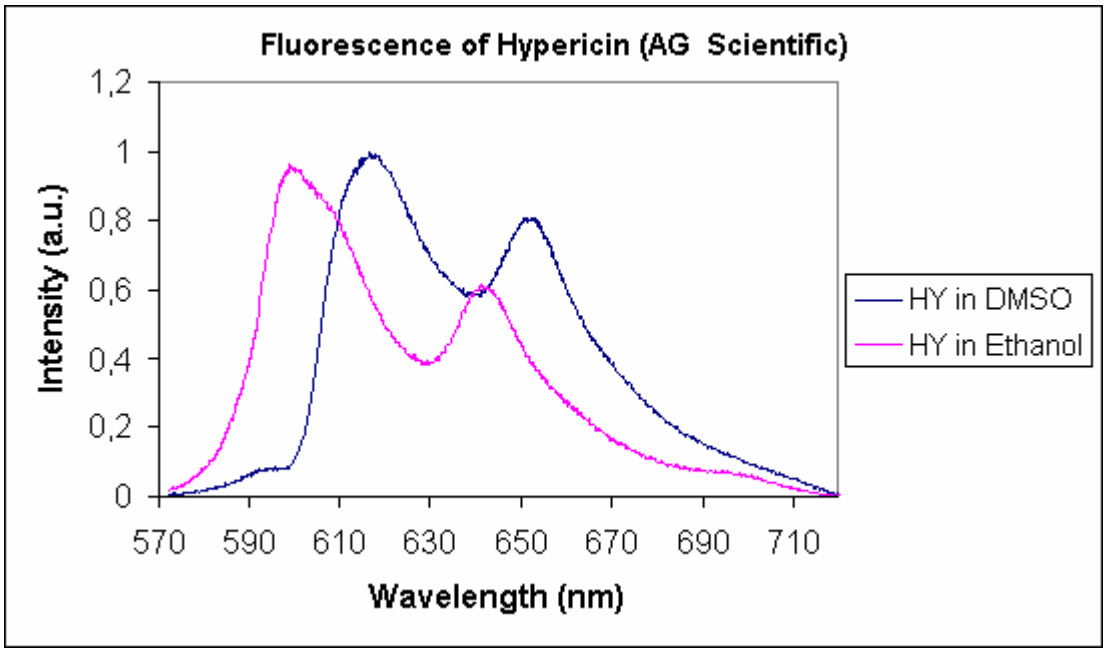

Figure 5.2: Normalize fluorescence of Hypericin in ethanol and in DMSO a.t. 10ms

One mg (66mM) of pure hypericin was diluted in DMSO and in ethanol and the fluorescence was measured in these two solvents (Fig. 5.2). A major peak appears at 618nm with a minor peak at 654nm in DMSO. The spectrum also shows a small peak coming up at 592nm. The difference between the major and the minor peak is 46nm. Fluorescence of hypericin in ethanol exhibits a major peak at 602nm and a minor at 642nm. The difference between the major and the minor peak is 40nm. Additionally there was a red shift of 16nm in the reordered spectrum in DMSO compared to the ethanol solution and this due to the different solvent.

There is a great similarity between the PMF and Hypericin spectra and this is supportive of the idea that the main fluorescent specie of the PMF and ME extracts is hypericin.

5.2 Fluorescence of PMF in the presence and absence of HL-60 cells

The fluorescence signal of the PMF extract in samples irradiated at various light doses with or without cells was measured. The first set concerned samples of 1 ml each containing 50μg of the PMF extract in a 1:1 ethanol: water solution. The samples were irradiated for 3, 5 and 7 minutes with the Millennia V laser at 532 nm at 4W power. The light doses respectively were 74.87, 124.79 and 174.7 J/cm^2. After the

irradiation the fluorescence was measured and compared with a reference sample which was not irradiated. For the excitation we used the 514nm line of Ar^+ laser at 100mW.

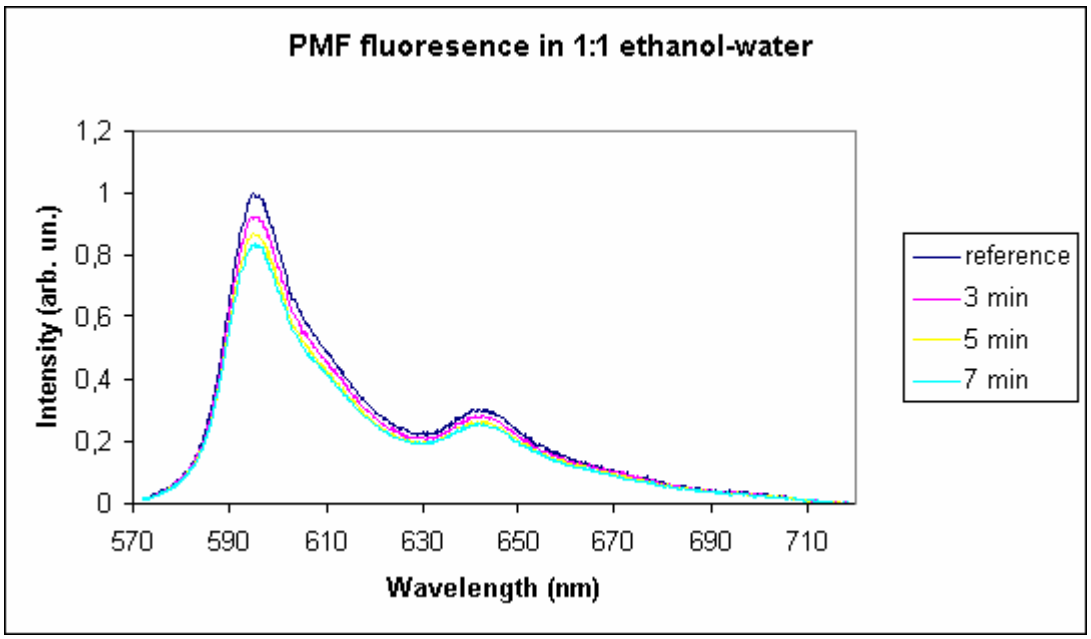

Figure 5.3: Normalized fluorescence of PMF in the absence of cells after being irradiated for 0, 3, 5 and 7 min. a.t. 400 ms

In all spectra in Fig.5.3 appears a major peak at 595 nm and a minor at 642 nm and their difference is 47nm. A decrease in the intensity of fluorescence can be observed as the duration of irradiation increases. Specifically the decrease of intensity at the peak compared to the reference sample is 7,3 % for the sample irradiated for 3 minutes, 12,85% for the sample irradiated for 5 minutes and 16,8% for the sample irradiated for 7 minutes. The decrease of intensity could be attributed to photobleaching. This decrease though is not considerable and it is linear.

The next step was to examine the fluorescence of the PMF extract in the presence of HL-60 cells. Samples with cells (3×10^6 cells/ml) were prepared, diluted in RPMI and 50 μg/ml of PMF extract was added. The samples were irradiated for 3, 5, and 7 minutes with the Millennia V laser at 532 nm and then their fluorescence with the Argon laser at 514 nm line for the excitation was measured. The major peak appears at 602 nm and a minor at 652 nm (Fig.5.4). There is a shift in the maximum of fluorescence compared to the samples without HL-60 cells and this could probably be due to the different solvent. The shift is $\Delta\lambda \approx +7$ nm. Also the net fluorescence is approximately 50% lower in the samples containing cells compared to those without cells. There is also a decrease in the intensity of fluorescence as the time of irradiation

increases. The decrease compared to the reference sample, which was not irradiated with the Millennia V laser, is 29.6% for the 3 minutes sample, 41.7% for the 5 minutes and 54.6% for the 7 minutes. The drop is much greater than the drop of intensity occurred in the absence of HL-60 cells. This is due to a partial photobleaching of PMF which is significant for the 7 minutes sample where the intensity drops to half. During the irradiation Type I reactions take place which gradually lead to the decomposition of the molecule of hypericin which is responsible for the fluorescence. It should be noticed that hypericin is still present in the solution even after 7 minutes of irradiation indicating that the PMF extract can be used as a photosensitizer in Photodynamic Therapy with the Millennia V laser even for prolonged exposure.

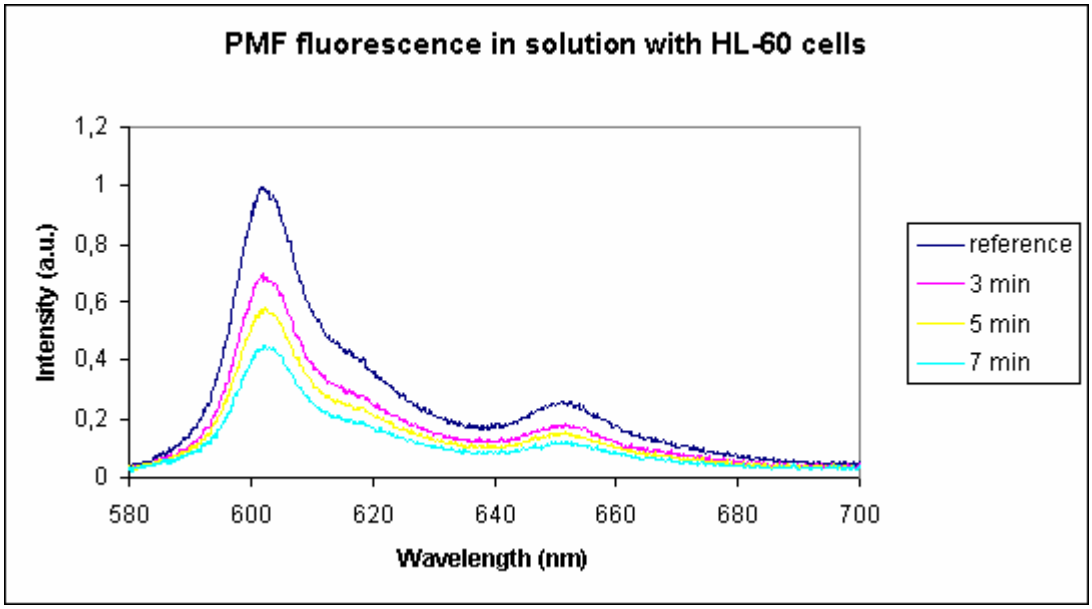

Figure 5.4: Normalized fluorescence of PMF in the presence of cells after being irradiated for 0, 3, 5 and 7 min. a.t 100ms

The decrease of the intensity can be also attributed to another fact. It is known that the fluorescence of Hypericin depends on the pH value of the environment [113,114]. During the irradiation oxygen species are produced which make the environment in the cell suspension more acidic. The intensity of fluorescence of Hypericin drops in an acidic environment compared to a neutral pH environment and it is possible that the decrease of fluorescence is related with the increased production of singlet oxygen as the time of irradiation increases. This could be suggestive of an even smaller percentage of photobleaching meaning that the PMF extract is even more resistant to irradiation.

5.3 Fluorescence of MC 540 in the presence and absence of HL-60 cells

We repeated the same fluorescence measurements for MC 540. 20 μg of MC 540 were diluted in 1ml of 1:1 ethanol water solution and samples with or without HL-60 cells were irradiated for 3, 5 and 7 minutes with the Millennia V laser at 532nm (energy doses 75 J/cm^2, 125 J/cm^2 and 175 J/cm^2). The Argon laser was used as an excitation source for fluorescence measurements. The results are presented in Fig 5.5.

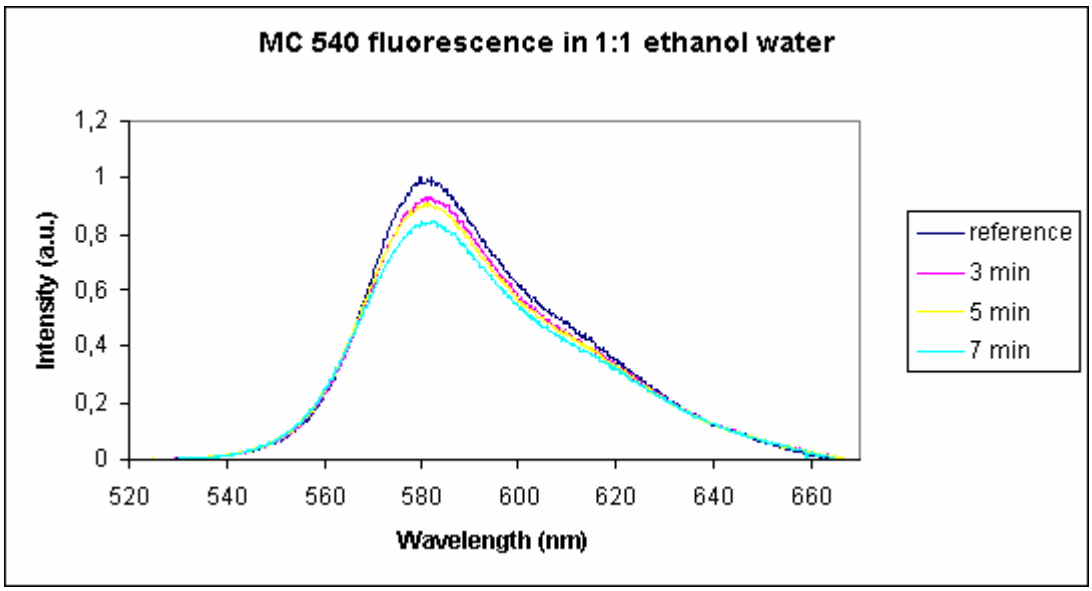

Figure 5.5: Normalized fluorescence of MC 540 in the absence of cells after being irradiated for 0, 3, 5 and 7 min. a.t 60ms

In the fluorescence measurement of MC 540 in the absence of cells a major peak appears at 582nm. Again as the time of irradiation increases the fluorescence signal decreases. The decrease for the sample which was irradiated for 3 minutes is 6.95%, for the 5min sample is 8.8% and for the 7 min is 15.5%. The decrease is comparable to that of the PMF extract where the decrease was 7.35, 12.8% and 16.3% for the 3, 5 an7 minutes samples respectively.

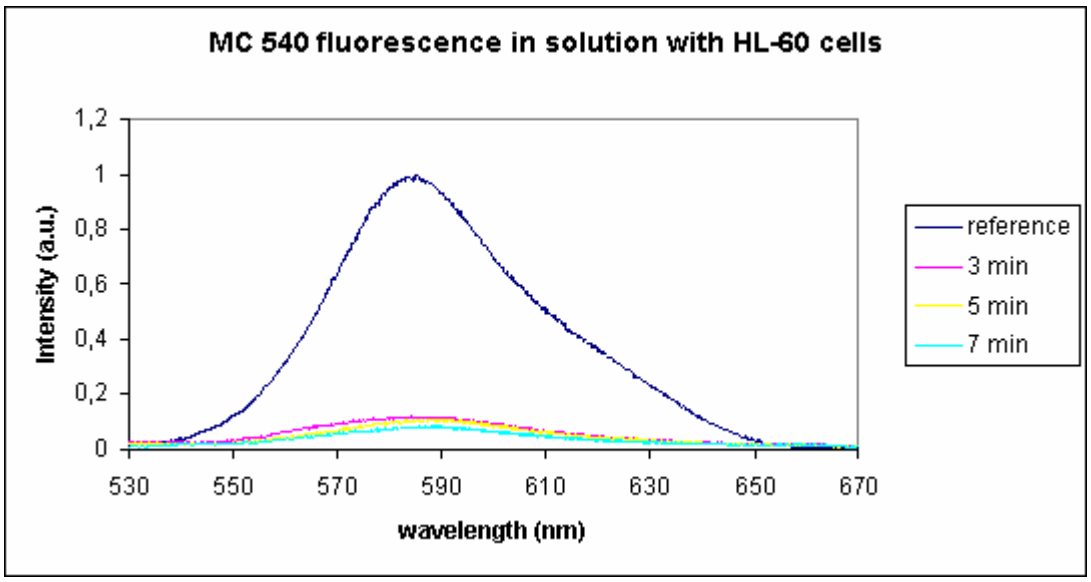

Figure 5.6: Normalized fluorescence of MC 540 in the presence of cells after being irradiated for 0, 3, 5 and 7 min. a.t. 60ms

The fluorescence of MC 540 in the presence of HL-60 cells appears (Fig.5.6) α peak at 585nm slightly shifted $\Delta\lambda$=3nm than the water-ethanol solution. A dramatic decrease of the fluorescence of the irradiated samples is observed. It reaches 87.9%, 88.8% and 91.7% for the 3, 5 and 7 minutes irradiated samples respectively compared to the reference sample. This result should be attributed to photobleaching of the chromophore. This also implies that MC 540 is destructed before inducing its photodynamic effect to cells. These observations suggest that MC 540 is not as photostable as Hypericin and PDT with MC 540 and the Millennia V laser is not recommended.

5.4 Conclusions

Decomposition of sensitizers occurs during PDT and it is often substantial [5] contributing to reduced efficacy of the photosensitizer. Previous studies report that the sensitizer Photofrin was nearly 60% photobleached after a typical PDT treatment *in vivo* and this photobleaching was responsible for reduced efficiency [5]. The mechanism of photobleaching is not very clear. Though indications suggest that photobleaching occurs through Type I reactions [138] deprotonization of sensitizers may result to their decomposition as well. In the present work photobleaching is observed in both PMF and MC 540. Photobleaching for MC 540 is around 90% while for PMF is over 30% for the 3 min irradiation. Hypericin has been found to be very photostable having a photobleaching factor (the fluence bleaching 50% of the

dye)BD_{50} over 100 J/cm^2 [139]. In our experiments this factor was found to be BD_{50}~99J/cm^2 for PMF. Therefore PMF and consequently hypericin prove to be much more stable than MC 540 and this means that PMF could be much more effective during PDT.

6. Photodynamic Therapy - Results

The parameters of photodynamic therapy which include the sensitizer concentration and the energy dose were examined. Since no previous study has been conducted concerning PDT on HL-60 leukemic cells in the presence of PMF and ME extracts, various concentrations of the sensitizer were tested and different energy doses applied.

Energy dose depends on two factors, the light intensity and the time of irradiation. We retained light intensity constant in all experiments as the photodynamic effect depends mainly on the total energy dose and not on the magnitude of the intensity. The power of the Millennia V laser at 532nm was kept constant at 4W and the irradiation duration tested was 3, 5 and 7 minutes. These correspond to energy doses of 74.9 J/cm^2, 124.8 J/cm^2 and 174,7 J/cm^2 respectively. These PDT parameters were tested for both PMF and ME extracts. After determining the optimum conditions for PDT with *Hypericum Perforatum* extracts the photodynamic effect under those parameters was investigated for pure Hypericin on HL-60 cells and for PMF on bone marrow and on cord blood progenitor cells

6.1 Laser toxicity and dark toxicity of PMF

According to our results the toxicity of the laser alone is not significant (Fig. 6.1). The number of samples in this experiment is n=6. For all irradiation times the cell survival is over 90%. The laser alone can not induce a photodynamic effect on HL-60 cells.

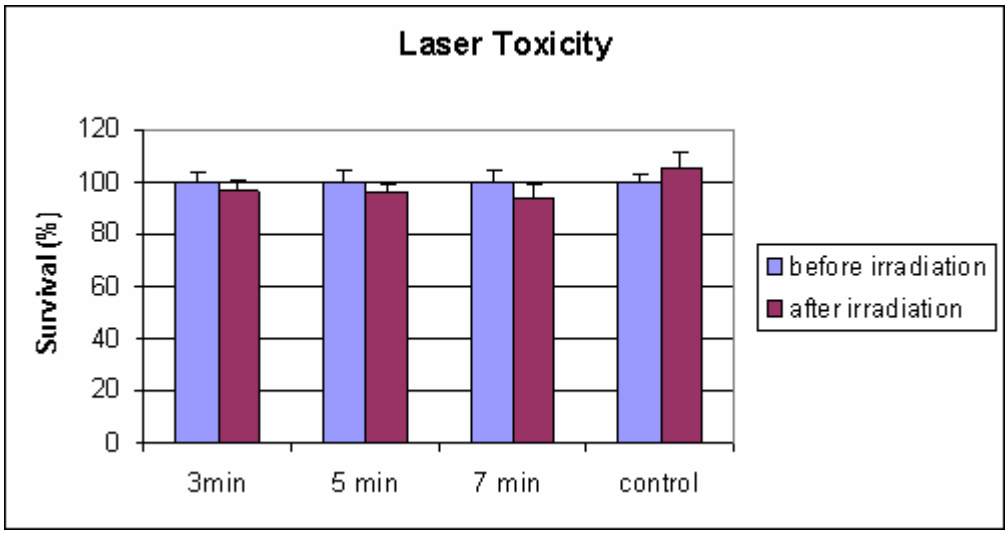

Figure 6.1: Laser toxicity at 4W

Cells were incubated with PMF only in order to estimate the dark toxicity of PMF. The cell survival was evaluated after 2 hours of incubation with the photosensitizer and revealed that there is no PMF dark toxicity. In another set of experiments cells were incubated with PMF for 24 hours. As it is depicted in Fig. 6.2 for PMF doses over 40μg/ml in that case the dark toxicity is over 90%. It has been reported that hypericin alone does not exert significant dark toxicity [76]. Other compounds, apart from hypericin, which are present in the extract, such as flavonoids and phloroglucinols, might be responsible for the dark toxicity of the extract after a prolonged period of incubation [140].

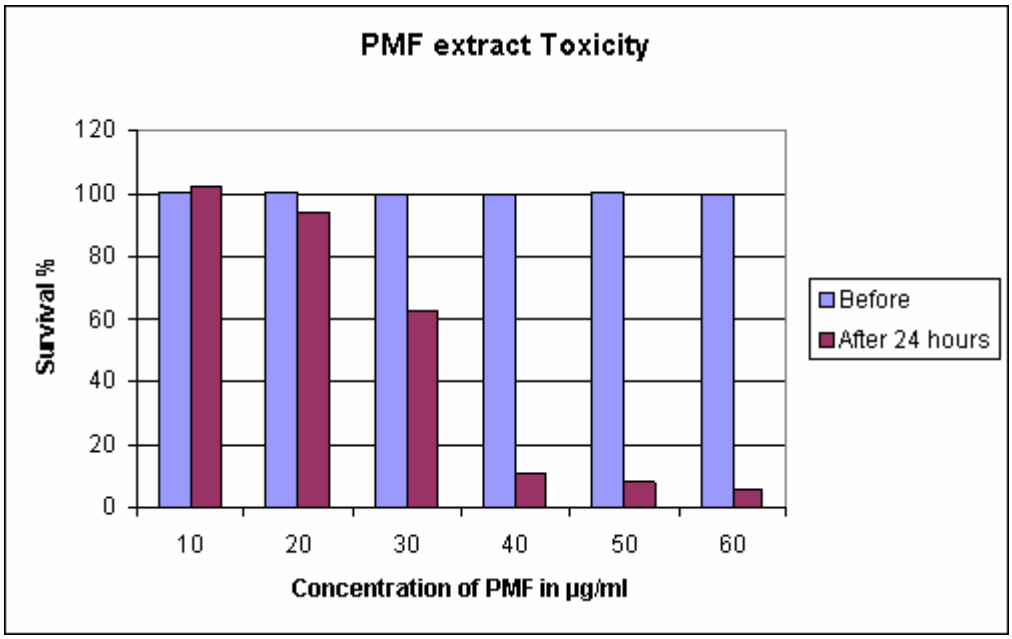

Figure 6.2: Dark toxicity of PMF after 24 hours of incubation

6.2 PDT with the PMF extract

The photodynamic effect of 30, 40, 50 and 60μg/ml concentration of PMF (n=9) is shown in the following Table.

Number of cells (%)	3 min	5 min	7 min	Control
Before irradiation	100 ± 7.44	100 ± 9,75	100 ±10,64	100 ± 16,05
After irradiation	7.75 ± 3.89	0.31 ± 0.21	0,41 ± 0,30	76,22 ± 19,68
24 hours	0.12 ± 0.12	0.10 ± 0.10	0 ± 0	169,28 ± 30,69
1st week	41.65 ± 18.98	0 ± 0	0,20 ± 0,20	98,96 ± 13,87
2nd week	18.88 ± 9.21	21.41 ± 19.28	54,63 ± 27,30	108,12 ± 48,72
3rd week	23.73 ± 10.88	37.92 ± 18.32	22,38 ±12,55	38,18 ± 18,51
4th week	6.73 ± 3.77	5.61 ± 2.66	4,58 ± 2,46	30,94 ± 14,75

Table 6.1: PDT results of 30μg/ml of PMF extract on HL-60 cells

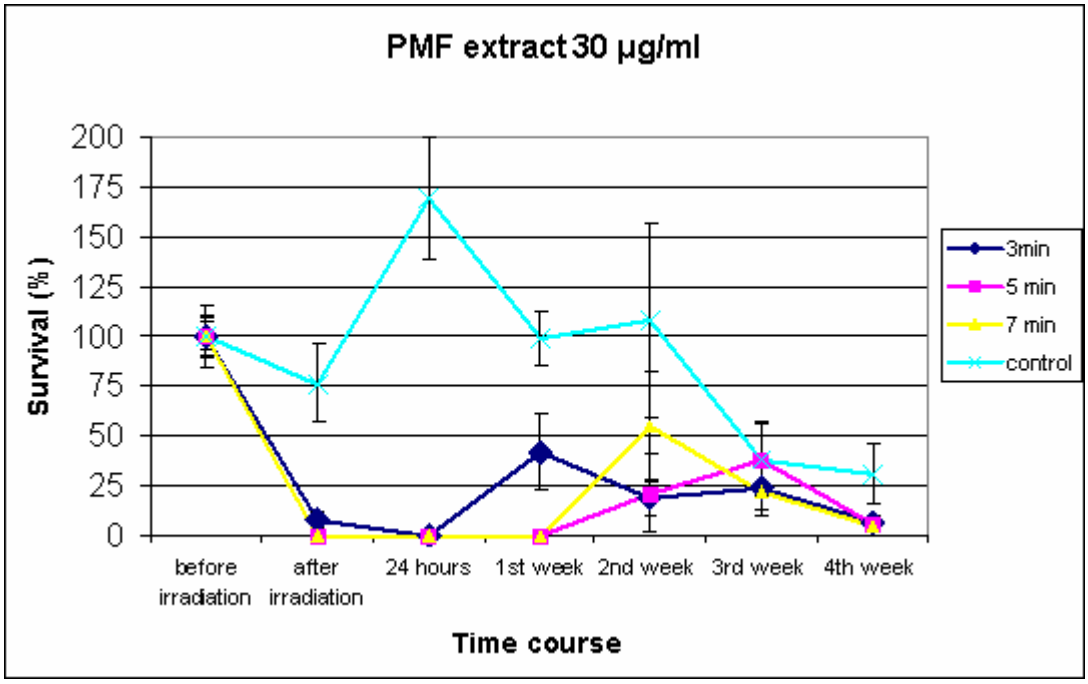

Figure 6.3: Survival of HL-60 cells after PDT with 30μg/ml of PMF extract at 4W

Immediately after irradiation the cell survival of those irradiated for 3 minutes is 7.75% and for the 5 and 7 minutes irradiated samples is 0% (Fig. 6.3). Cell survival is 0% 24 hours after irradiation for all samples. Following one week liquid culture though, the cell survival for the 3 min irradiation samples is 41.65%, and at the second week samples irradiated for 5 and 7 min showed 21.5% and 54.63% survival respectively. At the end of the culture, the fourth week, live cells are present in all samples. Therefore complete killing of cells is not achieved with 30μg/ml of PMF

Number of cells (%)	3 min	5 min	7 min	Control
Before irradiation	100 ± 3.73	100 ± 16.20	100 ±1 0.27	100±13.92
After irradiation	1,31 ± 1.05	0 ± 0	0,12 ± 0.12	85,35 ± 10.14
24 hours	0 ± 0	0 ± 0	0 ± 0	183,75 ± 9.65
1st week	0,47 ± 0.47	0 ± 0	0,47 ± 0.47	139,28 ± 15.13
2nd week	33,57 ± 17.85	0 ± 0	53,77 ± 35.90	108,21 ± 22.96
3rd week	30,95 ± 16.66	0 ± 0	16,04 ±1 0.24	29,91 ± 13.87
4th week	13,75 ± 9.58	7,92 ± 7.92	9,43 ± 6.56	35,53 ± 19.11

Table 6.2: PDT results of 40μg/ml of PMF extract on HL-60 cells

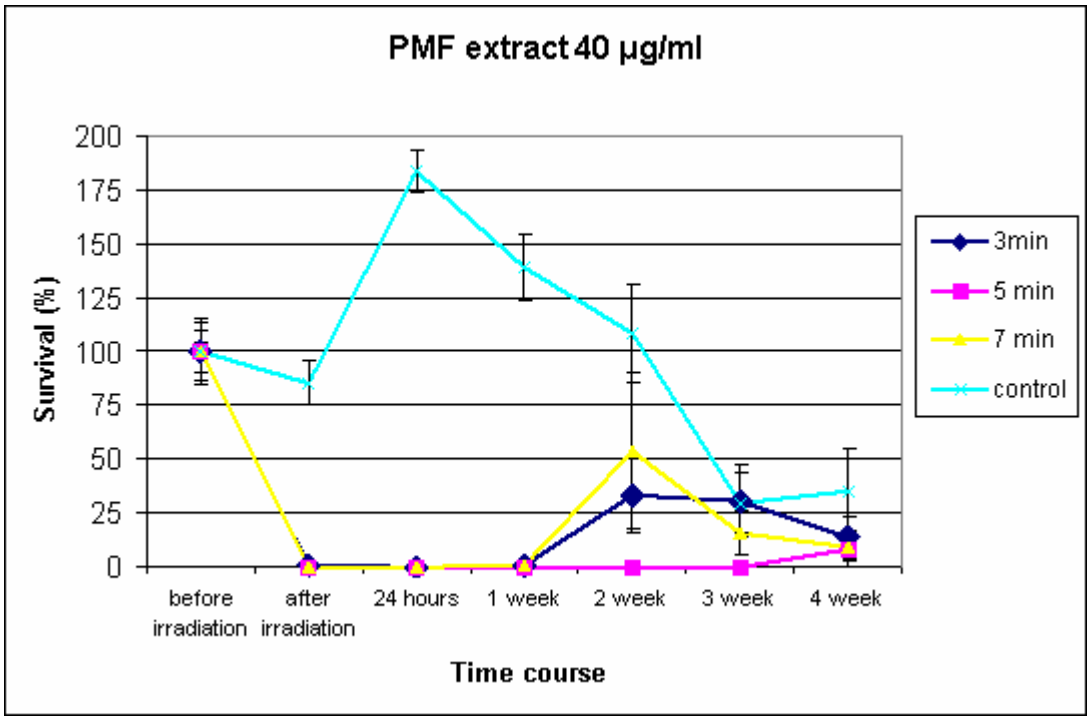

Figure 6.4: Survival of HL-60 cells after PDT with 40μg of PMF extract at 4W

The killing effect is more evident with PMF at 40μg/ml (Fig.6.4). No live cells were detected in the 5 min irradiated samples after irradiation and for the following 3 weeks. For the 3,5 and 7 min irradiated samples cell survival immediately after irradiation was about 1% and 0% 24 hours after Regrowth of the cells though is observed after the first week. At the end of the culture all samples contain live cells. This means that not all cells were killed during irradiation. Few survived and after a period of time they proliferated to give a measurable number of cells. Complete killing of cells is not achieved with 40μg/ml of PMF.

Number of cells (%)	3 min	5 min	7 min	Control
Before irradiation	100 ± 12.08	100±12.85	100 ± 12.23	100±15.60
After irradiation	0,24 ± 0,17	0 ± 0	0 ± 0	80,42 ± 12.99
24 hours	0 ± 0	0 ± 0	0 ± 0	117,56 ± 14.23
1st week	0 ± 0	0 ± 0	0 ± 0	96,34 ± 21.30
2nd week	0 ± 0	0 ± 0	0 ± 0	78,40 ± 14.40
3rd week	0 ± 0	0 ± 0	0 ± 0	79,78 ± 26.45
4th week	0 ± 0	0 ± 0	0 ± 0	69,62 ± 28.93

Table 6.3: PDT results of 50µg/ml of PMF extract on HL-60 cells

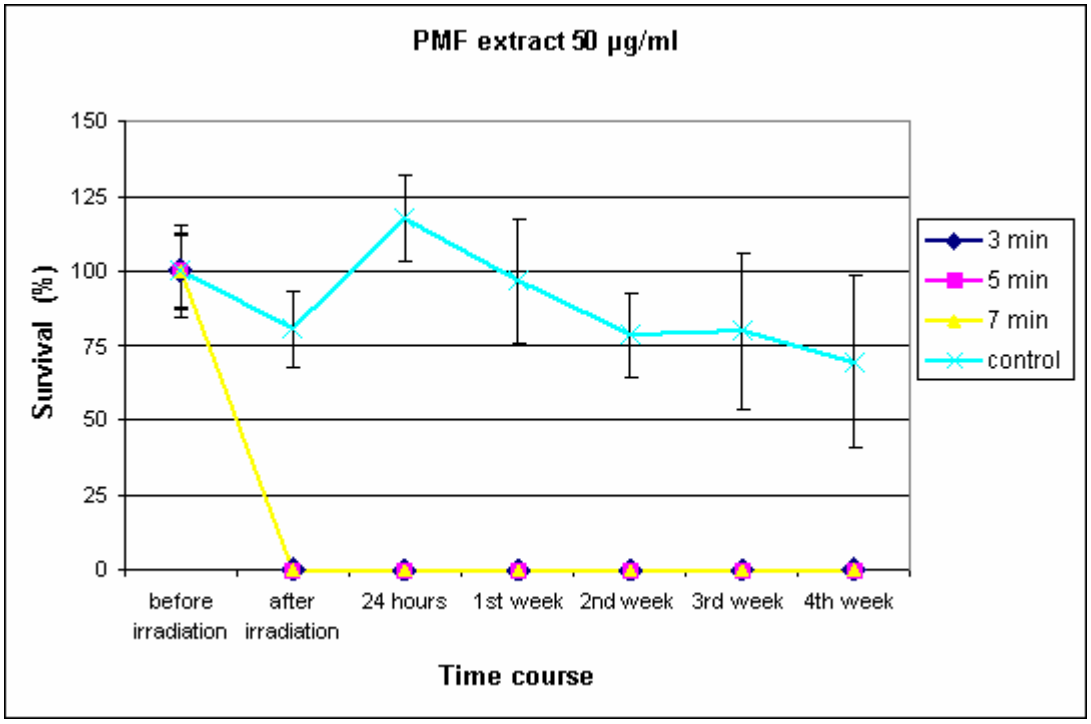

Figure 6.5: Survival of HL-60 cells after PDT with 50µg/ml of PMF extract at 4W

The killing effect of 50µg/ml of PMF is shown in Fig.6.5. Cell survival is 0% immediately after irradiation and remains 0% until the end of the culture for all times of irradiation. Complete killing of cells is achieved with 50µg/ml of PMF.

Number of cells (%)	3 min	5 min	7 min	Control
Before irradiation	100 ± 5.67	100 ± 8.44	100 ± 13.93	100 ± 11.76
After irradiation	0,24 ± 0,23	0 ± 0	0 ± 0	97,17 ± 11.82
24 hours	0 ± 0	0 ± 0	0 ± 0	116,28 ± 20.03
1st week	0 ± 0.23	0 ± 0	0 ± 0	78,86 ± 22.67
2nd week	0 ± 0	0 ± 0	0 ± 0	47,64 ± 8.47
3rd week	0 ± 0	0 ± 0	0 ± 0	44,57 ± 25.05
4th week	0 ± 0	0 ± 0	0 ± 0	13,12 ± 5.53

Table 6.4: PDT results of 60μg/ml of PMF extract on HL-60 cells

Complete cell death is also observed when PMF is used at 60μg/ml (Fig.6.6). The cell survival is 0% after irradiation and until the end of the culture for all time intervals. Complete cell death should be expected since the same result was achieved with lower concentration of PMF. These results though confirm that the concentration of 50μg/ml of PMF is the optimal for the eradication of HL-60 cells with PDT.

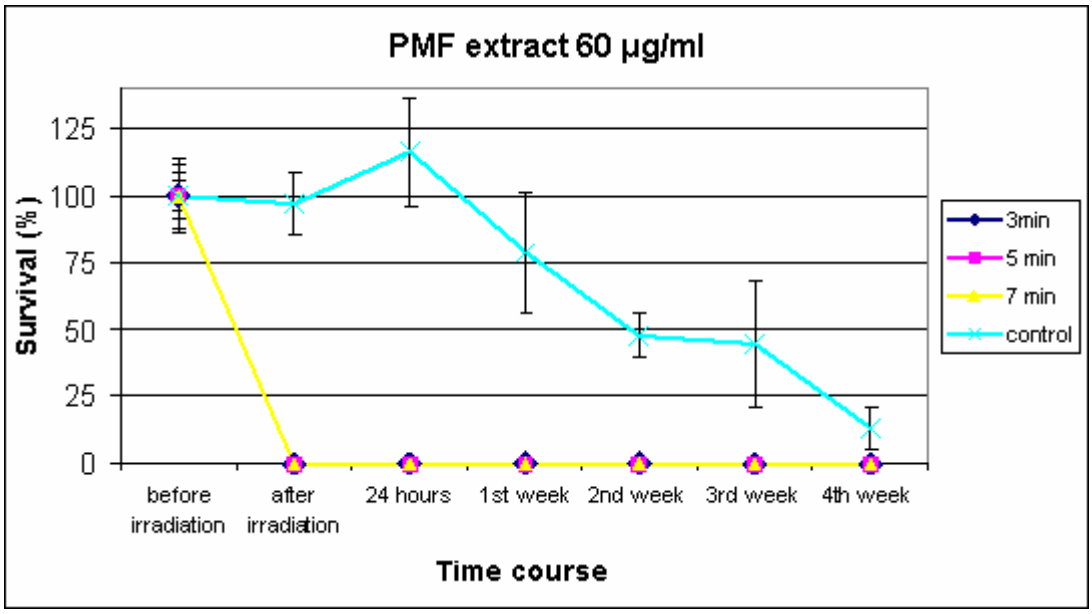

Figure 6.6: Survival of HL-60 cells after PDT with 60μg/ml of PMF extract at 4W

The survival of the control samples at the end of the culture varies and no cell growth is observed after 4 weeks of culture. This is due to the fact that no optimal culture conditions were applied for these cells as the amount of culture media –RPMI- added was not enough for the logarithmic growth of the cells of the control sample but only sufficient for their survival.

In conclusion, 50μg/ml of PMF and 3 minutes of irradiation with the laser are the optimum parameters in order to achieve complete death of HL-60 cells.

6.3 PDT with the ME extract

The parameters of PDT with the ME extract were investigated. The concentrations of 30, 40, 50, and 60μg/ml were used for 3, 5 and 7 minutes of irradiation. The number of samples is n=6

Number of cells (%)	3 min	5 min	7 min	Control
Before irradiation	100 ± 8.34	100 ± 17.43	100 ± 21.11	100 ± 17.84
After irradiation	20.58 ± 6,94	0.31± 0.34	0 ± 0	182.72 ± 59.3
24 hours	1.07 ± 6.20	0 ± 0	0 ± 0	160.0 ± 30.44
1st week	3.21 ± 0.62	0 ± 0	0 ± 0	150,1 ± 37.21
2nd week	99.46 ± 25,93	0 ± 0	0 ± 0	34.81 ± 11.38
3rd week	57,75 ± 6,17	0 ± 0	0 ± 0	68.63 ± 35.95
4th week	8.02 ± 1.54	67.39 ± 5.12	29.57 ± 17.07	16.81 ± 8.13

Table 6.5: PDT results of 30μg/ml of ME extract on HL-60 cells

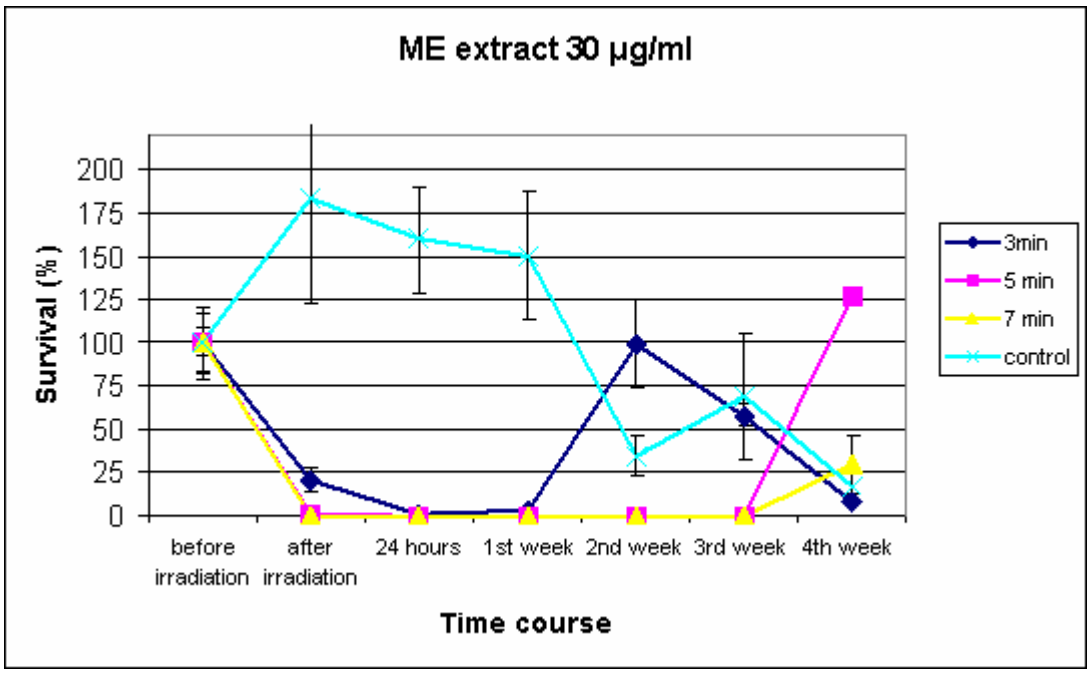

Figure 6.7: Survival of HL-60 cells after PDT with 30μg/ml of ME extract at 4W

There is no cell survival immediately after irradiation for the 5 and 7 min irradiated samples until the third week (Fig.6.7). For the 3 min irradiation sample the survival is 20% after irradiation and the cells regrow at the second week. At the end

of the culture, the fourth week, live cells are present in all samples. Complete cell death is not achieved and this is result is similar to the one observed when the same concentration of PMF extract was used in the PDT experiment

Number of cells (%)	3 min	5 min	7 min	Control
Before irradiation	100 ± 8.64	100 ± 16.06	100 ± 19.44	100 ± 20.23
After irradiation	6.58 ± 3,11	4.51 ± 1.73	0 ± 0	96.58 ± 12.33
24 hours	0 ± 0	0 ± 0	0 ± 0	171.79 ± 18.25
1st week	0 ± 0	0 ± 0	0 ± 0	122.3 ± 24.13
2nd week	23.35 ± 3.11	11.27 ± 3.91	0 ± 0	22.47 ± 4.78
3rd week	153.3 ± 38.72	64.66 ± 6.07	0 ± 0	64.52 ± 33.8
4th week	50,90 ± 12.1	48.87 ± 17.37	160.52 ± 7.6	48.29 ± 26.4

Table 6.6: PDT results of 40µg/ml of ME extract on HL-60 cells

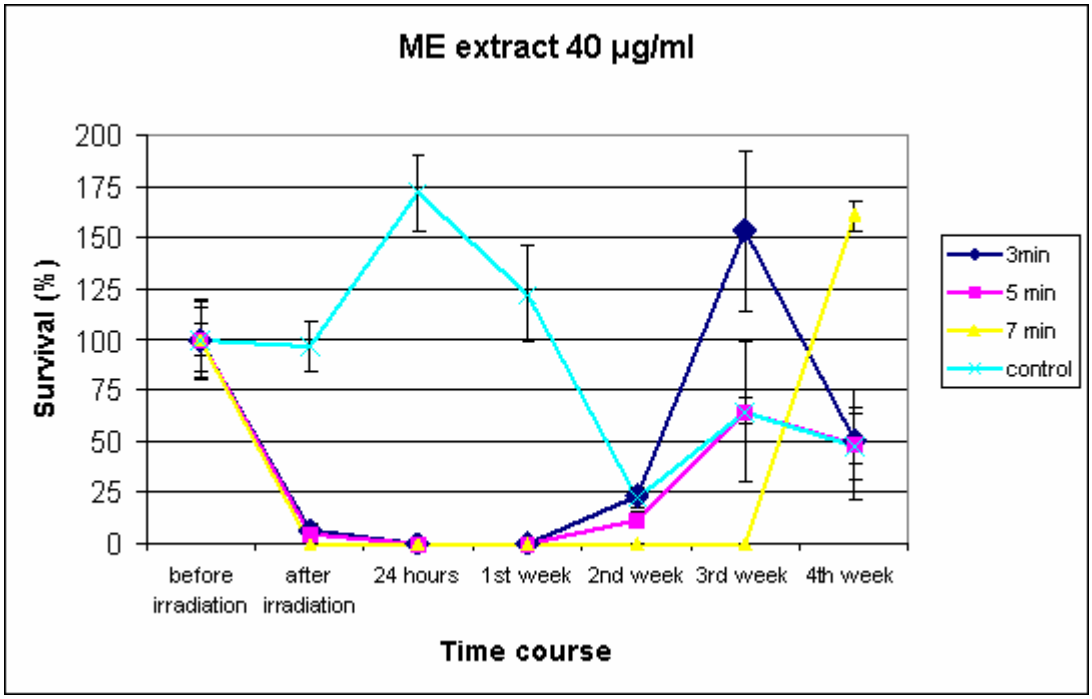

Figure 6.8: Survival of HL-60 cells after PDT with 40µg/ml of ME extract at 4W

The cell survival is 0% for all samples after 24 hours. Cell regrowth is observed the second week for the 3 and 5 min irradiated samples. At the end of the culture cells have recovered for all times of irradiation. Complete cell death with 40µg/ml of ME has not been achieved. This result is similar to the one observed when the same concentration of the PMF extract was used in the PDT experiment.

Number of cells (%)	3 min	5 min	7 min	Control
Before irradiation	100 ± 8.99	100± 3.99	100± 3.87	100 ± 4.47
After irradiation	0 ± 0	0 ± 0	0 ± 0	89,77 ± 6.23
24 hours	0.11 ± 0.11	0 ± 0	0 ± 0	135,37 ± 14.32
1st week	0 ± 0	0 ± 0	0 ± 0	60.39 ± 5.51
2nd week	0 ± 0	0 ± 0	0 ± 0	23.61 ± 8.71
3rd week	0 ± 0	0 ± 0	0 ± 0	11.84 ± 5.6
4th week	0 ± 0	0 ± 0	0 ± 0	3.78 ± 2.71

Table 6.7: PDT results of 50μg/ml of ME extract on HL-60 cells

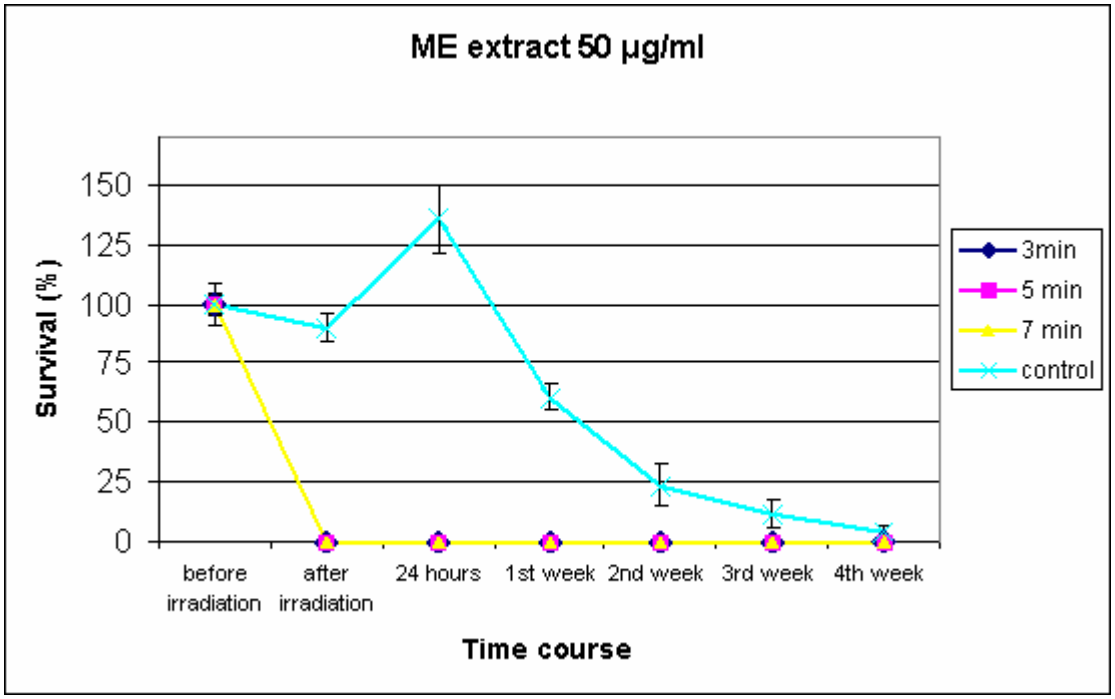

Figure 6. 9: Survival of HL-60 cells after PDT with 50μg/ml of ME extract at 4W

Immediately after irradiation cell survival is 0% for all samples and remains 0% until the end of the culture (Fig. 6.9). Complete cell death is achieved when 50μg/ml of ME extract is used. and the samples are irradiated for three minutes or equivalently when a 74,9 J/cm^2 energy dose is used. This result is similar with the results when the same PDT conditions as with the PMF extract are applied.

Number of cells (%)	3 min	5 min	7 min	Control
Before irradiation	100 ± 3.91	100± 1.85	100± 1.49	100± 4.42
After irradiation	0 ± 0	0 ± 0	0 ± 0	75.14 ± 8.41
24 hours	0 ± 0	0 ± 0	0 ± 0	159,28 ± 17.89
1st week	0 ± 0	0 ± 0	0 ± 0	82.63 ± 13.99
2nd week	0 ± 0	0 ± 0	0 ± 0	22.45 ± 1.27
3rd week	0 ± 0	0 ± 0	0 ± 0	21.55 ± 6.39
4th week	0 ± 0	0 ± 0	0 ± 0	10.77 ± 1.46

Table 6.8: PDT results of 60μg/ml of ME extract on HL-60 cells

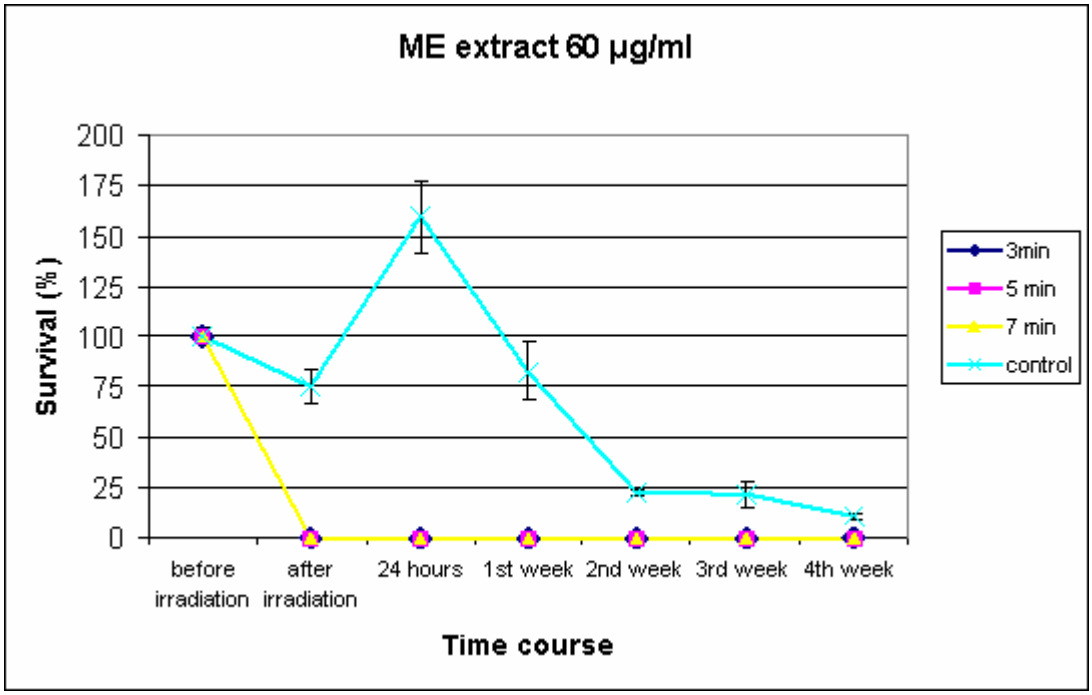

Figure 6.10: Survival of HL-60 cells after PDT with 60μg/ml of ME extract at 4W

Cell survival is 0% immediately after irradiation for all samples (Fig.6.10). The cells do not recover until the end of the culture. Complete cell death is achieved for all time intervals for PDT with 60μg/ml of ME.

As with the PDT experiments in the presence of PMF the survival of the control samples at the end of the culture varies and no cell growth is observed after 4 weeks of culture due to the culture conditions used.

The minimum concentration of ME required for complete cell death is 50μg/ml and the minimum irradiation duration is 3 minutes or 74.9 J/cm^2 of energy dose. These optimum parameters for achieving complete cell death with ME are similar with those of the PMF extract.

6.4 PDT with Hypericin

In order to compare the photodynamic effect of pure hypericin with that of PMF and ME extracts under the same parameters, Hypericin (Purity >98%) obtained by AG Scientific was used as sensitizer. The sensitizer dose was selected to correspond to the same amount of hypericin present in 50μg of PMF and was found to be 0,7μg. The 3, 5 and 7 minutes irradiation were tested. The number of samples is n=9

Number of cells (%)	3 min	5 min	7 min	Control
Before irradiation	100 ± 5.22	100± 4.54	100± 4.5	100± 4.2
After irradiation	0 ± 0	0 ± 0	0 ± 0	89.32 ± 9.32
24 hours	0 ± 0	0 ± 0	0 ± 0	147,21 ± 12.92
1st week	0 ± 0	0 ± 0	0 ± 0	81.61 ± 13.7
2nd week	0 ± 0	0 ± 0	0 ± 0	21.7 ± 8.78
3rd week	0 ± 0	0 ± 0	0 ± 0	9.31 ± 3.54
4th week	0 ± 0	0 ± 0	0 ± 0	5.11 ± 2.43

Table 6.9: PDT results of Hypericin on HL-60 cells

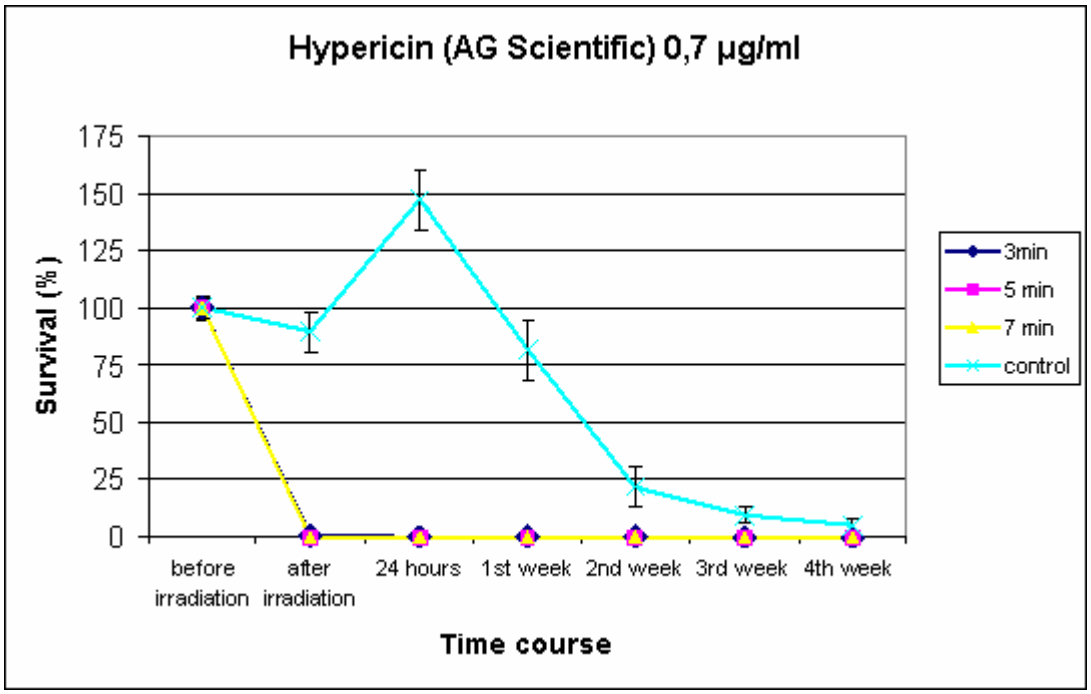

Figure 6.11: Survival of HL-60 cells after PDT with 0.7μg/ml of Hypericin at 4W

Complete cell death is achieved with 0.7μg/ml of Hypericin for 3, 5 and 7 minutes of irradiation (Fig.6.11) the same result with that of the PMF and ME

extracts. It is therefore suggested that the photoactive compound of the *Hypericum Perforatum L* extracts is hypericin.

6.5 PDT with PMF extract on hemopoietic progenitor cells

6.5.1 Cord Blood cells

After the establishment of optimum PDT experimental conditions for effective killing of leukemic cells, the same experiments were repeated with normal hemopoietic progenitors of cord blood in order to examine if PMF and/or ME extracts are selective uptaken by leukemic cells as it has been reported to be the case when MC 540 was used as photosensitizer [64].

Cord blood mononuclear cells were irradiated for 3 min in the presence of 30μg/ml PMF and for 5 minutes in the presence 50μg/ml PMF. In parallel the effect of PMF extract only on the normal hemopoietic progenitors was determined in PDT experiments in the presence of either 30μg/ml PMF or 50μg/ml PMF without irradiation. The number of samples is n=9.

	BFU-E	CFU-GM
Control No PMF, no Laser	321,58 ± 50,82	201 ± 40,5
PMF 30μg/ml 3 min	0,08 ± 0,08	1,67 ± 1,12
PMF 30μg/ml only	301,5 ± 60,69	216 ± 46,79
PMF 50μg/ml 5 min	0	0
PMF 50μg/ml only	259,8 ± 46,31	192 ± 37,16

Table 6.10: PDT effect in the presence of PMF extract on the development of Cord Blood progenitors

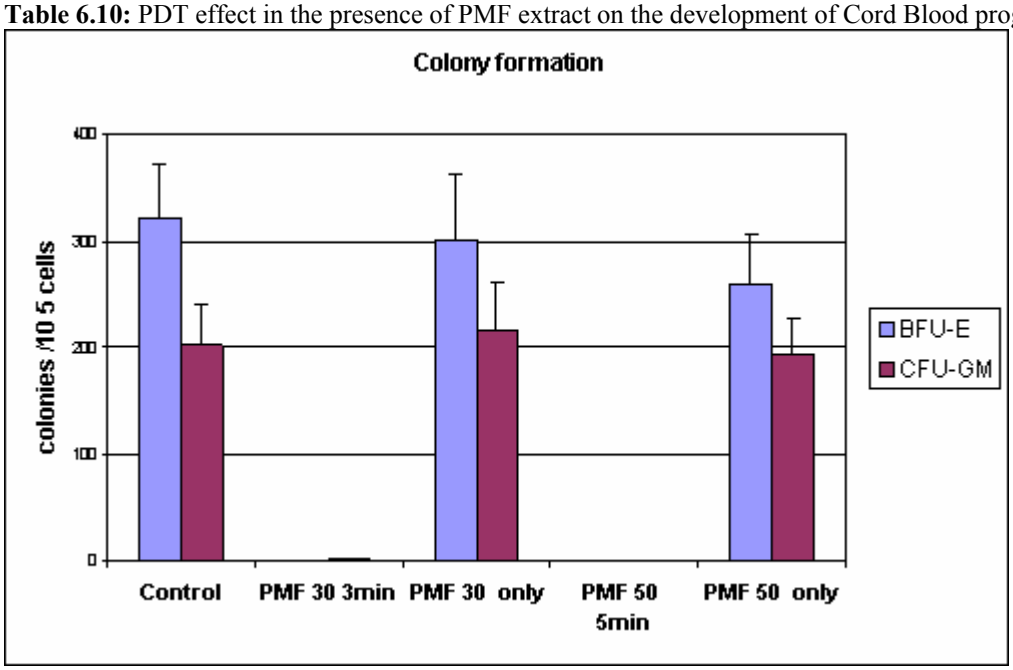

Figure 6.12: Results of PDT on Cord Blood progenitors with 30μg/ml and 50μg/ml of PMF extract

PMF exerts a cytotoxic effect on cord blood progenitors even under conditions which are not toxic for HL-60 leukemic cells (Fig. 6.12). No colonies were developed when cells were treated with 50μg/ml PMF and irradiated for 5 min. Samples treated with 30g/ml of PMF and irradiated for 3 min formed an extremely low number of colonies. No effect on the survival of cord blood progenitors was observed when cells were treated with PMF only.

6.5.2 Bone Marrow cells

The photodynamic effect of the PMF extract on bone marrow mononuclear cells from a patient with acute leukemia in remission was also examined. The PMF concentration was 50μg/ml and the light dose was 74.9J/cm^2 and 124.8 J/cm^2 -3 and 5 minutes of irradiation respectively.

	BFU-E	CFU-GM
Control	214 ± 5	159 ± 19
3 min	0	0
5 min	0	0
PMF only	45 ± 5	83 ± 12

Table 6.11: PDT results of 50μg/ml of PMF extract on Bone Marrow progenitor cells

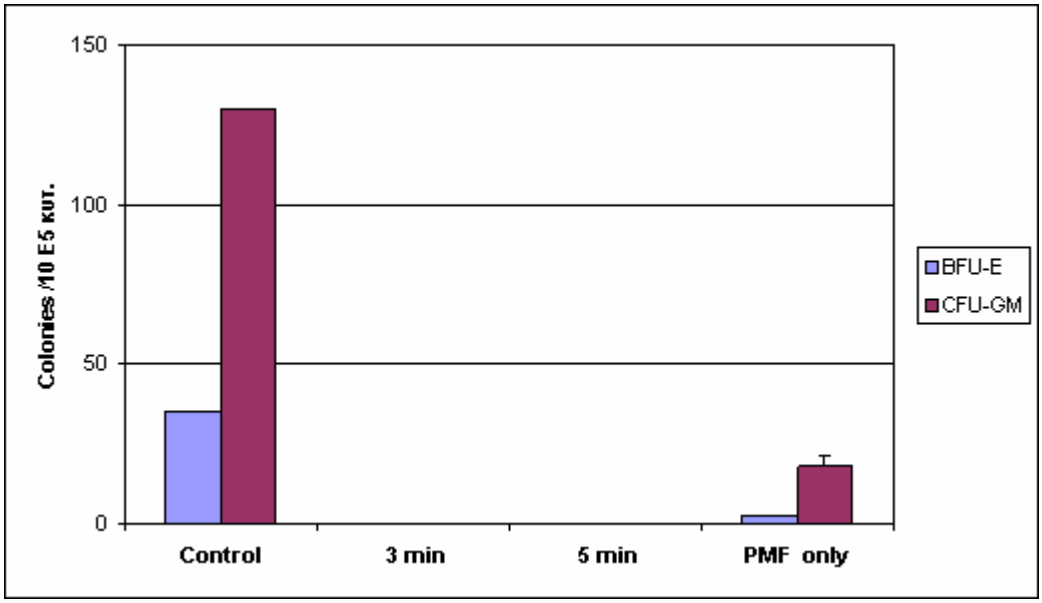

Figure 6.13: Results of PDT on Bone Marrow cells with 50μg/ml of PMF extract at 4W.

According to our results (Fig. 6.13) no colonies developed in the irradiated samples. In samples treated with PMF only, a decreased -compared to the control - colony growth was observed.

6.6 Conclusions

PMF and ME exert the same cytotoxic effect on leukemic cells during PDT. PMF could be the choice since it is easier to handle.

Complete cell death is achieved with the addition of 50μg/ml of both sensitizers for irradiation times of 3, 5 and 7 minutes. The concentrations of 30μg/ml and 40μg/ml of both PMF and ME are not enough to completely eradicate the leukemic cells. It therefore suggested 50μg/ml as the optimum concentration of sensitizer and 74.9 J/cm^2 as the optimum light dose.

The PDT effect in the presence of pure Hypericin is identical with that of the extracts.

PDT with PMF results in the killing of normal hemopoietic progenitors of either cord blood or bone marrow. It is profound that *Hypericum Perforatum L* extracts are not selectivity uptaken by leukemic cells and they exert their cytotoxic effect in any kind of hemopoetic cell under the same experimental conditions. Though this suggests that PDT/ PMF cannot be helpful in autologous bone marrow purging, PMF can however be beneficial in the PDT treatment of tumors.

7. Microscopy results

As stated in the photobiology section the localization of the sensitizer is very significant as it determines the effect of the excited sensitizer to the cell. Microscopy techniques such as confocal microscopy and non linear microscopy were used to examine the subcellular localization of the PMF extract and MC 540. Confocal microscopy is a high resolution technique and provides information on where the sensitizers are localized in two dimensions and indirectly in three dimensions. The incubation parameters were those of the photodynamic therapy protocol -1 hour incubation and 3×10^6 cells/ml concentration- since the localization of the sensitizers just before the irradiation were of interest.

7.1 Confocal Microscopy

7.1.1 Localization of PMF extract and Hypericin

The PMF extract localization was investigated after incubation of HL-60 cells with 50μg/ml of the extract and excitation with the He-Ne laser line 543nm. Fluorescence first appears at the upper part of the cell and disappears at its lower part. Therefore we get approximately the diameter of the cell by measuring the fluorescence signal in the z direction In Fig 7.1. the z distance scanned is 8μm. The periphery and areas inside the cell are stained. This figure is the projection of all the sections scanned in one picture.

The fluorescence signal was not strong enough so for the following stainings the amount of PMF was doubled to 100μg/ml.

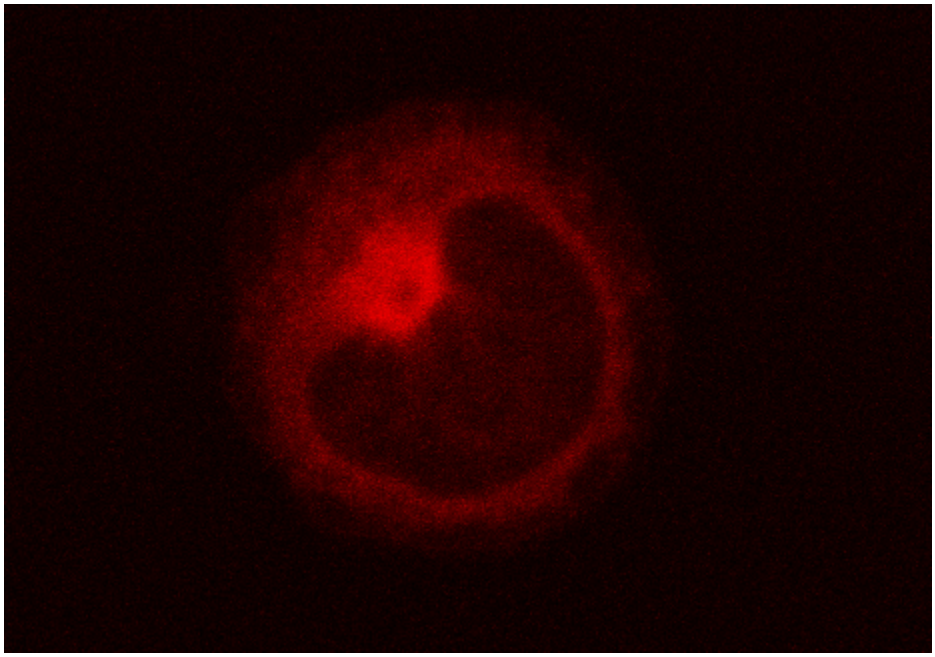

Figure 7.1: Cell stained with PMF. The cell was scanned with an objective lens (40x) with 1.3 NA (numerical aperture). The overall magnification was 400x as the 10x lens is standard on the microscope. The image was further digitally enlarged by a factor of 4.1x.

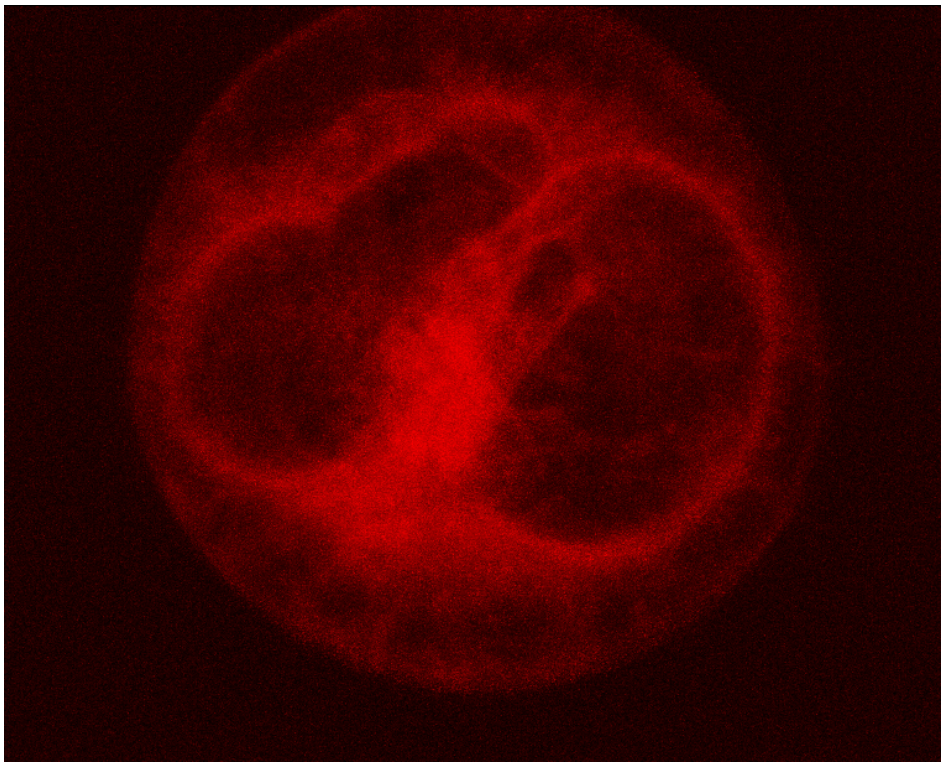

Figure 7.2: The projection of all sections scanned in one picture of a cell stained with PMF (100µg/ml).
Cell diameter 13µm. Optical magnification 400x and digital magnification 5x.

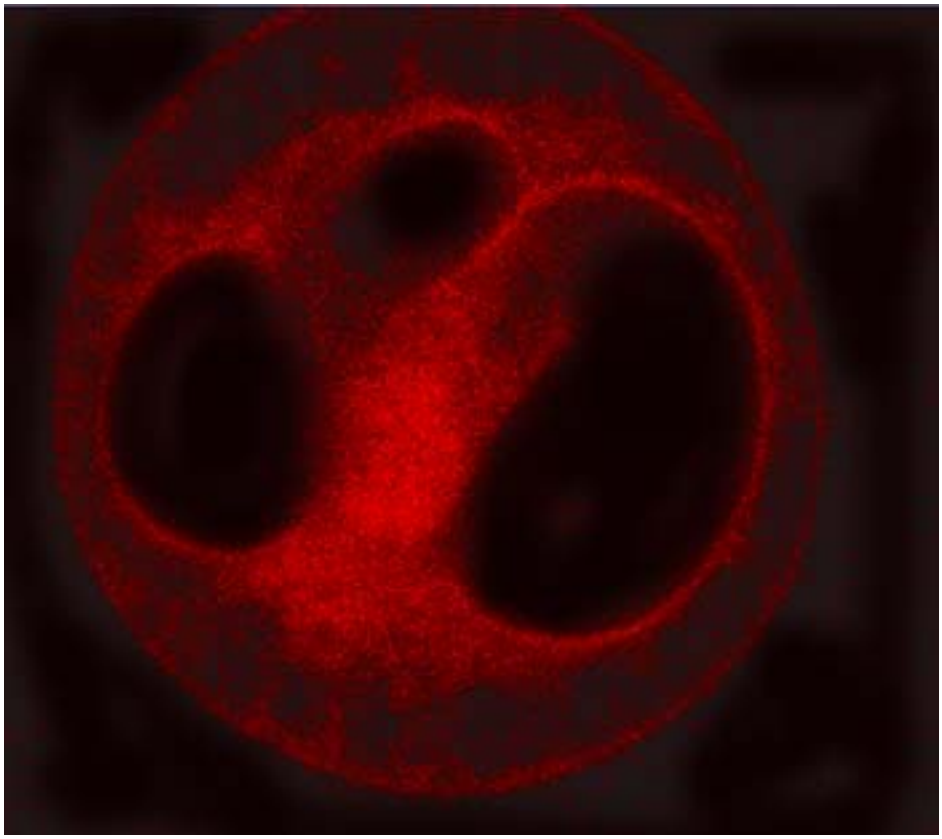

Figure 7.3: A section of the cell of Fig. 7.2

Figs. 7.2 and 7.3 represent the same cell stained with 100μg of PMF. The first figure is the projection of all sections scanned in one. Intense fluorescence on the periphery of the cell and the periphery of its nucleus can be interpreted as that hypericin of the PMF extract is localized on the cellular and nuclear membrane. Lower signal appears in the cytoplasm except from a region in the center of the cell. The same observations can be made also for Fig. 7.3 which is a section of the cell. What's new in Fig. 7.3 is that two dark regions appear. These dark regions is the nucleus which is folded. Intense fluorescence signal appears in the folding of the nucleus where the cytoplasm is concentrated. Organelles such as endoplasmic reticulum and Golgi are usually localized near the nucleus and they are consisted of membranes. It is possible that hypericin is localized on these membranous organelles.

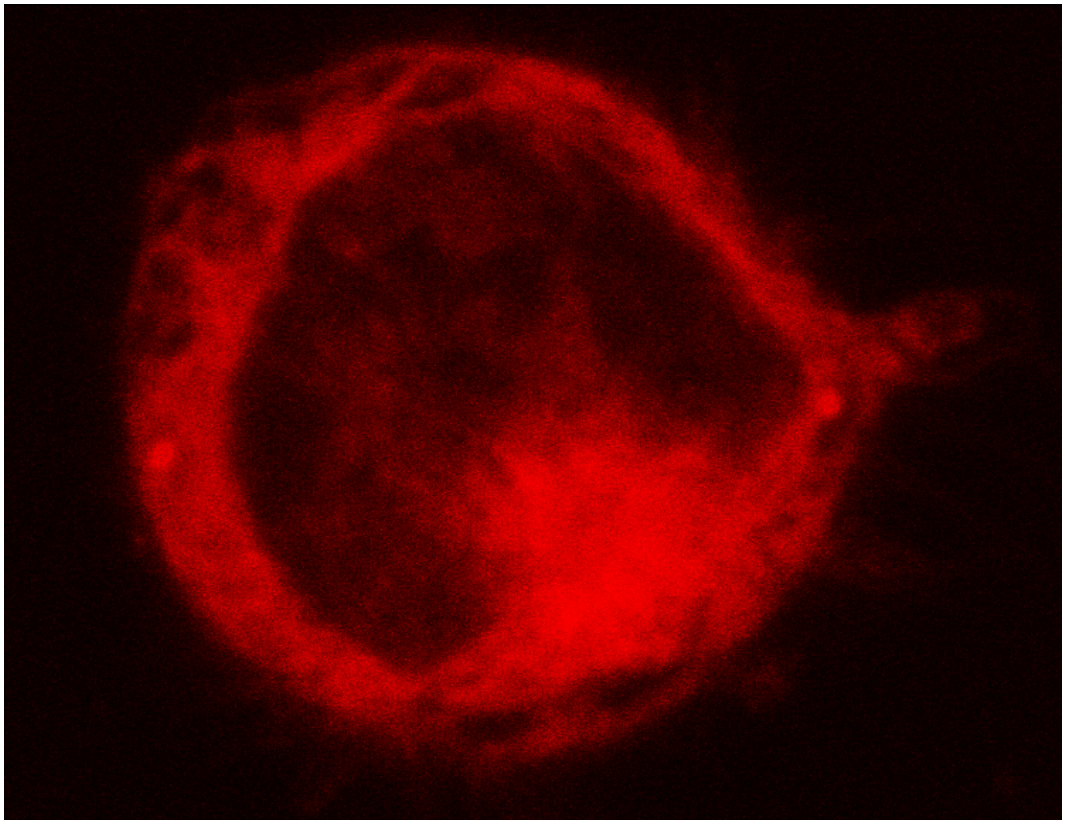

Figure 7.4: The projection of all sections scanned in one picture of a cell stained with PMF (100µg/ml).
Cell diameter 8,5µm . Digital magnification 6.5x.

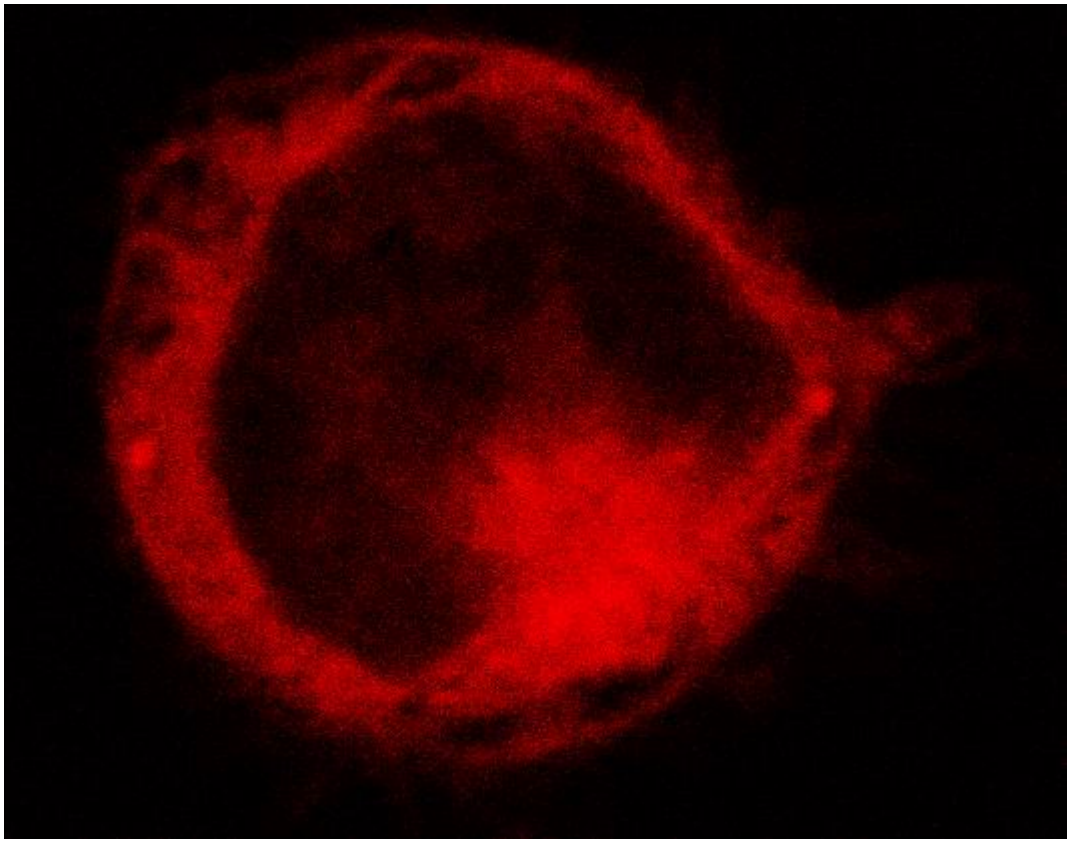

Figure 7.5: A section of the cell in Fig. 7.4 stained with PMF

One more set of Fig. 7.4 and 7.5 with another cell stained with 100μg of PMF. Again the first figure is the projection of all sections into one. Cell membrane, nuclear membrane and cytoplasm are stained. In figure 7.5 the nucleus is seen as one big dark region. In the lower part of the figure part of the cytoplasm has a stronger signal. This might be the region where endoplasmic reticulum and Golgi are localized The cell membrane though in this set of pictures is not clearly stained as in figures 7.2 and 7.3.

Finally in Fig. 7.6 cells stained with 10μg of pure hypericin (AG Scientific) are shown. The signal is much stronger compared to that of the cells stained with PMF. The localization pattern though is similar to the PMF stained cells.

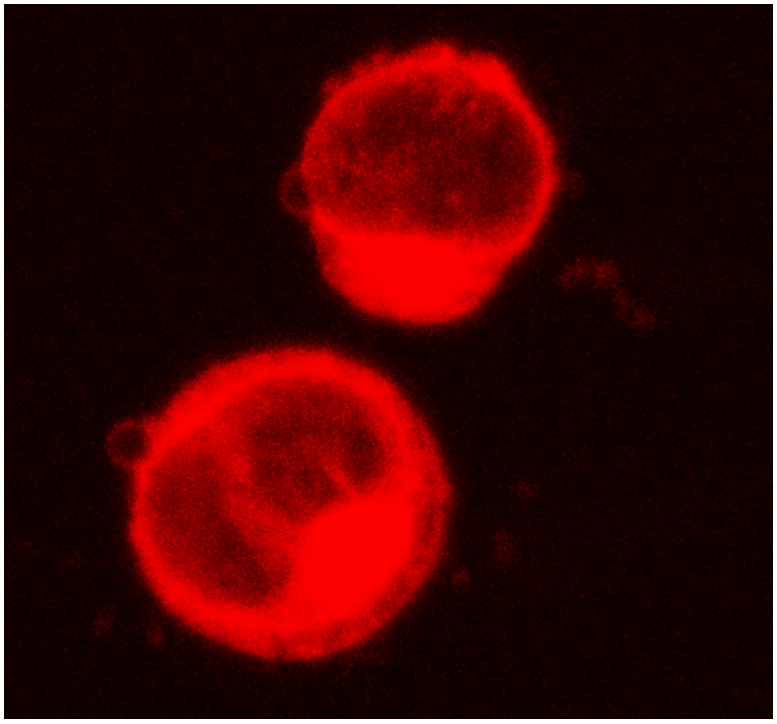

Figure 7.6: Cells stained with pure hypericin (10μg/ml). Digital zoom 3.9x

7.1.2 Localization of MC 540

The localization of MC 540 in the cell was examined. For this purpose 20μg of MC540 were added in 1ml of cell suspension. Fluorescence is seen on cell membrane and a stronger signal appears when the cells are in contact since their membranes are parallelized and their effective surface is greater.

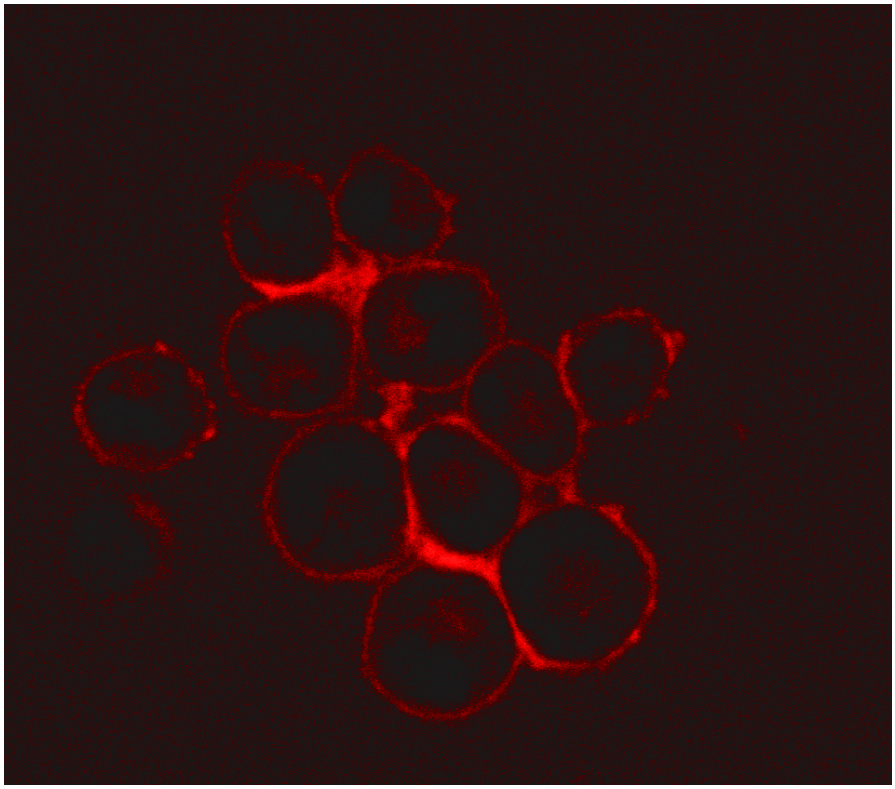

Figure 7.7: A group of cells stained with MC 540 (20µg/ml). Optical magnification 400x.

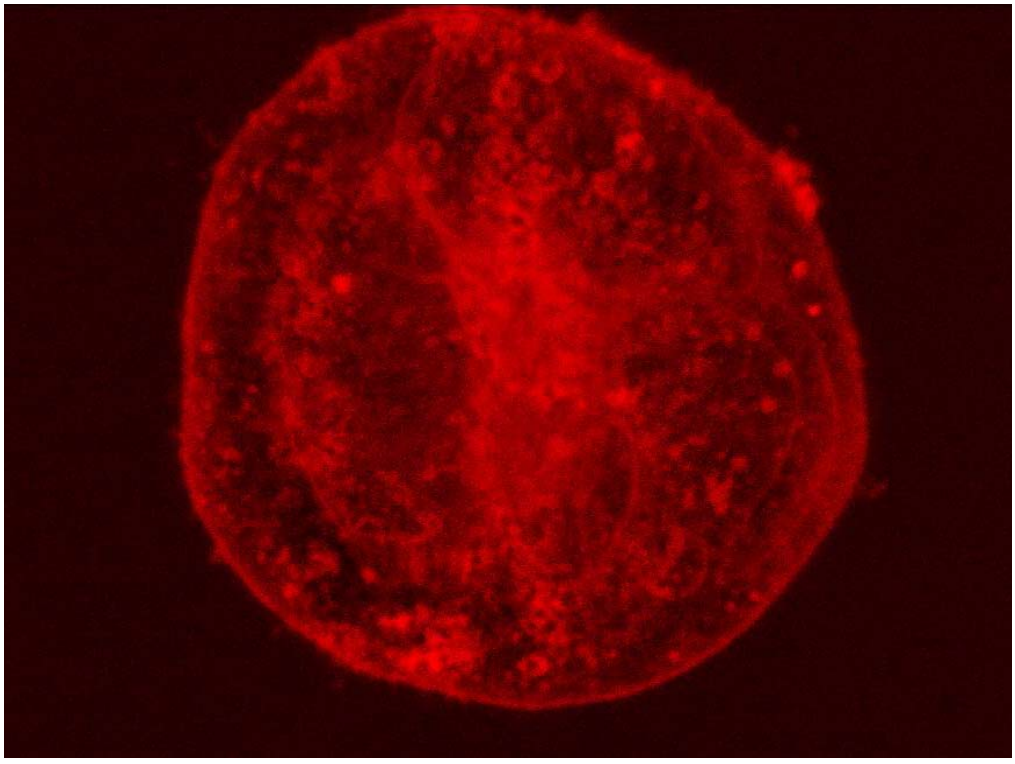

Figure 7.8: Projection of all the sections scanned of a cell stained with MC540 (20µg/ml). Diameter of the cell ~ 12µm. Digital zoom 4.7x.

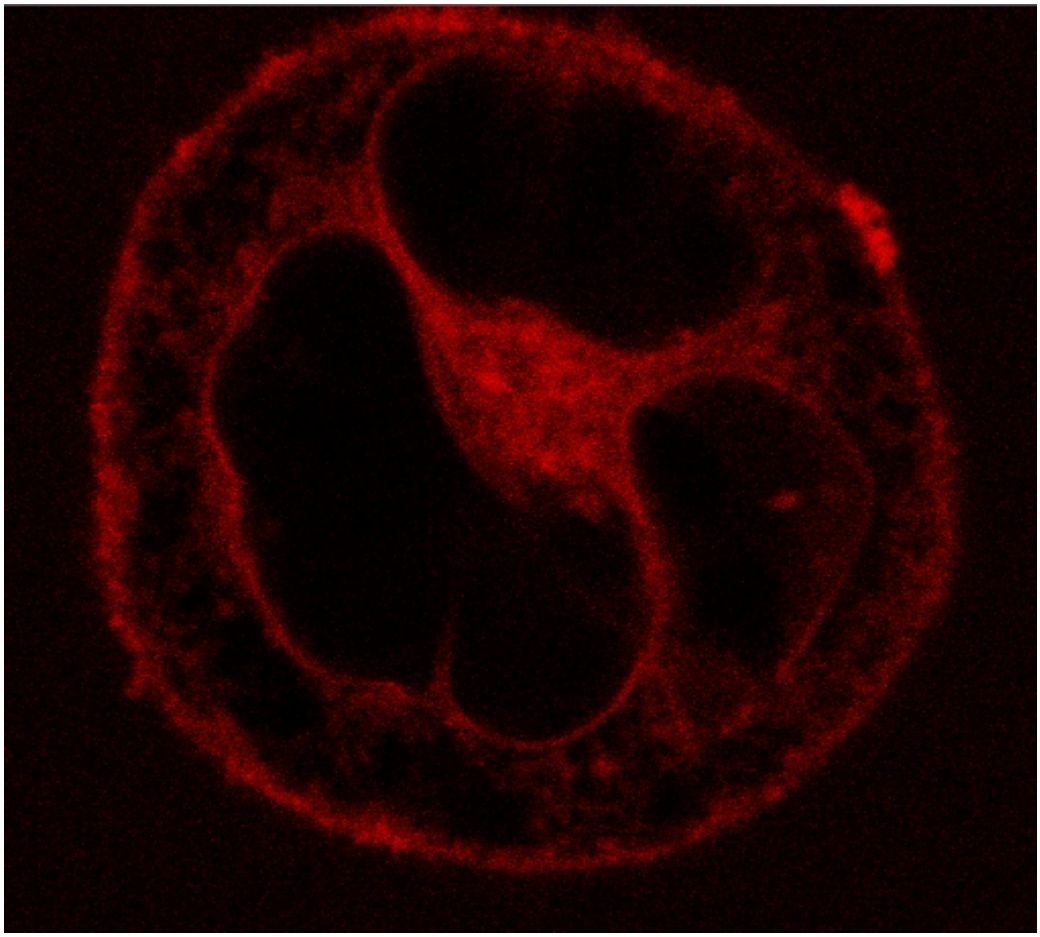

Figure 7.9: A section of the cell shown in Fig. 7.8

In Figs. 7.8 and 7.9 the staining of a single cell with MC 540 is shown. In Fig. 7.8 it appears that the whole cell is stained due to the projection of the round cell the membrane of which is stained giving the impression that the cell is totally stained. Sites in the cell with greater fluorescence –small red dots- can be observed. The 'equator' section of this cell in Fig. 7.9 gives a clearer insight. The chromophore doesn't stain the nucleus, which is the dark area inside the cell. One can see the staining of the cell and the nuclear membranes. The cytoplasm is not stained as strongly as the membranes except for region in the center of the cell. This region is very close to the nucleus.

7.1.3 Conclusions

Both chromophores PMF and MC 540 do stain HL-60 cells. The staining is obvious and reproducible. PMF stains the cell membrane, the nucleus membrane and the cytoplasm. As far as the cytoplasm is concerned it appears that some regions near the nucleus are more stained than others. It is hypothesize that membranous

organelles located near the nucleus, such as the endoplasmic reticulum and Golgi are possible sites of localization for hypericin. The same observation accounts for pure hypericin too. The areas of MC 540 localization is similar, with strong staining in the cell and nuclear membranes and in parts of the cytoplasm. These results for hypericin [124-126] and MC 540 [65,66] are in accordance with previous works.

The staining patterns, though, appear to have some differences. As is shown in Fig. 7.8, which are the projections of the sections scanned in one picture, the staining with MC 540 seems to be homogenous in the cell even though from the sections (Fig. 7.9) it is known that this is not true. However, in Fig. 7.2 and 7.4, where the projections of cells stained with PMF appear, the staining does not seem to be homogenous. Even in the projection the major components of the cell, cell membrane, nucleus and cytoplasm are distinguished. One reason for this difference might be that MC 540 is localized more efficiently on the cell membrane than PMF. This could also suggest that PMF and therefore, hypericin is not a molecule that binds very strongly to membranes but rather diffuses into the cytoplasm. The diffusion hypothesis can be also verified by the fact that the fluorescence signal of MC 540 in the cytoplasm is lower than that of PMF. This observation can be very well correlated with the fact that hypericin has not been found to accumulate in the mitochondria membranes [88]. However, it is known that hypericin can impair mitochondria function [126-128], which could be explained if we consider that having a diffused pattern along the cytoplasm it is often in close and effective proximity to these organelles.

In order to exactly determine the localization of hypericin experiments with the use of special markers for the various cell organelles should be carried out.

7.2 Two Photon Excited Fluorescence

We also investigated the localization of PMF and MC 540 with non linear microscopy. Their two photon fluorescence was measured. The resolution though of this microscope is lower compared to confocal. Even though an objective lens of higher magnification was used (100x, NA 1.25), its NA was lower compared to the 1.3 NA of the confocal objective and the results were poorer. The non linear microscope employs a step motor for the scanning, in contrast to the scan head of the confocal, and its step is 1μm limiting thus its lateral resolution to that dimension when

the lateral resolution of the confocal is around 300nm. Clear observations about the localization of sensitizers can not be made. Only rough estimations can be made.

7.2.1 Localization of PMF extract

For the staining 100μg of PMF was used. The scanning was made with 1μm step and the Edmund Scientific (100x, NA 1.25) oil immersion objective lens was used. In Fig. 7.10 we see a section of a cell. In Fig. 7.10.a) every pixel represents one datum. In fig 7.10.b) we see the same section of the cell but the data are fitted to contour lines. In 7.10.a) by counting the pixels we can assume that the diameter of the cell is around 15μm. As far it concerns the localization of the sensitizer two regions can be distinguished, one bigger region in the lower part of the picture and one smaller in the upper part. These regions must be parts of the cytoplasm. The lower region might be where endoplasmic reticulum is localized. In the center of the cell a darker region appears and it must be the nucleus.

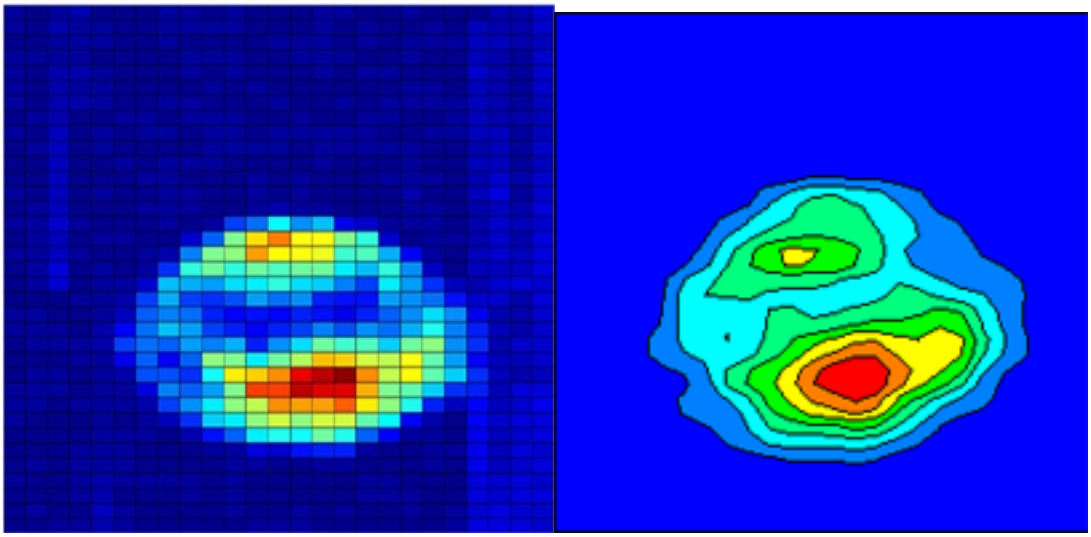

a b

Figure 7.10: A cell stained with PMF. a) Every point of measuring is represented by a pixel b) The same cell with the data fitted in contour lines

7.2.2 Localization of MC 540

Cells with 20μg of MC 540 were stained. The 100x objective was used. The diameter of the cell as defined by its fluorescence is around 15μm. In Fig. 7.11 we see two distinct fluorescing regions which must correspond to the cytoplasm. Also two darker regions can be distinguished which must correspond to the nucleus.

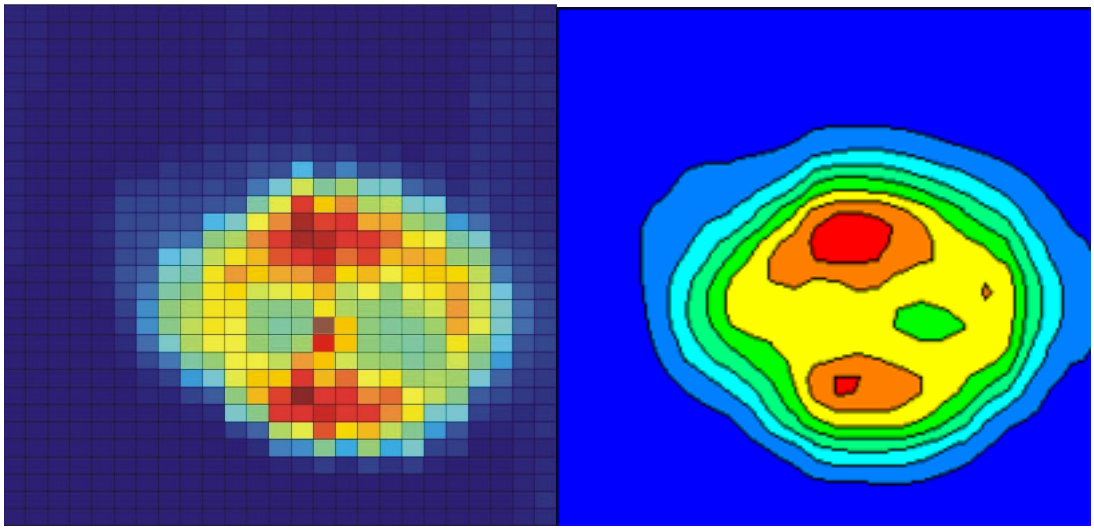

a b

Fig 7.11: A cell stained with MC 540. a) Every datum is represented by a pixel b) The same section of the cell with the data fitted in contour lines

We also investigated the optical sectioning capability of the non linear microscope. For this reason we used MC 540 as it exhibits a more distinct profile than PMF in different sections. This time we used a Nikon (50x, 0.8 NA) objective lens. The cell selected had approximately 15μm diameter. We scanned three sections with 7 μm distance in the z axis between them. In Fig. 7.12.a) which is the upper part of the cell we see two photon fluorescence arising from the center. This fluorescence is owed the cell membrane which we know that MC 540 stains. In Fig. 7.12.b) we see the middle section of the cell. The fluorescence has shifted to the left of the cell. From cell anatomy we know that the nucleus is in the center of the cell. So, fluorescence arises from the cytoplasm which is constrained between the nucleus and the cell membrane. In the final section from the lower part of the cell in Fig. 7.12.c fluorescence is appears at the center. Again fluorescence is owed to MC 540 molecules bound to the cell membrane.

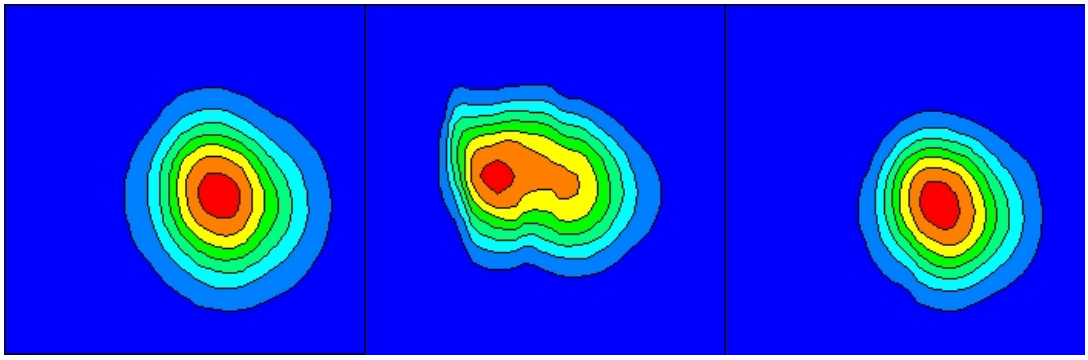

a b c

Fig 7.12: Section of a cell stained with MC 540 a) upper section b) midlle section c) lower section. The shift of fluorescence from the center of the cell to the left and again to the center as the scanning level in the z axis changes can be seen.

Comparing this non linear microscope sectioning with the confocal sectioning we can find similarities but also differences. The important feature is that we observe distinctions in the various sections as with the confocal microscope. In the middle section in Fig 7.12.b we see the fluorescence shifting away from the nucleus and closer to the membrane. This was observed also in confocal images in figure 7.8. But the strong fluorescence arising from the periphery of the cell was not observed as it was observed in confocal images.

Finally we should mention that we investigated the possibility of measuring SHG in cells stained with MC 540. We know that MC 540 is an asymmetric molecule and binds on the cell membrane. The cell membrane is a very well organized lipid bilayer where MC 540 penetrates with its lipophilic region leaving its hydrophilic region outside. In this situation the molecules of MC 540 are specifically oriented providing the appropriate conditions for Second Harmonic Generation. SHG signal was not detected. The failure of the SHG imaging forced us to consider two possible explanations: First, the photosensitizer penetrates the cellular membrane thus having a small concentration of molecules bound on the membrane. Due to the small concentration, the SHG signal, produced by the MC 540 molecules, is not detectable. Second, it is very likely that the molecules that remain bound to the cellular membrane lack a global orientation, and therefore their SHG signal is negligible and not detectable.

7.2.3 Conclusions

The non linear images of the microscope used provide poorer imaging quality compared to the confocal. The lateral resolution in the non linear microscope is 1μm,

which is defined by the minimum step of the step motor, when the resolution of the confocal is around 0,3μm. Confocal has higher lateral and axial resolution. For this reason the confocal can resolve clearer the major components of the cell while the non linear microscope can provide us with rough estimations only. If an objective lens with higher NA and a step motor with smaller step were employed on this device the results could be improved. On the other hand the non linear microscope uses an IR beam which has higher penetration depth into the tissue and the photodamage and photobleaching are reduced as the excitation takes place only at the focal point. This comparison proves that the operation of the non linear microscope is correct and imaging of larger specimens could provide a much better quality.

8. Discussion – Future Plans

The properties of the PMF and ME extracts of *Hypericum Perforatum L* were studied in order to evaluate the substances as photosensitizers in the Photodynamic treatment for the purging of autologous bone marrow grafts. The spectrum characteristics as well as the localization of Hypericin were compared with those of MC 540 which has been successfully used as sensitizer in PDT of bone marrow cells. PMF was also compared with pure Hypericin available in the market in order to evaluate the cost -effect ratio.

PMF and ME extracts exhibit maximum emission corresponding to that of Hypericin. The fluorescence properties after the photodynamic irradiation in presence and in absence of cells for the PMF extract prove it to be very resistant to photobleaching. The comparison with MC 540 revealed that PMF extract is a very stable compound since in high energy doses (170 J/cm^2), in the presence of cells, fluorescence of PMF decreases 50% while MC 540 had no the fluorescence at all, suggesting that PMF extract is a very stable compound and can be used successfully for prolonged irradiation in procedures where required.

The photodynamic effect of PMF and ME extracts on both leukemic and normal hemopoietic progenitor cells were studied. The results were identical for both extracts. Different concentrations of the sensitizer and different energy doses were tested in order to define the optimal PDT conditions that will cause eradication of malignant cells without killing the normal ones. Under our experimental conditions the effective killing of HL- 60 leukemic cells was achieved in the presence of 50μg/ml extract and 75 J/cm^2 energy dose. Cord blood mononuclear cells as well as bone marrow mononuclear cells from a child with acute leukemia in remission were found to be equally sensitive to PMF mediated photolysis.

These results indicate that there is no preferential cytotoxicity of PMF mediated photoirradiation in neoplastic cells.

There was not noted any cytotoxic effect when Laser light or PME/ME extract alone were used. It was noted though that PMF extract was very toxic after prolonged incubation period. Since it has been reported that Hypericin which is the chromophore of the extract, has not be found to exhibit significant dark toxicity [76] other compounds present in the extract, and mainly flavonols and phloroglucinols which have been identified as cytotoxic [140], could have attributed to this effect. Therefore

improvement of the extracts and mainly extracts free of flavonols and phloroglucinols should be prepared and evaluated.

PDT carried out with pure hypericin exerted the same effect. This may suggest that the main photoactive compound of the PMF extract is hypericin.

In an attempt to explore the localization of the sensitizer confocal microscopy was employed. PMF was observed to stain the cytoplasm and the nuclear membrane while cell membrane was slightly stained. These observations suggest that PMF and therefore, hypericin is a molecule that does not bind very strongly to membranes but rather diffuses into the cytoplasm in accordance with previous reports [139]. Further microscopic investigations with special markers for the various cell organelles should be carried out in order to define the exact localization of PMF inside the cell. MC 540 on the contrary was found to bind more efficiently than PMF on the cell membrane and further accumulates on the cytoplasm and the nuclear membrane. Valinsky *et al.* [65] have reported that the initial site of accumulation of Merocyanine 540 is the cell membrane. Taken together that the cell membrane of leukemic cells is different than the one of normal cells and that MC540 is selectively uptaken by leukemic cells and localized at different sites of the cell than Hypericin, further studies on the localization of the sensitizers on the cell would clarify the exhibited properties of the PMF extract .

In conclusion, PMF and ME extracts cannot be helpful in autologous bone marrow purging where leukemic cells and normal hemopoietic progenitor cells coexist. These extracts though have shown promising results in bladder cancer PDT [141]. Given their effect against tumor growth *in vivo* and *in vitro,* the photostability of PMF in combination with their low cost, they comprise potent photosensitizers for the photodynamic therapy of tumors

References

1] Niemz M. H. Laser tissue interactions. Springer (1996)

2] Boulnois J. L. Photophysical processes in recent medical laser developments. *Lasers Med. Sci*. **1**, 47-66 (1996).

3] Ackroyd, R., Kelty, C., Brown, N. & Reed, M. The history of photodetection and photodynamic therapy. *Photochem. Photobiol.* **74**, 656–669 (2001).

4] von Tappeiner, H. & Jodlbauer, A. *Die sensiblilisierende Wirkung fluoreszierender Substanzer Gesammte Untersuchungen uber die photodynamische Erscheinerung* (Voger, F. C., Leipzig, 1907).

5] Macdonald, I. J. & Dougherty, T. J. Basic principles of photodynamic therapy. *J. Porphyrins Phthalocyanines* **5,** 105–129 (2001).

6] Dolmans, D., Fukumura, D. & Jain, R. K. Photodynamic therapy for cancer. *Nature Reviews Cancer* **3**, 380 (2003).

7] Epstein, J. H. Phototoxicity and photoallergy. *Semin. Cutan. Med. Surg.* **18**, 274–284 (1999).

8] Epstein, J. H. Phototherapy and photochemotherapy. *N. Engl. J. Med.* **322**, 1149–1151 (1990).

9] Diamond I., Granelli SG, McDonagh AF, Nielsen S, Wilson CB, Jaenicke R. Photodynamic therapy of malignant tumours. *Lancet* **2**, 1175–1177 (1972).

10] Dougherty, T. J., Grindey, G. B., Fiel, R., Weishaupt, K. R. & Boyle, D. G. Photoradiation therapy. II. Cure of animal tumors with hematoporphyrin and light. *J. Natl. Cancer Inst.* **55**, 115–121 (1975).

11] Kelly, J. F., Snell, M. E. & Berenbaum, M. C. Photodynamic destruction of human bladder carcinoma. *Br. J. Cancer* **31**, 237–244 (1975).

12] Kelly, J. F. & Snell, M. E. Hematoporphyrin derivative: a possible aid in the diagnosis and therapy of carcinoma of the bladder. *J. Urol.* **115**, 150–151 (1976).

13] Hayata, Y., Kato, H., Konaka, C., Ono, J. & Takizawa, N. Hematoporphyrin derivative and laser photoradiation in the treatment of lung cancer. *Chest* **81**, 269–277 (1982).

14] McCaughan, J. S. Jr., Hicks, W., Laufman, L., May, E. & Roach, R.. Palliation of esophageal malignancy with photoradiation therapy. *Cancer* **54**, 2905–2910 (1984).

15] Balchum, O. J., Doiron, D. R. & Huth, G. C., Photoradiation therapy of endobronchial lung cancers employing the photodynamic action of hematoporphyrin derivative. *Lasers Surg. Med.* **4**, 13–30 (1984).

16] Hayata, Y., Kato, H., Okitsu, H., Kawaguchi, M. & Konaka, C. Photodynamic therapy with hematoporphyrin derivative in cancer of the upper gastrointestinal tract. *Semin. Surg. Oncol.* **1**, 1–11 (1985).

17] Dougherty, T.J., Lawrence G, Kaufman JH, Boyle D, Weishaupt KR, Goldfarb A. Photoradiation in the treatment of recurrent breast carcinoma. *J. Natl. Cancer Inst.* **62**, 231–237 (1979).

18] Dimofte, A., Zhu, T. C., Hahn, S. M. & Lustig, R. A. *In vivo* light dosimetry for motexafin lutetium-mediated PDT of breast cancer. *Lasers Surg. Med.* **31**, 305–312 (2002).

19] Ward, B. G., Forbes, I. J., Cowled, P. A., McEvoy, M. M.& Cox, L. W., The treatment of vaginal recurrences of gynecologic malignancy with phototherapy following hematoporphyrin derivative pre-treatment. *Am. J. Obstet. Gynecol.* **142**, 356–357 (1982).

20] Hornung, R. Photomedical approaches for the diagnosis and treatment of gynecologic cancers. *Curr. Drug Targets Immune Endocr. Metabol. Disord.* **1**, 165–177 (2001).

21] Fehr, M. K., Hornung R, Degen A, Schwarz VA, Fink D, Haller U, Wyss P.Photodynamic therapy of vulvar intraepithelial neoplasia III using topically applied 5-aminolevulinic acid. *Gynecol. Oncol*. **84**, 62–66 (2002).

22] Gomer, C. J., Doiron, D. R., Jester, J. V., Szirth, B. C. & Murphree, A. L., Hematoporphyrin derivative photoradiation therapy for the treatment of intraocular tumors: examination of acute normal ocular tissue toxicity. *Cancer Res.* **43**, 721–727 (1983).

23] Favilla, I., Favilla ML, Gosbell AD, Barry WR, Ellims P, Hill JS, Byrne JR. Photodynamic therapy: a 5 year study of its effectiveness in the treatment of posterior uveal melanoma, and evaluation of haematoporphyrin uptake and photocytotoxicity of melanoma cells in tissue culture. *Melanoma Res.* **5**, 355–364 (1995).

24] Landau, I. M., Steen, B. & Seregard, S. Photodynamic therapy for circumscribed choroidal haemangioma. *Acta Ophthalmol. Scand,* **80**, 531–536 (2002).

25] Sandeman, D. R. Photodynamic therapy in the management of malignant gliomas: a review. *Lasers Med. Sci.* **1**, 163–167 (1986).

26] Popovic, E. A., Kaye, A. H. & Hill, J. S. Photodynamic therapy of brain tumors. *J. Clin. Laser Med. Surg.* **14**, 251–261 (1996).

27] Rosenthal, M. A., Kavar B, Hill JS, Morgan DJ, Nation RL, Stylli SS, Basser RL, Uren S, Geldard H, Green MD, Kahl SB, Kaye AH. Phase I and pharmacokinetic study of photodynamic therapy for high-grade gliomas using a novel boronated porphyrin. *J. Clin. Oncol.* **19**, 519–524 (2001).

28] Schweitzer, V. G. Photodynamic therapy for treatment of head and neck cancer. *Otolaryngol. Head Neck Surg.* **102**, 225–232 (1990).

29] Biel, M. A. Photodynamic therapy and the treatment of head and neck neoplasia. *Laryngoscop,* **108**, 1259–1268 (1998).

30] Barr, H., Krasner, N., Boulos, P. B., Chatlani, P. & Bown, S. G. Photodynamic therapy for colorectal cancer: a quantitative pilot study. *Br. J. Surg.* **77**, 93–96 (1990).

31] Mlkvy, P., Messmann H, Regula J, Conio M, Pauer M, Millson CE, MacRobert AJ, Bown SG. Photodynamic therapy for gastrointestinal tumors using three photosensitizers — ALA induced PPIX, Photofrin and MTHPC. A pilot study. *Neoplasma* **45**, 157–161 (1998).

32] Allison, R. R., Mang, T. S. & Wilson, B. D. Photodynamic therapy for the treatment of nonmelanomatous cutaneous malignancies. *Semin. Cutan. Med. Surg.* **17**, 153–163 (1998).

33] Taber, S. W., Fingar, V. H., Coots, C. T. & Wieman, T. J. Photodynamic therapy using mono-L-aspartyl chlorin e6 (Npe6) for the treatment of cutaneous disease: a Phase I clinical study. *Clin. Cancer Res.* **4**, 2741–2746 (1998).

34] DeLaney, T. F Sindelar WF, Tochner Z, Smith PD, Friauf WS, Thomas G, Dachowski L, Cole JW, Steinberg SM, Glatstein E. Phase I study of debulking surgery and photodynamic therapy for disseminated intraperitoneal tumors. *Int. J. Radiat. Oncol. Biol. Phys.* **25**, 445–457 (1993).

35] Pass, H. I Pass HI, DeLaney TF, Tochner Z, Smith PE, Temeck BK, Pogrebniak HW, Kranda KC, Russo A, Friauf WS, Cole JW, et al.. Intrapleural photodynamic therapy: results of a phase I trial. *Ann. Surg. Oncol.* **1**, 28–37 (1994).

36] Ortner, M. A., Liebetruth J, Schreiber S, Hanft M, Wruck U, Fusco V, Muller JM, Hortnagl H, Lochs H. Photodynamic therapy of nonresectable cholangiocarcinoma. *Gastroenterology* **114**, 536–542 (1998).

37] Bown, S. G., Rogowska AZ, Whitelaw DE, Lees WR, Lovat LB, Ripley P, Jones L, Wyld P, Gillams A, Hatfield AW. Photodynamic therapy for cancer of the pancreas. *Gut* **50**, 549–557 (2002).

38] McBride, G. Studies expand potential uses of photodynamic therapy. *JNCI Cancer Spectrum* **94**, 1740–1742 (2002).

39] Dougherty, T. J., Gomer, C. J., Henderson, B. W., Jori, S., Kessel, D., Korbelik, M., et al. Photodynamic therapy. J. Natl. Cancer Inst. **90**, 889-905 (1998).

40] Leman, J. A. & Morton, C. A. Photodynamic therapy applications in dermatology. *Expert Opin. Biol. Ther.* **2**, 45–53 (2002).

41] Ortu, P., LaMuraglia, G. M., Roberts, W. G., Flotte, T. J. & Hasan, T. Photodynamic therapy of arteries. A novel approach for treatment of experimental intimal hyperplasia. *Circulation* **85**, 1189–1196 (1992).

42] Soukos, N. S., Ximenez-Fyvie, L. A., Hamblin, M. R., Socranski, S. S. & Hasan, T. Targeted antimicrobial photochemotherapy. *Antimicrob. Agents Chemother.* **42**, 2595–2601 (1998).

43] Trauner, K. B., Gandour-Edwards R, Bamberg M, Shortkroff S, Sledge C, Hasan T. Photodynamic synovectomy using benzoporphyrin derivative in an antigen-induced arthritis model for rheumatoid arthritis. *Photochem. Photobiol.* **67**, 133–139 (1998).

44] Mittra, R. A. & Singerman, L. J. Recent advances in the management of age-related macular degeneration. *Optom. Vis. Sci.* **79**, 218–224 (2002).

45] Meruelo, D., Lavie, G. & Lavie, D. Therapeutic agents with dramatic antiretroviral activity and little toxicity at effective doses: aromatic polycyclic diones hypericin and pseudohypericin. Proc. Natl. Acad. Sci. U.S.A. **85**, 5230–5234 (1988).

46] Mycek, M. A. & Pogue, B. W. Handbook of Biomedical Fluorescence. *Marcel Dekker* (2003)

47] Luksiene, Z. Photodynamic therapy: mechanism of action and ways to improve the efficiency of treatment. *Medicina* **39**, 1137-1150 (2003).

48] Fiers, W., Beyaert, R., Declercq, W. & Vandenabeele, P. More than one way to die: apoptosis, necrosis and reactive oxygen damage. *Oncogene* **18**, 7719–7730 (1999).

49] Ellis, R. E., Yuan, J. & Horvitz, H. R. Mechanisms and functions of cell death. *Ann. Rev. Cell. Biol.* **7**, 663–698 (1991).

50] Moan, J. & Berg, K. The photodegradation of porphyrins in cells can be used to estimate the lifetime of singlet oxygen. *Photochem. Photobiol*. **53**, 549–553 (1991).

51] Kessel, D., Luo, Y., Deng, Y. & Chang, C.K. The role of subcellular localization in initiation of apoptosis by photodynamic therapy. *Photochem. Photobiol.* **65**, 422–425 (1997).

52] Moor, A. C. Signaling pathways in cell death and survival after photodynamic therapy. *J. Photochem. Photobiol.* **57**, 1–13 (2000).

53] Forman, S. J. & Blume, K. G. Allogeneic bone marrow transplantation for acute leukemia. *Hematol. Oncol. Clin. North Am*. **4**, 517 (1990).

54] Zittoun, R. A., Mandelli, F., Willemze, R., et al. Autologous or allogeneic bone marrow transplantation compared with intensive chemotherapy in acute myelogenous leukemia. *N. Engl. J. Med.* **332**, 217 (1995).

55] Shulman, H. M. & Hinterberg, W. Hepatic veno-occlusive diseaseliver toxicity syndrome after bone marrow transplantation. *Bone Marrow Trans.* **10**, 197 (1992).

56] Zaia, J. A. Viral infections associated with bone marrow transplantation. *Hem. Oncol. Clin. North Am.* **4**, 603 (1990).

57] Kaizer, H. & Chow, H. S. Autologous bone marrow transplantation (ABMT) in the treatment of cancer. *Cancer Inv.* **2**, 203 (1984).

58] Champlin, R. Purging: the separation of normal from malignant cells for autologous transplantation. *Transfusion* **36**, 910 (1996).

59] Selvaggi, K. J., Wilson, J. W., Mills, L. E., et al. Improved outcome for high risk acute myeloid leukemia patients using autologous bone marrow transplantation and monoclonal antibody-purged bone marrow. *Blood* **83**, 1698 (1994).

60] Laport, J. P., Douay, L., Lopez M., et al. One hundred twenty-five adult patients with primary acute leukemia autografted with marrow purged by mafosfamide: A 10-year single institution experience. *Blood* **84**, 3810 (1994).

61] Udomsakdi, C., Eaves, C. J., Swolin, B., et al. Rapid decline of chronic myeloid leukemic cells in long term culture due to a defect at the leukemic stem cell level. *Proc. Nat. Acad. Sc. U.S.A.* **89**, 6192 (1992).

62] Mulroney, C. M., Gluck, S. & Ho, A. D. The use of photodynamic therapy in bone marrow purging. *Semin. Oncol.* 21, 24-7 (1994).

63] Gulati, S., Atzpodien, J., Lemoli, R. M., Shimazaki, C. & Clarkson, B. Photoradiation methods for purging autologous bone marrow grafts. *Prog. Clin. Biol. Res*. **333**, 87-102 (1990).

64] Danilatou V., Lydaki E., Dimitriou H., Papazoglou T., Kalmanti M., Bone marrow purging by photodynamic treatment in children with acute leukaemia Cytoprotective action of Amifostine. *Leukemia Research* **24**, 427–435, (2000)

65] Valinsky, J. F., Easton, T. G. & Reich, E. Merocyanine 540 as a fluorescent probe of membranes: selective staining of leukemic and immature hemapoietic cells. *Cell* **13**, 487 (1978).

66] Onganer, Y. & Quitevis, E. Dynamics of merocyanine 540 in model biomembranes: photoisomerization in small unulamellar vesicles. *J. Leukoc. Biochem. Biophys. Acta* **1192**, 27 (1994).

67] Mc Evoy, L., Schlegel, R. & Williamson, P. Merocyanine 540 as a flow cytometric probe of membrane lipid organization in leukocytes. *J. Leukoc. Biol*. **44**, 337 (1988).

68] Giese, A. C. Hypericism. *Photochem. Photobiol. Rev.* **5**, 229–255 (1980).

69] Kitanov, G. M. Hypericin and pseudohypericin in some *Hypericum* species. *Biochem. Syst. Ecol.* **29**, 171–178 (2001).

70] Delaey, E. M., Kamuhabwa, A., Vandenbogaerde, A. L. & de Witte, P. A. M. Photocytotoxicity of protohypericin after photoconversion to hypericin. *Planta Me*d. **65**, 719–722 (1999).

71] Schempp, C. M., Muller, K., Winghofer, B., Schulte-Monting, J. & Simon, J. C. Single-dose and steady state administrationof *Hypericum perforatum* extract St. John's wort does not influence skin sensitivity to UV radiation, visible light, and solar-simulated radiation. *Arch. Dermatol.* **137**, 512–513 (2001).

72] Linde, K., Ramirez, G., Mulrow, C. D., Pauls, A., Weidenhammer, W. & Melchart, D. St. John's wort for depressionan overview and meta-analysis of randomised clinical trials. *Br. Med. J.* **313**, 565–576 (1996).

73] Chatterjee, S. S., Bhattacharya, S. K., Wonnemann, M., Singer, A. & Muller, W. E. Hyperforin as a possible antidepressant component of *Hypericum* extracts. *Life Sci*. **63**, 499–510 (1998).

74] Ehrenberg, B., Anderson, J. L. & Foote, C. S. Kinetics and yield of singlet oxygen photosensitized by hypericin in organic and biological media. *Photochem. Photobiol.* **68**, 135–140 (1998).

75] Redmond, R. W. & Gamlin, J. N. A compilation of singlet oxygen yields from biologically relevant molecules. *Photochem. Photobiol.* **70**, 391–475 (1999).

76] Vandenbogaerde, A. L., Cuveele, J. F., Proot, P., Himpens, B., Marlevede, W. J. & DeWitte, P. A. Differential cytotoxic effects induced after photosensitization by hypericin. *J. Photochem. Photobiol.* **38**, 136-142 (1997).

77] Lavie, G., Mazur, Y., Lavie, D. & Meruelo, D. The chemical and biological properties of hypericin: a compound with a broad spectrum of biological activities. *Med. Res. Rev.* **15**, 111–119 (1995).

78] Tang, J., Colacino, J. M., Larsen, L. H., Spitzer, W. Virucidal activity of hypericin against enveloped and non-enveloped DNA and RNA viruses. *Antiviral Res.* **13**, 313–325 (1990).

79] Hudson, J. B., Lopez-Bazzocchi, I. & Towers, G. H. Antiviral activities of hypericin. *Antiviral Res.* **15**, 101–112 (1991).

80] Hudson, J. B., Harris, L. & Towers, G. H. The importance of light in the anti-HIV effect of hypericin. *Antiviral Res.* **20**, 173–178 (1993).

81] Lavie, G., Mazur, Y., Lavie, D., Prince, A. M., Pascual, D., Liebes, L., Levin, B. & Meruelo, D. Hypericin as an inactivator of infectious viruses in blood components. *Transfusion* **35,** 392–400 (1995).

82] Gulick, R. M., McAuliffe, V., Holden-Wiltse, J., Crumpacker, C., Liebes, L., Stein, D. S., Meehan, P., Hussey, S., Forcht, J. & Valentine, F. T. Phase I studies of hypericin, the active compound in St. John's wort, as an antiretroviral agent in HIV-infected adults. AIDS Clinical Trials Group Protocols 150 and 258. *Ann. Intern. Med.* **130**, 510–514 (1999).

83] Prince, A.M., Pascual, D., Meruelo, D., Liebes, L., Mazur, Y., Dubovi, E., Mandel, M. & Lavie, G. Strategies for evaluation of enveloped virus inactivation in red cell concentrates using hypericin. *Photochem. Photobiol.* **71**, 188–195 (2000).

84] Takahashi, I., Nakanishi, S., Kobayashi, E., Nakano, H., Suzuki, K. & Tamaoki, T. Hypericin and pseudohypericin specifically inhibit protein kinase C: possible relation to their antiretroviral activity. *Biochem. Biophys. Res. Commun.* **165**, 1207–1212 (1989).

85] de Witte, P. A. M., Agostinis, P., Van Lint, J., Merlevede, W. &. Vandenheede, J. R. Inhibition of epidermal growth factor receptor tyrosine kinase activity by hypericin. *Biochem. Pharmacol.* **46**, 1929–1936 (1993).

86] Agostinis, P., Vandenbogaerde, A., Donella-Deana, A., Pinna, L. A., Lee, K. T., Goris, J., Merlevede, W., Vandenheede, J. R. & de Witte P. A. M. Photosensitized inhibition of growth factor-regulated protein kinases by hypericin. *Biochem. Pharmacol.* **49**, 1615–1622 (1995).

87] Hadjur, C., Richard, M. J., Parat, M. O., Jardon, P. & Favier, A. Photodynamic effects of hypericin on lipid peroxidation and antioxidant status in melanoma cells. *Photochem. Photobiol.* **64**, 375–381 (1996).

88] Chaloupka, R., Obsil, T., Plasek, J. & Sureau, F. The effect of hypericin and hypocrellin-A on lipid membranes and membrane potential of 3T3 fibroblasts. *Biochem. Biophys. Acta* **1418**, 39–47 (1999).

89] Miccoli, L., Beurdeley-Thomas, A., De Pinieux, G., Sureau, F., Oudard, S., Dutrillaux, B. & Poupon, M. F. Light-induced photoactivation of hypericin affects the energy metabolism of human glioma cells by inhibiting hexokinase bound to mitochondria. *Cancer Res.* **58**, 5777–5786 (1998).

90] Weiner, L., Roth, E., Mazur, Y. & Silman, I. Targeted cross-linking of a molten globule form of acetylcholinesterase by the virucidal agent hypericin *Biochemistry* **38**, 11401–11405 (1999).

91] Schey, K. L., Patat, S., Chignell, C. F., Datillo, M., Wang, R. H. & Roberts, J. E. Photooxidation of lens alpha-crystallin by hypericin (active ingredient in St. John's wort). *Photochem. Photobiol.* **72,** 200–203 (2000).

92] Bouirig, H., Eloy, D. & Jardon, P. *J. Chim. Phys.* Fluorescence and triplet-triplet absorption quenching of hypericin in liposomes of dipalmitoylphoshpatidylcholine Application to the study of intervesicular diffusion of hypericin. **90**, 2021- 2038 (1993).

93] Yamazaki, T., Ohta, N., Yamazaki, I. & Song, P. S. Excited-state properties of hypericin: electronic spectra and fluorescence decay kinetics. *J. Phys. Chem.* ***97,*** 7870-7885 (1993).

94] Gai, F., Fehr, M. J. & Petrich, J. W. Role of Solvent in Excited-State Proton Transfer in Hypericin**.** *J. Phys. Chem.* ***98***, 8352- 8358 (1994).

95] Carpenter, S., Fehr, M. J., Kraus, G. A. & Petrich, J. W. Chemiluminescent activation of the antiviral activity of hypericin: a molecular flashlight. *Proc. Natl. Acad. Sci. U.S.A.* ***91***, 12273-12277 (1994).

96] Meruelo, D., Lavie, G. & Lavie, D. Therapeutic agents with dramatic antiretroviral activity and little toxicity at effective doses: aromatic polycyclic diones hypericin and pseudohypericin. *Proc. Natl. Acad. Sci. U.S.A.* ***85***, 5230-5234 (1988).

97] Malkin, J. & Mazur, Y. Hypericin derived triplet states and transients in alcohols and water. *Photochem. Photobiol.* **57**, 929–933 (1993).

98] Michaeli, A., Regev, A., Mazur, Y., Feitelson, J. & Levanon, H. Triplet-state reactions of hypericin. Time-resolved laser photolysis and electron paramagnetic resonance spectroscopy. *J. Phys. Chem.* **97**, 9154–9160 (1993).

99] Roslaniec, M., Weitman, H., Freeman, D., Mazur, Y. & Ehrenberg, B. Liposome binding constants and singlet oxygen quantum yields of hypericin, tetrahydroxy helianthrone and their derivatives: studies in organic solutions and in liposomes. *Journal of Photochemistry and Photobiology* **57**, 149–158 (2000).

100] Darmanyan, A.P., Burel, L., Eloy, D. & Jardon, P. Singlet oxygen production by hypericin in various solvents. *J. Chim. Phys.* **91**, 1774–1785 (1994).

101] Bouirig, H., Eloy, D. & Jardon, P. Formation et reactivite de l'oxygene singulet photosensibilise par l'hypericine dans des liposomes de dipalmitoylphosphatidyl-choline. Mise en evidince d'une photooxydation retardee. *J. Chem. Phys.* **89**, 1391–1411 (1992).

102] Ehrenberg, B., Anderson, J. L. & Foote, C. S. Kinetics and yield of singlet oxygen photosensitized by hypericin in organic and biological media. *Photochem. Photobiol.* **68**, 135–140 (1998).

103) Jardon, P., Lazortchak, N., Gautron, R. Generation of singlet oxygen delta-1g photosensitized by hypericin – Characterization and study of the mechanism by lase spectroscopy. *J. Chim. Phys.*, ***84***, 1143-1145 (1987).

104] Thomas, C. & Pardini, R. S. Oxygen dependence of hypericin-induced phototoxicity to EMT6 mouse mammary carcinoma cells. *Photochem. Photobiol.* ***55***, 831-837 (1992).

105] Kraus, G. A., Zhang, W., Fehr, M. J., Petrich, J. W., Wannemuehler, Y. & Carpenter, S. Research at the interface between chemistry and virology: development of a molecular flashlight. *Chem. Rev.* **96,** 523–535 (1996).

106] Couldwell, W. T., Gopalakrishna, R., Hinton, D. R., He, S., Weiss, M. H., Law, R. E. & Apuzzo, M. L. *J. Neurosurgery* ***35***, 705-710 (1994).

107] Weiner, L. & Mazur, Y. EPR studies of hypericin. Photogeneration of free radicals and superoxide. *J. Chem. Soc., Perkins Trans.* **2**, 1439–1442 (1992).

108] Redepenning, J. & Tao, N. Measurement of formal for hypericin in dimethylsulfoxide. *Photochem. Photobiol.* ***58***, 532-535 (1993).

108] Diwu, Z. & Lowen, J. W. Photosensitization with anticancer agents.17. EPR studies of photodynamic action of hypericin – formation of semiquinone radical and activated oxygen species on illumination. *Free Radical Biol. Med*. **14**, 209-215 (1993).

109] Malkin, J. & Mazur, Y. Hypericin derived triplet states and transients in alcohols and water. *Photochem. Photobiol.* **57**, 929–933 (1993).

110] Darmanyan, A. P., Burel, L., Eloy, D. & Jardon, P. Singlet oxygen production by hypericin in various solvents. *J. Chem. Phys.* **91**, 1774–1785 (1994).

111] Hadjur, C., Jeunet, A. & Jardon, P. Photosensitization by hypericin: electron spin resonance (ESR) evidence for the formation of singlet oxygen and superoxide anion radicals in an in vitro model. *J. Photochem. Photobiol.* **26**, 67–74 (1994).

112] Hadjur, C., Richard, M. J., Parat, M. O., Favier, A. & Jardon, P. Photodynamically induced cytotoxicity of hypericin dye on human fibroblast cell line MRC5. *J. Photochem. Photobiol.* **27**, 139–146 (1995).

113] Sureau, F., Miskovsky, P., Chinsky, L. & Turpin P. Y. Hypericin-Induced Cell Photosensitization Involves an Intracellular pH Decrease. *J. Am. Chem. Soc.* **118**, 9484-9487 (1996).

114] Chowdhury, P. K., Ashby, K. D., Datta, A. & Petrich, J. W. Effect of pH on the Fluorescence and Absorption Spectra of Hypericin in Reverse Micelles. *Photochem Photobiol.* **72**, 612–618 (2000).

115] Fehr, M. J., Mc Closkey, A. & Petrich, J. W. Light induced acidification by the antiviral agent hypericin. *J. Am. Chem. Soc.* **117**, 1833-1836 (1995).

116] Pinto, L. H., Holsinger, L. J. & Lamb, R. A. *Cell* **69**, 517-528 (1992).

117] Barry, M. A., Reynold, J. E. & Eastman, A. Eteposide-induced apoptosis in human HL-60 cells is associated with intracellular acidification. *Cancer Res.* **53**, 2349-2357 (1993).

118] Zhang, W., Lawa, R. E., Hintona, D. R., Su, Y. & Couldwell, W. T. Growth-inhibition and apoptosis in human neuroblastoma SK-N-SH cells induced by hypericin, a potent inhibitor of protein- kinase-c. *Cancer Let.* **96**, 31-35(1995).

119] Li, J. & Eastman, A. Apoptosis in interleukin-2- dependent cytotoxic-T lemphocyte cell-line is associated with intracellular acidification – role of the NA^+/H^+ antiport. *J. Biol. Chem.* **270**, 3203-3211 (1995).

120] Couldwell, W. T., Gopalakrishna, R., Hinton, D. R., He, S., Weiss, M. H., Law, R. E. & Apuzzo, M. L. J. Hypericin: a potential antiglioma therapy. *Neurosurgery* **35**, 705-710 (1994).

121] Miccoli, L., Oudard, S., Sureau, F., Poirson, F., Dutrillaux, B. & Poupon, M.F. Intracellular pH governs the subcellular distribution of hexokinase in a glioma cell line. *Biochem J.* **313**, 957-962 (1995).

122] Uzdensky, A B., Iani, V., Ma, L. W. & Moan J. Photobleaching of Hypericin Bound to Human Serum Albumin. *Cultured Adenocarcinoma Cells and Nude Mice Skin Photochemistry and Photobiology* **76**, 320–328 (2002).

123] D'Hallewin, M. A., Bezdetnaya, L. & Guillemin, F. Fluorescence detection of bladder cancer :A Review. *European Urology* **42**, 417-425 (2002).

124] Vandenbogaerde, A L., Cuveele, J. F., Proot, P. Himpens, B. E., Merlevede, W. J. & de Witte P. A. M. Differential cytotoxic effects induced after photosensitization by hypericin. *J. Photochem. Photobiol.* **38**, 136–142 (1997).

125] Weber, N. D., Murray, B. K., North, J. A. & Wood S. G. The antiviral agent hypericin has in vitro activity against HSV-1 through non-specific association with viral and cellular membranes. *Antiviral Chem. Chemother.* **5**, 83–90 (1994).

126] English, D. S., Doyle, R. T., Petrich, J. W. & Haydon, P.G. Subcellular distributions and excited state processes of hypericin in neurons. *Photochem. Photobiol.* **69**, 301–305 (1999).

127] Sattler, S., Schaefer, U., Schneider, W., Hoelzl, J. & Lehr, C.M. Binding, uptake, and transport of hypericin, by Caco-2 cell monolayers. *J. Pharm. Sci.* **86**, 1120–1126 (1997).

128] Miccoli, L., Beurdeley-Thomas, A., De Pinieux, G., Sureau, F., Oudard, S., Dutrillaux, B. & Poupon, M.F. Light-induced photoactivation of hypericin affects the energy metabolism of human glioma cells by inhibiting hexokinase bound to mitochondria. Cancer Res. **58**, 5777–5786 (1998).

129] Utsumi, T., Okuma, M., Kanno, T., Takehara, Y., Yoshioka, T., Fujita, Y., Horton, A. A. & Utsumi, K. Effect of the antiretroviral agent hypericin on rat liver mitochondria. *Biochem. Pharmacol.* **50**, 655–662 (1995).

130] Johnson, S. A. S. & Pardini, R. S. Antioxidant enzyme response to hypericin in EMT6 mouse mammary carcinoma cells. *Free Rad. Biol. Med.* **24**, 817–826 (1998)

131] Pawley, J. B. *Handbook of Biological Confocal Microscopy* 2nd edn, (New York: Plenum) (1995)

132] Webb, R. H. Confocal optical microscopy. *Rep. Prog. Phys.* **59**, 427–471 (1996).

133] White, N. S, Errington, R. J., Fricker, M. D. & Wood, J. L. *Journal of Microscopy* **181**, 99-116 (1996).

134] Denk, W., Strickler, J. H. & Webb, W. W. Two-photon laser scanning fluorescence microscopy. *Science* **73**, 248, (1990).

135] http://www.loci.wisc.edu/multiphoton/mp.html

136] Bloembergen, N. Nonlinear Optics. *World Scientific* (1965)

137] Κουλουμέντας, Χ. Απεικόνιση δομών και διεργασιών του Νηματώδους *C.elegans* με χρήση Μη Γραμμικής Μικροσκοπίας. Μεταπτυχιακή Διατριβή, Πανεπιστήμιο Κρήτης-Τμήμα Φυσικής, (2004).

138] Geirgakoudi, I. & Foster, T. H. Singlet oxygen versus nonsinglet oxygen-mediated mechanisms of sensitizer photobleaching and their effects on photodynamic dosimetry. *Photochem. Photobiol.* **67**, 612–625 (1998).

139] Uzdensky, A. B., Ma, L. W, Iani, V., Hjortland, G.O., Steen H.B., Moan, J., Intracellular localization of hypericin in human glioblastoma and carcinoma cell lines, *Lasers Med. Sci.,* **16**, 276–283 (2001).

140] Shen, S. C., Chen, Y. C., Hsu, F. L. & Lee, W. R. Differential apoptosis-inducing effect of quercetin and its glycosides in human promyeloleukemic HL-60 cells by alternative activation of the caspase 3 cascade. *J. Cell Biochem.* **89**, 1044-55 (2003).

141] Nseyo U. O., Kim A. H., Nseyo U. U., Stayropoulos N. E., Skalkos D. Photodynamic therapy (PDT) with Hypericum Perforatum L. extract induced significant in vitro cytotoxicity of human bladder cancer cells. *Proceedings of the American Assoc. for Cancer Resear.* **45**, 4319 (2004)